

1-1-2005

Fatigue damage assessment of unidirectional GRP and CFRP composites

Morteza Panbechi
Ryerson University

Follow this and additional works at: <http://digitalcommons.ryerson.ca/dissertations>

 Part of the [Mechanical Engineering Commons](#)

Recommended Citation

Panbechi, Morteza, "Fatigue damage assessment of unidirectional GRP and CFRP composites" (2005). *Theses and dissertations*. Paper 376.

This Thesis is brought to you for free and open access by Digital Commons @ Ryerson. It has been accepted for inclusion in Theses and dissertations by an authorized administrator of Digital Commons @ Ryerson. For more information, please contact bcameron@ryerson.ca.

NOTE TO USERS

This reproduction is the best copy available.

UMI[®]

b17760641

TA
403
.P36
2805

FATIGUE DAMAGE ASSESSMENT OF UNIDIRECTIONAL GRP AND CFRP COMPOSITES

By

Morteza Panbechi

BSc, Sharif University of Technology, Tehran Iran, 1989

A thesis to the Ryerson University

in fulfillment of the

thesis requirement for the degree of

Master of Applied Science

in

Mechanical Engineering

Toronto, Ontario, Canada, 2005

© Morteza Panbechi 2005

**PROPERTY OF
RYERSON UNIVERSITY LIBRARY**

UMI Number: EC53750

INFORMATION TO USERS

The quality of this reproduction is dependent upon the quality of the copy submitted. Broken or indistinct print, colored or poor quality illustrations and photographs, print bleed-through, substandard margins, and improper alignment can adversely affect reproduction.

In the unlikely event that the author did not send a complete manuscript and there are missing pages, these will be noted. Also, if unauthorized copyright material had to be removed, a note will indicate the deletion.

UMI[®]

UMI Microform EC53750

Copyright 2009 by ProQuest LLC

All rights reserved. This microform edition is protected against unauthorized copying under Title 17, United States Code.

ProQuest LLC
789 East Eisenhower Parkway
P.O. Box 1346
Ann Arbor, MI 48106-1346

AUTHOR'S DECLARATION

I hereby declare that I am the sole author of this thesis.

I authorize the Ryerson University to lend this thesis to other institutions or individuals for the purpose of scholarly research.

I further authorize the Ryerson University to reproduce this thesis by photocopying or by other means, in total or in part, at the request of other institutions or individuals for the purpose of scholarly research.

The Ryerson University requires the signatures of all persons using or photocopying this thesis.
Please sign below, and give address and date.

To the Memories of
My late Father Mr. Mostafa Panbechi

ABSTRACT

Fatigue Damage Assessment of Unidirectional GRP and CFRP Composites, Morteza Panbechi, MA Sc, Mechanical Engineering, Ryerson University, 2005

The present thesis has developed an energy-based critical plane fatigue damage parameter to assess the fatigue damage of unidirectional GRP and CFRP composites. The proposed model is based on the physics and the mechanism of fatigue cracking within three damage regions of the matrix (I), the fiber-matrix interface (II), and the fiber (III) in unidirectional GRP and CFRP composites as the number of cycles progresses. The model involves the shear and normal energies calculated from stress and strain components acting on (i) a relatively ductile matrix, (ii) the matrix-fiber interface, and (iii) the unidirectional brittle fibers. For the regions III, and I the cracking is dominantly based on the maximum shear stress and the maximum normal principal stress, respectively and the fatigue damage was assessed based on the Varvani-Farahani damage approach. For region II, the damage progress along the matrix-fiber interface was evaluated based on the Plumtree-Cheng approach.

The proposed fatigue damage analysis has addressed the cracking and damage progress within three regions over the life of unidirectional GRP and CFRP composites and showed a good capability in unifying the experimentally obtained fatigue lives with various off-axis angles and stress ratios as compared with other well-known damage criteria available in the literature.

ACKNOWLEDGEMENTS

I would like to thank my supervisor, Professor A. Varvani-Farahani, for his support, advice, and his guidance through my Masters program in the Department of Mechanical and Industrial Engineering at Ryerson University.

The financial support of NSERC through Professor A. Varvani-Farahani of the Department of Mechanical and Industrial Engineering, Ryerson University and partial support of a Ryerson Graduate Scholarship are greatly appreciated.

I would also like to thank my family and friends who supported me and stood beside me during the ups and downs in last two years.

TABLE OF CONTENTENTS

AUTHOR'S

DECLARATION.....	ii
ABSTRACT.....	iv
ACKNOWLEDGEMENTS.....	v
TABLE OF CONTENTS.....	vi
LIST OF FIGURES.....	ix
LIST OF TABLES.....	xiv
NOMENCLATURE.....	xv
OBJECTIVE AND SCOPE OF PRESENT STUDY.....	xviii
PREFACE OF THESIS.....	xix

Chapter 1: Introduction and Background in Fatigue of Reinforced Composite Materials

1.1 Introduction.....	1
1.2 General Considerations on Fatigue Damage Modeling for FRPs.....	1
1.3 Review of Fatigue Models.....	2
1.4 Fatigue Life Models.....	2
1.4.1 Stress-Based Models.....	2
1.4.2 Eenergy-Based Models.....	4
1.5 Phenomenological Models to Predict Residual Stiffness/Strength.....	5
1.5.1 Residual Stiffness Models.....	5
1.5.2 Residual Strength Models.....	7
1.6 Progressive Damage Models.....	9
1.6.1 Progressive Damage Models Predicting Damage Growth.....	9
1.6.2 Progressive Damage Models Predicting Residual Mechanical Properties.....	9
1.7 The Objective of This Study.....	10

Chapter 2: Materials Behavior and Industrial Application of Unidirectional GRP and CFRP Composites

2.1 The Nature of Reinforced Plastics.....	11
2.2 Unidirectional continuous-fiber composites.....	12
2.2.1 Progressive Damage and Failure in Unidirectional Composites.....	15
2.2.2 Transverse Strength.....	16
2.2.3 Orientation-Dependence of Composite Strength.....	17
2.2.4 Effect of Polyester Resin Properties.....	18
2.3 Glass Fiber Reinforcement.....	18
2.4 Carbon-Fiber-Reinforced Plastics.....	21
2.5 Applications.....	24
2.5.1 Aerospace and Military Applications.....	24
2.5.1.1 Composite Materials in U.S. Army Applications.....	25
2.5.1.2 Seawater Ball Valves.....	25
2.5.1.3 Aero-engine Application.....	25
2.5.2 Offshore Application.....	26
2.5.3 Wind Power Plant Application.....	27
2.5.4 Highway Infrastructure Application.....	27

Chapter 3: Stress and Strain Constitutive Relationship in FRP Composites

3.1 Displacements, Strains, and Stresses.....	28
3.2 Stress-Strain Relationships.....	30
3.2.1 Generally Anisotropic Material.....	30
3.2.2 Transversely Isotropic Material.....	33
3.3 Macromechanical analysis of a unidirectional lamina.....	38

Chapter 4: Fatigue Damage Modeling for GRP and CFRP Composites

4.1. Failure Damage Mechanism in FRP composites.....	46
4.2 The Proposed Fatigue Damage Model in this Thesis.....	47
4.3 Fatigue Damage Analysis Procedures and Methodology.....	53

Chapter 5: Fatigue Damage Assessment Results of Unidirectional GRP and CFRP

5.1 GRP and CFRP Data.....	55
5.1.1 Hashin Data.....	55
5.1.2 Ellyin and El Kadi Data.....	56
5.1.3 Xiao and Bathias Data.....	56
5.1.3 Zheng Data.....	57
5.1.4 Kawai Data.....	57
5.2 Evaluation of Proposed Fatigue Damage Model.....	58

Chapter 6: Evaluation of Proposed Damage Model and Discussion.....69

6.1 Evaluation of Proposed Damage Assessment Model	70
6.2 Fatigue Damage Theories for Fibrous Composites.....	70
6.2.1 Kawai Damage Model.....	70
6.2.2 Ellyin and El Kadi Strain Energy Model.....	71
6.2.3 Plumtree and Cheng Energy-Based Model.....	72
6.3 Comparison of Results of Proposed Model with other Models.....	74

Chapter 7: Conclusion and Recommendation

7.1 Conclusion.....	87
7.2 Recommendation.....	88
References.....	89
Appendix A: Material Property and Data.....	A1
Appendix B: Programming Code.....	B1

LIST OF FIGURES

Figure 2.1 A simple unidirectional composite lamina under tensile load.....	12
Figure 2.2 Schematic illustrations of the stress/strain curves of composites with a ductile matrix and as derived from the stress/strain behavior of the constituents.....	13
Figure 2.3 Schematic illustration of the strength of a unidirectional composite with fiber content.....	14
Figure 2.4 Schematic representation of the development of damage during the fatigue life of composite materials.....	16
Figure 2.5 Variation of Tensile strength various off-axis angles for CFRP	17
Figure 2.6 Variation of Tensile strength various off-axis angles for GRP	18
Figure 2.7 Measured properties of glass fiber and polyester resin and GRP.	
(a) Polyester stress-strain curve.....	20
(b) Glass fiber stress-strain curve.....	20
(c) GRP stress-strain curve.....	21
Figure 2.8(a) Stress-Strain response for Graphite Epoxy tensile test.....	23
Figure 2.8(b) Stress-Strain response for Graphite Epoxy shear test.....	24
Figure 3.1 The global x, y, z and local 1, 2, 3 coordinate systems.....	29
Figure 3.2 The stresses in the global x, y, z and the local 1, 2, 3 coordinate system.....	29
Figure 3.3a Material with three planes of symmetry.....	35

Figure 3.3b Example of a fiber-reinforced, transversely isotropic composite.....	35
Figure 3.4 For an off-axis unidirectional specimen under uniaxial tension the on-axis stresses are found by transforming the off-axis stress from the off-axis to on axis directions.....	39
Figure 3.5 The elastic modulus response as off-axis angle changes for a typical unidirectional GRP.....	42
Figure 3.6 The shear modulus response as off-axis angle changes for a typical unidirectional GRP.....	43
Figure 3.7 The elastic modulus response as off-axis angle changes for a typical unidirectional GRP.....	44
Figure 3.8 The Shear modulus response as off-axis angle changes for a typical unidirectional CFRP.....	45
Figure 4.1 Three regions of cracking in unidirectional of composites :(I) Matrix Failure, (II) Matrix – fiber cracking, and (III) Fiber failure.....	47
Figure 4.2 Strain history, strain Mohr’s circle, and stress Mohr’s circle for uniaxial loading condition.....	49
Figure 4.3 Three regions of cracking mechanism in unidirectional composites.....	52
Figure 4.4 Procedure of fatigue damage analysis for unidirectional GRP and CFRP composites.....	54
Figure 5.1 Experimentally obtained fatigue lives of GRP composite of Ellyin at various off-axis angles and $R = 0$: (a) stress-fatigue life, and (b) proposed fatigue damage parameter versus life.....	59

Figure 5.2 Experimentally obtained fatigue lives of GRP composite of Ellyin at various off-axis angles and $R = 0.5$: (a) stress-fatigue life, and (b) proposed fatigue damage parameter versus life.....	60
Figure 5.3 Experimentally obtained fatigue lives of GRP composite of Ellyin at various off-axis angles and $R = -1$: (a) stress-fatigue life, and (b) proposed fatigue damage parameter versus life	61
Figure 5.4 Experimentally obtained fatigue lives of GRP composite of Hashin at various off-axis angles and $R = 0.1$: (a) stress-fatigue life, and (b) proposed fatigue damage parameter versus life.....	62
Figure 5.5 Experimentally obtained fatigue lives of GRP composite of Xiao at various off-axis angles and $R = -1$: (a) stress-fatigue life, and (b) proposed fatigue damage parameter versus life	63
Figure 5.6 Experimentally obtained fatigue lives of CFRP composite of Kawai at various off-axis angles and $R = 0.1$: (a) stress-fatigue life, and (b) proposed fatigue damage parameter versus life	64
Figure 5.7 Experimentally obtained fatigue lives of CFRP composite of Kawai at various off-axis angles and $R = 0.5$: (a) stress-fatigue life, and (b) proposed fatigue damage parameter versus life	65
Figure 5.8 Experimentally obtained fatigue lives of CFRP composite of Kawai at various off-axis angles and $R = -1$: (a) stress-fatigue life, and (b) proposed fatigue damage parameter versus life	66
Figure 5.9 Experimentally obtained fatigue lives of CFRP composite of Zheng at various off-axis angles and $R = 0.1$: (a) stress-fatigue life, and (b) proposed fatigue damage parameter versus life	67

Figure 6.1 The strain energy for different values of stress ratio. (a) $R=0$ (b) $R>0$	72
Figure 6.2 Deformations in fracture plane	74
Figure 6.3 Fatigue life correlation of unidirectional GRP composites at different off-axis angles and stress ratio of $R=0$ using (a) Ellyin-El Kadi, (b) Kawai model, (c) Plumtree-Cheng model, (d) the proposed model.	76
Figure 6.4 Fatigue life correlation of unidirectional GRP composites at different off-axis angles and stress ratio of $R=0.5$ using (a) Ellyin-El Kadi, (b) Kawai model, (c) Plumtree-Cheng model, (d) the proposed model.....	77
Fig 6.5 Fatigue life correlation of unidirectional GRP composites at different off-axis angles and stress ratio of $R=-1$ using (a) Ellyin-El Kadi, (b) Kawai model, (c) Plumtree-Cheng model, (d) the proposed model.	78
Fig 6.6 Fatigue life correlation of unidirectional GRP composites at different off-axis angles and stress ratio of $R=0.5$ using (a) Ellyin-El Kadi, (b) Kawai model, (c) Plumtree-Cheng model, (d) the proposed model.....	79
Fig 6.7 Fatigue life correlation of unidirectional GRP composites at different off-axis angles and stress ratio of $R=-1$ using (a) Ellyin-El Kadi, (b) Kawai model, (c) Plumtree-Cheng model, (d) the proposed model.....	80
Fig 6.8 Fatigue life correlation of unidirectional CFRP composites at different off-axis angles and stress ratio of $R=0.1$ using (a) Ellyin-El Kadi, (b) Kawai model, (c) Plumtree-Cheng model, (d) the proposed model.	81

Fig 6.9 Fatigue life correlation of unidirectional CFRP composites at different off-axis angles and stress ratio of $R= 0.5$ using (a) Ellyin-El Kadi, (b) Kawai model, (c) Plumtree-Cheng model, (d) the proposed model.....82

Fig 6.10 Fatigue life correlation of unidirectional CFRP composites at different off-axis angles and stress ratio of $R= -1$ using (a) Ellyin-El Kadi, (b) Kawai model, (c) Plumtree-Cheng model, (d) the proposed model.83

Fig 6.11 Fatigue life correlation of unidirectional CFRP composites at different off-axis angles and stress ratio of $R= 0.1$ using (a) Ellyin-El Kadi, (b) Kawai model, (c) Plumtree-Cheng model, (d) the proposed model.....84

LIST OF TABLES

Table 2.1 E glass fibers properties.....	19
Table 2.2 Typical properties of commercially produced Carbon Fibers	22
Table 2.3 Properties of a unidirectional composite containing 60% fiber by volume	22
Table 3.1: The elements of the compliance matrix in the x, y, z systems.....	32
Table 3.2 Element of the compliance matrix in terms of the engineering constants for monoclinic materials.....	36
Table 5.1 Table of evaluation of proposed model in life correlation of GRP and CFRP.....	67
Table 6.1 Summery of models and modes of failure:.....	84
Table 6.2 Table of evaluation of models in life correlation of GRP and CFRP.....	85

NOMENCLATURE

σ_A :	Stresses along the Fibers
σ_T :	Stresses along Transverse to the Fibers
σ_A^U :	Ultimate Tensile Stress
σ_T^u :	Ultimate Transverse Tensile Stress
τ^u :	Ultimate Shear Stress
ΔW^t :	Total Input Energy
N_f :	Cycles to Failure
κ, α :	Material Constants
σ_{ij}^m :	Average Stress in Matrix
σ_{ij}^f :	Average Stress in Fibers
X^f :	Fatigue Failure Function under Tensile Loading for Fiber
X^m :	Fatigue Failure Function under Tensile Loading for Matrix
S^m :	Fatigue Failure Function under Shear Loading for Matrix
σ_{22} :	Normal Stress Transverse to the Fiber
τ_{12} :	Shear Stress Along to the fiber
σ_{\max} :	Maximum Applied Stress
R :	Stress Ratio ($\frac{\sigma_{\min}}{\sigma_{\max}}$)
σ_{\min} :	Minimum Applied Stress
E :	Modulus of Elasticity
σ_a :	Applied Stress
$F(n_i)$:	Fatigue Modulus Loading Cycle n_i
$\epsilon(n_i)$:	Strain at Loading Cycle n_i
σ_B :	Ultimate Static Strength

ΔD_i :	The Amount of Damage Accumulation During Fatigue at Stresses Level r_i
Ψ :	The Fatigue Strength Ratio
N^* :	Ratio of Applied Cycles to the Fatigue Life N
$E(0)$:	Initial Modulus
E_f :	Failure Stiffness
$R(n)$:	Residual Stress at n Cycles
$(\sigma)_c$:	Stress Level at Composite
$(\sigma)_f$:	Stress in Fibers
$(\sigma)_m$:	Stress in Matrix
E_f :	Modulus of Elasticity of Fiber
E_m :	Modulus of Elasticity of Matrix
V_f :	Volume Fraction of Fiber
σ_{my} :	Yield strength of Matrix
σ_{fu} :	Ultimate Tensile Strength of Fiber
σ'_m :	Stress in the Matrix at the Fiber's Failure Strain
σ_{mu} :	Ultimate Strength of Matrix
\overline{C}_{ij} :	Elements of the Stiffness Matrix $[\overline{C}]$ in x, y, z Coordination System
\overline{S}_{ij} :	Elements of the Compliance Matrix $[\overline{S}]$ in x, y, z Coordination System
C_{ij} :	Elements of the Stiffness Matrix $[C]$ in the 1,2,3 Coordinate System
S_{ij} :	Elements of the Compliance Matrix $[S]$ in the 1, 2, 3 Coordinate System
$\Delta W_I, \Delta W_{II}, \Delta W_{III}$:	Three Regions of Progressive Fatigue Damage Energy Range
$\Delta \epsilon_n, \Delta(\frac{\gamma_{max}}{2})$:	Maximum Normal and Shear Strain Ranges on the Critical Plane
$\Delta \sigma_n, \Delta \tau_{max}$:	Maximum Normal and Shear Stress Ranges on the Critical Plane
$\epsilon_{11}, \epsilon_{22}, \epsilon_{33}$:	Principal Strains ($\epsilon_{11} > \epsilon_{22} > \epsilon_{33}$)
$\sigma_{11}, \sigma_{22}, \sigma_{33}$:	Principal Stresses ($\sigma_{11} > \sigma_{22} > \sigma_{33}$)
$(\tau_{ULT})_m$:	Ultimate Shear Stress of Matrix
$(\sigma_{UTL})_F$:	Ultimate Tensile Stress of Fibers
G_m :	Shear Modulus of Matrix

E_f :	Elastic Modulus of Fiber
$\Delta\gamma_{12}$:	Shear Strain Range in the Fiber-Matrix Interface
$\Delta\tau_{12}$:	Shear Range in the Fiber-Matrix Interface
θ :	Off-Axis Angles
GRP:	Glass-Fiber Reinforced Polymer
CFRP:	Carbon-Fiber Reinforced Polymer
CSM:	Chop Strand Mat Fibrous Composites
WR:	Woven Roving Fibrous Composites
UD:	Unidirectional Fibrous Composites
FRP:	Fiber Reinforced Plastics
SWT:	Smith-Watson-Topper

OBJECTIVE AND SCOPE OF PRESENT STUDY

The present study was intended to develop a fatigue damage model for unidirectional GRP and CFRP composite materials. To predict the fatigue behavior of plies with arbitrary off-axis angles, an appropriate damage mechanism is required. In this study the progressive nature of damage accumulation based on the physics of cracking in constituents of unidirectional GRP and CFRP composite materials was modeled. The proposed damage analysis has taken into account the three regions of the damage development based on the physics and mechanism of cracking in the matrix, the matrix-fiber interface, and the fiber. This model has characterized the damage progress in regions I and II and III based on strain energy criterion developed earlier by Varvani-Farahani [40] and a criterion by Plumtree-Cheng [7].

The proposed fatigue damage parameter successfully correlated the fatigue data of unidirectional GRP and CFRP composites at different off-axis angles θ and stress ratios R .

The result of damage assessment showed that the proposed damage model correlated fatigue data with a greater success as compared with fatigue damage models developed by Kawai, Ellyn-El Kadi, and Plumtree- cheng [14, 6, 7].

PREFACE OF THESIS

The following provides a brief description of material covered in chapters of this thesis.

Chapter 1 covers a review of the major fatigue models and life time prediction methodologies for fiber-reinforced polymer composites in recent years. In this chapter the fatigue models were introduced in three categories of fatigue life model, phenomenological models, and progressive damage models.

Chapter 2 addresses the GRP and CFRP characteristics and shows how the mechanical properties of these materials are influenced by matrix, fiber, volume fraction and orientation of the fiber. This chapter reviews the practical application of GRP and CFRP in industrial fields. These applications aim to show how fatigue damage assessment is important in engineering design.

The stress and strain relationship and constitutive models for FRP composites have been reviewed in chapter 3.

Chapter 4 discusses all the requirements for fatigue damage assessment of GRP and CFRP unidirectional composites by the proposed model in this thesis. This chapter develops a fatigue damage criterion based on the physics and mechanism of cracking in three regions of the matrix, the fiber, and the fiber-matrix interface and represents the procedures of fatigue damage analysis in a stepwise algorithm.

Chapter 5 discusses the results of fatigue damage assessment using the proposed fatigue damage model in this thesis. The available experimental data from various laboratories were used to evaluate the capability of the proposed model. The results of damage assessment by the proposed model have been compared with stress-life data extracted from the literature and verified how

· closely the proposed model unifies the fatigue data in unidirectional GRP and CFRP composites over various off-axis and R-ratios.

Chapter 6 evaluates the proposed model and compares the capability of the proposed model in correlating fatigue data in unidirectional GRP and CFRP composites. This chapter shows how superior the proposed damage model is over other models in evaluating unidirectional GRP and CFRP composites.

Chapter 7 summarizes the conclusion obtained in this study. It gives the key points related to the fatigue damage assessment of unidirectional GRP and CFRP composites. It also includes a recommendation for researchers who are interested to carry out further studies on the topic.

CHAPTER ONE

Introduction and Background in Fatigue of FRP Composite Materials

1.1 Introduction

In recent years, the use of fiber-reinforced plastics (FRPs) in aerospace, automotive, marine, and civil infrastructure applications has been constantly increasing. In such applications, structures are constantly subjected to repetitive loadings, prompting questions about fatigue of the FRP materials. Proper prediction of life of those applications is a very important problem and any underestimation can cause catastrophic failure. Improved damage accumulation models and life time prediction methodologies may result in a more efficient and safer use of these materials.

1.2 General Considerations on Fatigue Damage Modeling for FRPs

In general, fatigue of fiber-reinforced composite materials is a quite complex phenomenon, and a large research effort is being spent on it today. Fiber-reinforced composites have a rather good rating as regards to life time in fatigue. Composite materials are inhomogeneous and anisotropic, and their behavior is more complicated than that of homogeneous and isotropic materials such as metals. The main reasons for this are the different types of damage that can occur. Cracking in FRP composites are in the forms of fiber fracture, matrix cracking, matrix crazing, fiber buckling, fiber-matrix interface failure, delaminations, and their interactions at different growth rates.

As a consequence the microstructural mechanisms of damage accumulation, damage mechanism occurs sometimes independently and sometimes interactively, and the predominance of one can strongly affect the durability of FRP composites. There are a number of differences between the fatigue behavior of metals and FRP composites. In metals, no significant reduction of stiffness is observed during the fatigue process. The final stage of the process starts with the formation of small cracks, which are the only form of

microscopically observable damage. Gradual growth and coalescence of microcracks quickly produce a large crack and final failure of the structural component. As the stiffness of a metal remains quasi unaffected, the linear relation between stress and strain remains valid, and the fatigue process can be simulated by a linear elastic analysis and linear fracture mechanics.

In a FRP composite fatigue damage starts very early and the extent of the damage zones grows steadily. As the number of cycle progresses, the damage type in these zones changes. For example, small matrix cracks generated early stage of life of FRP component leads to large size delaminations at higher fatigue cycles. The gradual deterioration of a FRP composite, with a loss of stiffness in the damaged zones, leads to a continuous redistribution of stress and a reduction of stress concentrations inside a structural component. As a consequence, the failure damage assessment in FRP composites requires the simulation of the complete path of successive damage states [1].

1.3 Review of Fatigue Models

This review aims to outline the most important fatigue models and life time prediction methodologies developed up to date for damage assessment of FRP composites. According to Sendekyj [2], fatigue criteria can be classified in four major categories: the macroscopic strength fatigue criteria, criteria based on residual strength and those based on residual stiffness, and finally the criteria based on the actual damage mechanisms. The existing fatigue models for composite laminates consist of three major categories: (i) fatigue life models, (ii) phenomenological models for residual stiffness/strength; and (iii) progressive damage models.

1.4 Fatigue Life Models

1.4.1 Stress-Based Models

Although the fatigue behavior of FRP composites is fundamentally different from the behavior exposed by metals, many models have been established which are based on the well-known S-N curves. These models make up the first class of so-called 'fatigue life models'. This approach requires extensive experimental work and does not take into account the actual damage mechanisms, such as matrix cracks and fiber fracture.

One of the first fatigue failure criteria was proposed by Hashin and Rotem [3]. A simple fatigue failure criterion for unidirectional fiber reinforced laminate under oscillatory states of combined plane stress has been established. Since the ultimate strengths are function of fatigue stress

level, stress ratio and the number of cycles, the criterion is expressed in terms of three S-N curves which are easily obtained from fatigue testing of off-axis unidirectional specimens under uniaxial oscillatory load. Hashin and Rotem [3] expressed Eq 1.1 for fiber-failure and matrix-failure mode, respectively as:

$$\sigma_A = \sigma_A^u$$

$$\left(\frac{\sigma_T}{\sigma_T^u} \right)^2 + \left(\frac{\tau}{\tau^u} \right)^2 = 1 \quad (1.1)$$

where σ_A and σ_T are the stresses along the fibers and transverse to the fibers, τ is the shear stress and σ_A^u , σ_T^u and τ^u are the ultimate tensile, transverse tensile and shear stresses, respectively. The fiber failure mode corresponds to a progressive failure of fibers and the matrix failure mode occurs when a crack runs parallel to the fibers through the matrix.

Reifsnider and Gao [4] established a fatigue failure criterion, based upon an average stress formulation of composite materials derived from the Mori-Tanaka method (a method to calculate the average stress fields in composites). The criterion is at the micromechanics level and takes into account the properties of the constituents and the interfacial bond. Although very similar to the fatigue failure criteria proposed by Hashin and Rotem [3], the failure criteria for matrix-dominated and fiber-dominated failure are expressed in terms of the average stresses (σ_{ij}^m) and (σ_{ij}^f) in the matrix and fibers, respectively. These average stresses are calculated by applying the Mori-Tanaka method, while taking into account the problem of non-perfectly bonded interfaces between fibers and matrix by modeling the interface as a thin layer with spring-like behavior. These failure functions for the two failure mechanisms are given by Eq1.2:

$$(\sigma_{11}^f) = X^f$$

$$\left(\frac{\sigma_{22}^m}{X^m} \right) + \left(\frac{\sigma_{12}^m}{S^m} \right) = 1 \quad (1.2)$$

where X^f and X^m are fatigue failure functions under tensile loading for fiber and pure matrix materials respectively, In equation 1.2 the fatigue failure function of the pure matrix under shear loading is

defined by S^m . These failure functions depend on the stress ratio R , the number of cycles N and the frequency f .

Epaarachchi and Clausen [5] proposed an empirical fatigue law to predict the fatigue life of glass fiber-reinforced plastic composites as:

$$\frac{d\sigma}{dt} = -a\sigma_{\max} (1-R)^{\gamma} t^{-k} \quad (1.3)$$

where a and k are constants, exponent γ is derived from crack growth propagation rate, σ_{\max} is the applied stress level, R is the stress ratio and t is a measure of time. Equation (1.3) is rewritten as:

$$\left(\frac{\sigma_{ult}}{\sigma_{\max}} - 1 \right) \frac{1}{(R-1)^{\gamma}} f^{\beta} = \alpha (N^{\beta} - 1) \quad (1.4)$$

where N is the number of cycles to failure, f is the loading frequency and, α and β are material constants.

1.4.2 Energy-Based Models

Ellyin and El-Kadi [6] established that the strain energy density can be used in a fatigue failure criterion for fiber-reinforced materials. The fatigue life N_f was related to the total energy input ΔW^t through a power law type relation of the form of Eq 1.5:

$$\Delta W^t = \kappa N_f^{\alpha} \quad (1.5)$$

where κ and α were shown to be functions of the fiber off-axis angle. In comparison with experimental data from tests on GRP composites, the expression for α and κ as a function of the fiber off-axis angle were established. The strain energy density was calculated under an elastic plane stress hypothesis.

Plumtree and Cheng [7] indicated that for multiaxial fatigue of metals, the Smith-Watson-Topper (SWT) parameter appeared to be a valid fatigue parameter. This parameter has the same dimensions as the strain energy density and is defined as the maximum stress times the tensile strain

range. Plumtree and Cheng proposed an energy-based fatigue damage model for unidirectional FRP composite as:

$$\Delta W^* = \sigma_{22}^{\max} \Delta \varepsilon_{22} + \tau_{12}^{\max} \gamma_{12} / 2 \quad (1.6)$$

The fatigue parameter ΔW^* accounts for the crack opening modes in off-axis loading. Subscripts “11” and “22” represent two directions of parallel and normal to the fiber direction.

1.5 Phenomenological Models to Predict Residual Stiffness/Strength

Phenomenological models propose are developed based on gradual deterioration of the stiffness or strength of the composite specimens.

1.5.1 Residual Stiffness Models

Residual stiffness models account for the degradation of the elastic properties during fatigue. Stiffness can be measured frequently during fatigue experiments, and can be measured without further degrading the material (Highsmith and Reifsnider [8]). To describe stiffness loss, the variable D is often used, which in the one-dimensional case is defined by:

$$D = 1 - \frac{E}{E_0} \quad (1.7)$$

where E_0 is the initial modulus of elasticity prior to the materials degradation and E corresponds to the instantaneous modulus of materials during damage evolution.

Hwang and Han [9-10] introduced the concept of the 'fatigue modulus', which is defined as the slope of applied stress and resultant strain at a specific cycle. The fatigue modulus degradation rate is assumed to follow a power function of the number of fatigue cycles expressed as:

$$\frac{dF}{dn} = -A n^{C-1} \quad (1.8)$$

where A and c are material constants. Further it was assumed that applied stress σ_a varies linearly with the resultant strain in any arbitrary loading cycle, so that this variation is given by:

$$\sigma_a = F(n_i)\varepsilon(n_i) \quad (1.9)$$

where $F(n_i)$ and $\varepsilon(n_i)$ are the fatigue modulus and corresponding strain at loading cycle n_i , respectively. After integration and introducing the strain failure criterion, the fatigue life N is calculated using:

$$N = [B(1-r)]^{1/c} \quad (1.10)$$

In Eq (1.10), the ratio of the applied cyclic stress to the ultimate static stress is denoted by $r = \frac{\sigma_a}{\sigma_u}$,

and B and c are material constants.

Hwang and Han [9] proposed three cumulative damage models based on the fatigue modulus $F(n)$ and the resultant strain. The presented model shows good agreement with experimental data. It can be proposed as:

$$D = \frac{r}{1-r} \left[\frac{F_0}{F(n)} - 1 \right] \quad (1.11)$$

where damage D is given by:

$$D = \sum_{i=1}^m \Delta D_i = 1 \quad (1.12)$$

In Eq (1.12), ΔD_i is the amount of damage accumulation during fatigue at any stress level σ_i and m is the number of load sequences until final failure.

The cumulative damage models proposed by Hwang and Han have been used by Kam *et al.* [11, 12] to study the fatigue reliability of graphite/epoxy composite laminates under uniaxial loading conditions.

Sidoroff and Subagio [13] proposed a fatigue damage growth model as expressed by equation (1.13):

$$\frac{dD}{dN} = \begin{cases} \frac{A(\Delta\epsilon)^c}{(1-D)^b} & \text{(a)} \\ 0 & \text{(b)} \end{cases} \quad (1.13)$$

Equation (1.13 a) is applied for tensile and equation (1.13 b) is used for compressive loading. In this equation, A, b and c are three material constants and are obtained experimentally. This model has successfully evaluated the damage growth rate of unidirectional GRP composites fatigue tested by a three-point bending set up.

Kawai [14] developed a phenomenological fatigue model for the off-axis fatigue behavior of a class of unidirectional matrix composites subjected to constant-amplitude stress cycling with non-negative mean stresses. In this model, the maximum fatigue stress σ_{\max} is normalized by the static strength σ_B in the loading direction. This non-dimensional fatigue damage parameter is expressed by:

$$\Psi = \frac{\sigma_{\max}}{\sigma_B} \quad (1.14)$$

In Eq1.14, the fatigue strength ratio Ψ corresponds to a quantitative measure of tendency of composite material to static failure.

1.5.2 Residual Strength Models

The other approach is based on the composite's strength. In many applications of composite materials it is important to know the residual strength of the composite structure and as a consequence the remaining life time during which the structure can bear the applied load. From their early use, strength-based models have generally been inherently statistical. Most commonly, two-parameter Weibull functions are used to describe the residual strength and probability of failure for a set of laminates after an arbitrary number of cycles.

Residual strength models can be categorized into types: (i) the sudden death model and (ii) the wear out model. At low-cycle fatigue regime, where composite specimens are subjected to a high stresses, the residual strength is initially nearly constant and it decreases drastically when the number of cycles to failure is being reached. The sudden death model [15-16] is a suitable technique to describe this behavior and is especially used for high-strength unidirectional composites. However, at high cycle fatigue regime the residual strength of the laminate degrades gradually at the number of cycles increases. This behavior is described by degradation models which are often referred to as wear out models. These models generally incorporate the 'strength-life equal rank assumption' which states that the strongest specimen has either the longest fatigue life or the highest residual strength at run out. This assumption has been experimentally proved by Hahn and Kim [17]. In the wear out model [18], it is assumed that the residual strength $R(n)$ is monotonically decreasing as a function of the number of cycles n , and that the change of the residual strength can be approximated by a power-law growth equation:

$$\frac{dR(n)}{dn} = \frac{-A(\sigma)}{m[R(n)]^{m-1}} \quad (1.15)$$

where $A(\sigma)$ is a function of the maximum cyclic stress and m is a material constant.

Caprino and D'Amore [19] developed a fatigue damage parameter based on decay of the residual strength as the number of cycles progressed:

$$\frac{d\sigma_n}{dn} = -a_0 \Delta\sigma \cdot n^{-b} \quad (1.16)$$

In this equation, σ_n is the residual strength after n cycles, $\Delta\sigma = \sigma_{\max} - \sigma_{\min}$ is the applied stress range, R is the stress ratio and a_0 and b are material constants. Caprino and D'Amore stressed the fact that a reliable model should reflect both the influence of the stress ratio R and the fatigue response of composites at low- and high-cycle fatigue regimes. In another study, Caprino and Giorleo [20] have evaluated the fatigue results of glass-fabric/epoxy composites tested under bending loading and reported the capability of their model in damage assessment of GRP composites.

1.6 Progressive Damage Models

Progressive damage models have been developed based on the physics of materials damage leading to degradation of the mechanical properties. These models have been subdivided into two categories: (i) the damage models which predict the damage progress in the form of matrix transverse cracks per unit length and (ii) the models which correlate the damage progress with the residual mechanical properties [1].

1.6.1 Progressive Damage Models Predicting Damage Growth

Owen and Bishop [21] were among the first researchers to investigate a wide range of GRP composites. They investigated the initiation of damage at central holes in the specimens under static and fatigue loading. Because the measurement of the crack lengths was experimentally difficult to do, Owen and Bishop related crack length to the specimen compliance. They concluded that the Paris equation is applicable to evaluate the fatigue crack growth rate in GRP composite tests they conducted.

Feng *et al* [22] developed a model to predict fatigue damage growth in CFRP composite specimens. They performed fatigue tests on CFRP composite components and evaluated the crack growth in on theses components using a modified Paris-type equation:

$$\frac{dA}{dN} = DG_{\max}^n \quad (1.17)$$

In this equation A is the damage area due to matrix cracking, N is the number of fatigue cycles, G_{\max} is the maximum strain-energy release rate in a fatigue cycle, and coefficient D and exponent n are material constants.

1.6.2 Progressive Damage Models Predicting Residual Mechanical Properties

The progressive damage models relate the damage variables with the residual mechanical properties such as stiffness and strength of the composite laminate. The damage growth rate equations are often based on damage mechanics, thermodynamics, micromechanical failure criteria and other specific damage characteristics such as crack spacing, and delamination area. One of the first methods to calculate stiffness reduction due to matrix cracking is the shear-lag model, established by Highsmith and Reifsnider [8]. Through careful assessment of edge replicas of crack patterns in composite specimens, Highsmith and

Reifsnider observed that the shear cracks in any given ply were restricted to the interfaces of that ply with adjacent plies. Further, this region tended to be resin-rich, and thus was less stiff in response to shear than the central portion of the lamina. Transverse cracks advanced the interface region, but usually did not extend into it.

1.7 The Objective of This Study

A comprehensive literature review on fatigue damage assessment of FRP composites has motivated the present investigation. The literature lacks a universal damage model to enjoy assessing the damage and cracking mechanisms within phases and constituents of FRP composites and adhering damage analysis methodology with the fundamentals of continuum mechanics.

The present study has attempted to address the damage accumulation over fatigue cycles by means of the strain energy density concept and includes damage and cracking mechanisms within the matrix, the fiber-matrix and the fibers consistent with a simple damage map which is supported by numerous evidences in the literature. The thesis has addressed the fatigue damage analysis of unidirectional GRP and CFRP composites.

In damage map, for the Regions I and III, the fracture criteria are expressed respectively based on the maximum shear and the maximum normal principal stress. Fatigue damage within these two regions was characterized by Varvani's fatigue damage parameter [40]. For the Region II, the damage criterion is developed based on the Plumtree-Cheng parameter [7]. In this Region, the normal and shear stress and strain components are calculated from transformation of applied stress/strain loads to the directions normal to and along the unidirectional fibers, respectively.

CHAPTER TWO

Materials Behaviour and Industrial Applications of Unidirectional GRP and CFRP Composites

2.1 The Nature of FRP Composites

A range of different GRP and CFRP materials is now available depending on the choice of matrix materials and the method of glass or carbon reinforcement. There are three main types: (i) chopped strand mat (CSM), which consists of chopped fibres held randomly oriented in a mat by chemical binder, (ii) woven roving (WR), which is a coarse fabric and (iii) unidirectional aligned (UD) long fibres held together by a thin weft or by chemical binder.

GRP and CFRP composites have taken their place as materials in a wide range of industries, including marine and land transport, aerospace, building and process plant. The general characteristics of these composites include corrosion and wear resistance, high strength/weight ratio, convenient maintenance, better manufacturability, and higher thermal and electrical insulations.

Although it is frequently a combination of non-mechanical properties which leads to initial selection of these materials, the success of an application depends largely on the mechanical properties of materials. Compared with a traditional structural material such as mild steel, a GRP laminate has a strength/weight ratio typically 2 to 5 higher, but a stiffness/weight ratio a factor 2 or 3 lower. In common with most engineering materials, reinforced plastics are subject to fatigue under long term repeated loads and like metals, they may creep under sustained load and ambient temperature. Therefore, there is an urgent need for the establishment of a safe-life design procedure for engineering structures and components made of FRP composite materials [23].

2.2 Unidirectional Continuous-Fiber Composites

Consider a simple unidirectional composite lamina reinforced with continuous fibers which are initially well-bonded to the matrix so that, under load, fibers and matrix deform together, as shown in figure 2.1. The applied load is transferred to the matrix and fibers, and the stress on the composite, $(\sigma)_c$, can be expressed by the rule of mixtures:

$$(\sigma)_c = (\sigma)_f V_f + (\sigma)_m (1 - V_f). \quad (2.1)$$

where $(\sigma)_f$ and $(\sigma)_m$ are the stresses in fibers and matrix, respectively. In Eq (2.1), V_f corresponds to the volume fraction of fibers. In most practical composites, the high-performance reinforcing fibers are regarded as being brittle, *i.e.*, they deform elastically to failure, showing little or no non-linear deformation. In metal- and polymer-matrix composites, the matrix is usually capable of some irreversible plastic deformation and in such materials the matrix failure strain is usually much greater than that of the fibers.

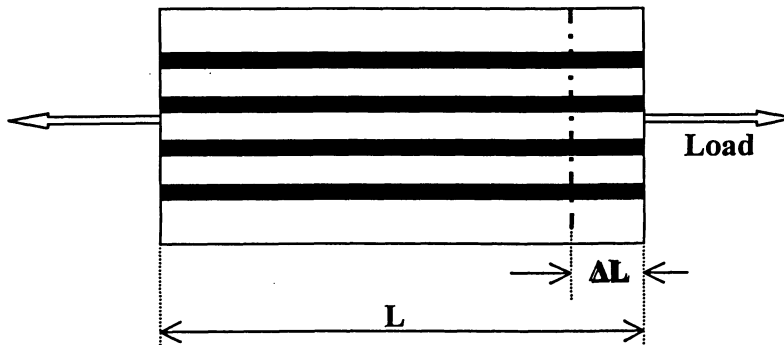


Figure 2.1: A simple unidirectional composite lamina under tensile load [24].

As Figure 2.2 shows, when the stress in the ductile matrix reaches the matrix yield stress, σ_{my} , the matrix continues to bear load, although the slope of the stress/strain curve falls somewhat. If the fibers are carrying most of the load, when the stress on the fibers reaches σ_{fu} (the fibre tensile strength), failure will occur and the stress on the composite at this point, $(\sigma)_c$, defines the composite strength:

$$\sigma_c = \sigma_{fu} V_f + \sigma'_m (1 - V_f) \quad (2.2)$$

where σ'_m is the stress in the matrix at the fiber failure strain.

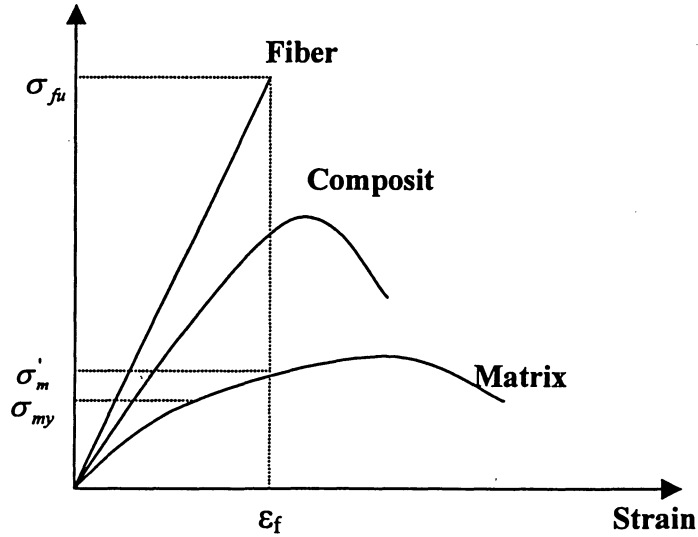


Figure 2.2: Schematic illustrations of the stress/strain curves of a composite and its fiber and matrix phases.

Considering now the brittle-ductile system shown in Figure 2.3, equation 2.2 can be represented on a diagram showing composite strength as a function of fiber content, V_f . When there are very few fibers present (i.e, for $V_f < V_{\min}$), the stress on the composite may be high enough to break the fibers [24].

But even if the fibers rupture and cease to carry load, because of its work-hardening ability, the matrix is still able to support the load on the composite until its tensile strength, σ_{mu} , is reached. Figure 2.3 shows the variation of composite strength with fiber volume fraction.

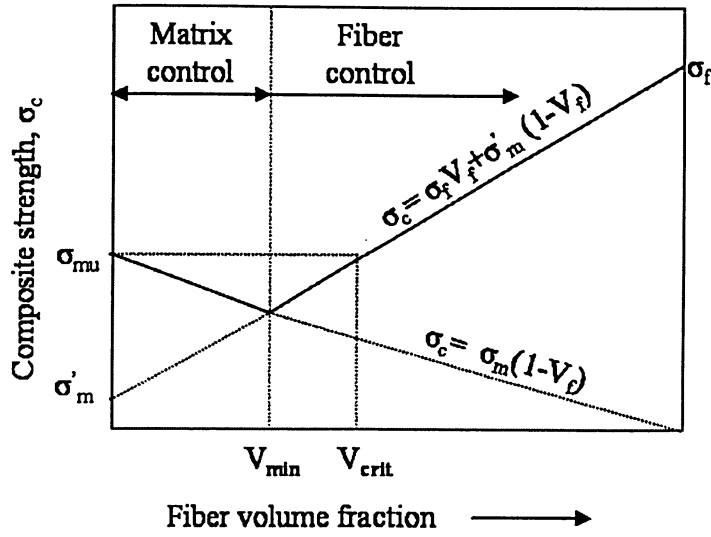


Figure 2.3: Schematic illustration of the strength of a unidirectional composite with fiber content [24].

In Figure 2.3 the matrix exerts control of failure behavior when V_f is less than V_{min} . Thus, there are sufficient fibres to bear some of the load when the matrix reaches its failure stress, and the rule-of-mixtures relationship defined by equation 2.2 then begins to operate. As the volume fraction of fibers exceeds V_{min} , the strength of the composite reduces following Eq 2.3:

$$\sigma_m = \sigma_{mu}(1 - V_f) \quad (2.3)$$

An increase in strength beyond the matrix tensile strength only occurs above the critical V_f level, V_{crit} :

$$V_{crit} = \frac{\sigma_{mu} - \sigma'_m}{\sigma_f - \sigma'_m} \quad (2.4)$$

In composites, when the ultimate strength of fiber and matrix are approximately equal ($\sigma_{fu} \approx \sigma_{mu}$), the critical volume fraction of the fiber, V_{crit} , is very low and of the order of only 0.01, then $\sigma_{mu} \cong \sigma'_m$.

2.2.1 Progressive Damage and Failure in Unidirectional Composites

Fatigue loading of composite laminates consists of the application of loads or strains that vary with time, usually in a cycle. By definition, the loads or strains reach amplitudes which are less than the values required to fracture the laminates in monotonic loading tests. If eventual failure due to cyclic loading occurs, then damage must have developed in the laminate during the fatigue damage progress. The damage process in composite laminates consists of the initiation and growth of several different damage modes and complex interactions between damage modes. The number of unique damage and the interactions between damage modes and subsequent effects on fatigue behavior are dependent on material, load, geometry, and environment. The progressive development of damage during fatigue life can be overviewed with the aid of figure 2.4, which traces the damage process as a function of percentage of life of composite laminates which contain 0° plies and off-axis plies subjected to cyclic tension-compression loading. Under such conditions, there is some combination of damage modes to occur as illustrated schematically in Figure 2.4.

Cracks initially initiate within the matrix and upon cyclic loading. These cracks are the source of subsequent damage development and form the interfacial debonding and delaminations in stage 2 and 3. In the Stages 2 and 3 cracks develop in directions parallel to fibers in continuous-fiber-reinforced materials. In duration between stages 1-4, a fiber bundle embedded in a matrix does not behave like a free fiber bundle. When the local load level reaches the failure stress at a weak point in a given fiber it breaks and the carried load is transferred back into the neighboring matrix regions. But away from the broken ends the fiber carries its full share of the load, by contrast with what happens in an unbounded bundle. The stress carried by neighboring fibers in the vicinity of the break will be disturbed, but the stress concentration may not be great enough to break a neighboring fiber (or fibers). As the load on the composite increases, more fibers will fail, but without seriously damaging the overall load-bearing ability of the composite. This is mainly due to the fact that the tensile load supported by the broken fiber within a short distance, will rapidly build up again to its original level.

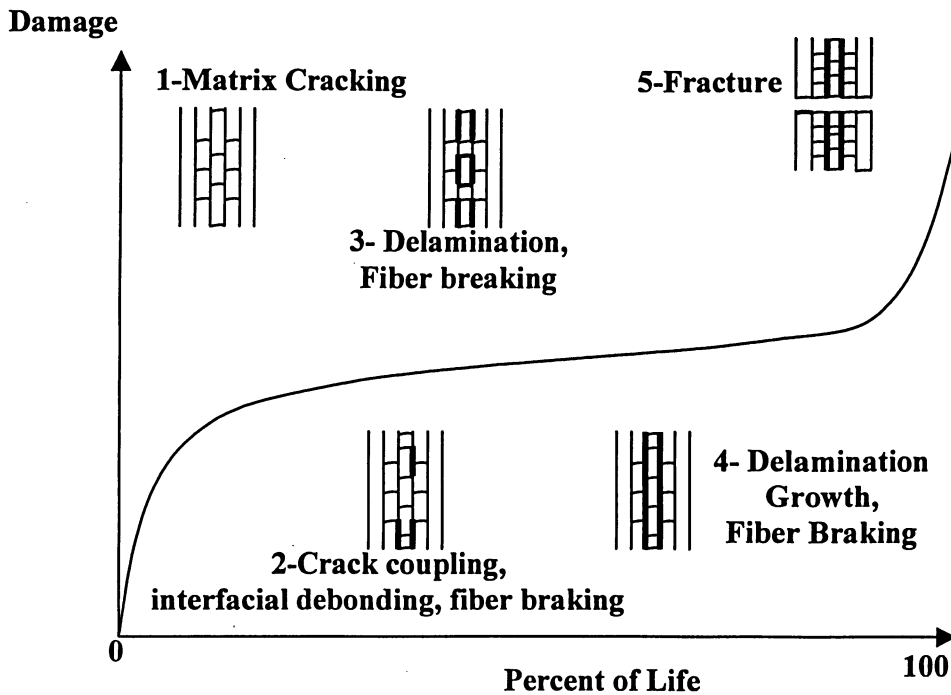


Figure 2.4: Schematic representation of the development of damage during the fatigue life of composite materials [25].

If the process is repeated a number of times, the cross section where the breaks are occurring will rapidly become too weak to support the applied load and catastrophic brittle failure will follow in stage 5. Fiber breaks accumulate randomly throughout the whole sample or structure. The final failure may then occur when the number of breaks in any one cross section has effectively reduced the local V_f below that required to support the applied load [25].

2.2.2 Transverse Strength

The strengths of unidirectional composites are highly anisotropic. Perpendicular to the reinforcing fibers most composites are weak and failure is controlled by rupture or plastic flow of the matrix, or by fiber/matrix separation. The damage mechanism in FRP composites will depend on the capacity of the matrix for plastic deformation and the strength of the fiber/matrix bond. If the matrix is a metal or polymer, its intrinsic yield strength will govern the transverse behavior of a composite containing only a few fibers. Such low levels of transverse strength mean that

unidirectional FRP composites are incapable of bearing transverse loads, and cross-ply laminates may even develop cracks during processing as a result of thermal stresses. Strain concentrations in the matrix may also lead to brittle failure at low strains, even in composites with otherwise ductile matrix materials. While this transverse cracking may not weaken the load-bearing ability of the composite materials in a major fiber direction [24].

2.2.3 Orientation-Dependence of Composite Strength

The strength of FRP composites is highly dependent on the damage mechanisms leading to failure. Figure 2.5 and 2.6 show that the tensile strength is maximum for 0° unidirectional CFRP and GRP composites, respectively, and drops rapidly as the off-axis angle increases to 90° . Figures 2.5 and 2.6 also show that FRP composites with low off-axis angles, fail dominantly due to fiber failure while, at higher off-axis angles, failure of the composite is mainly due to matrix cracking.

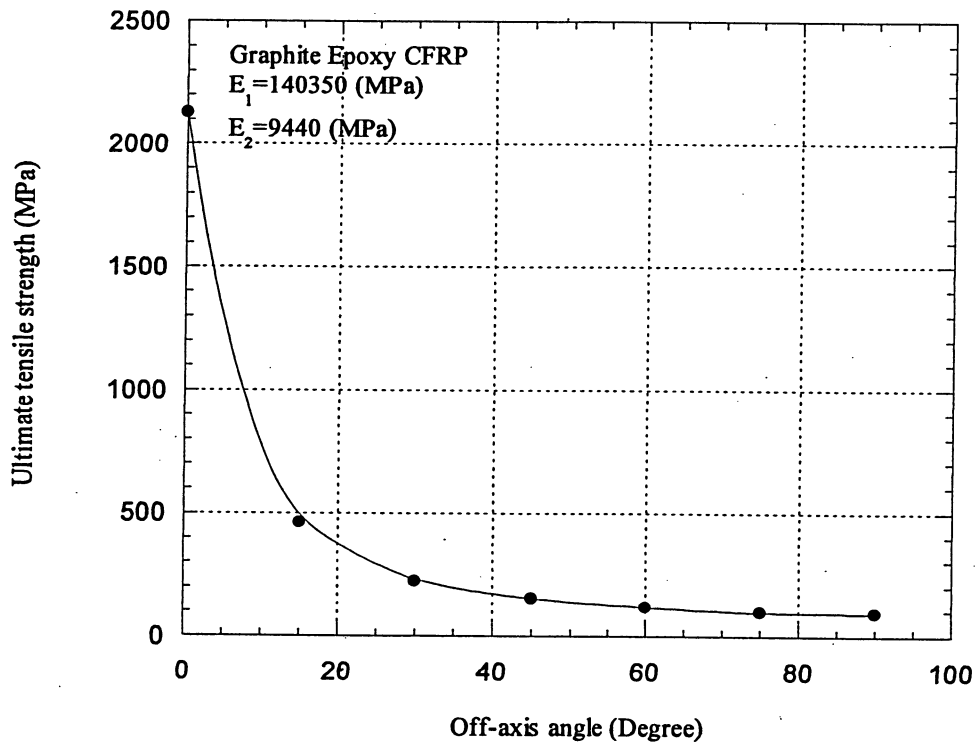


Figure 2.5: Variation of Tensile strength versus off-axis angles for CFRP [26]

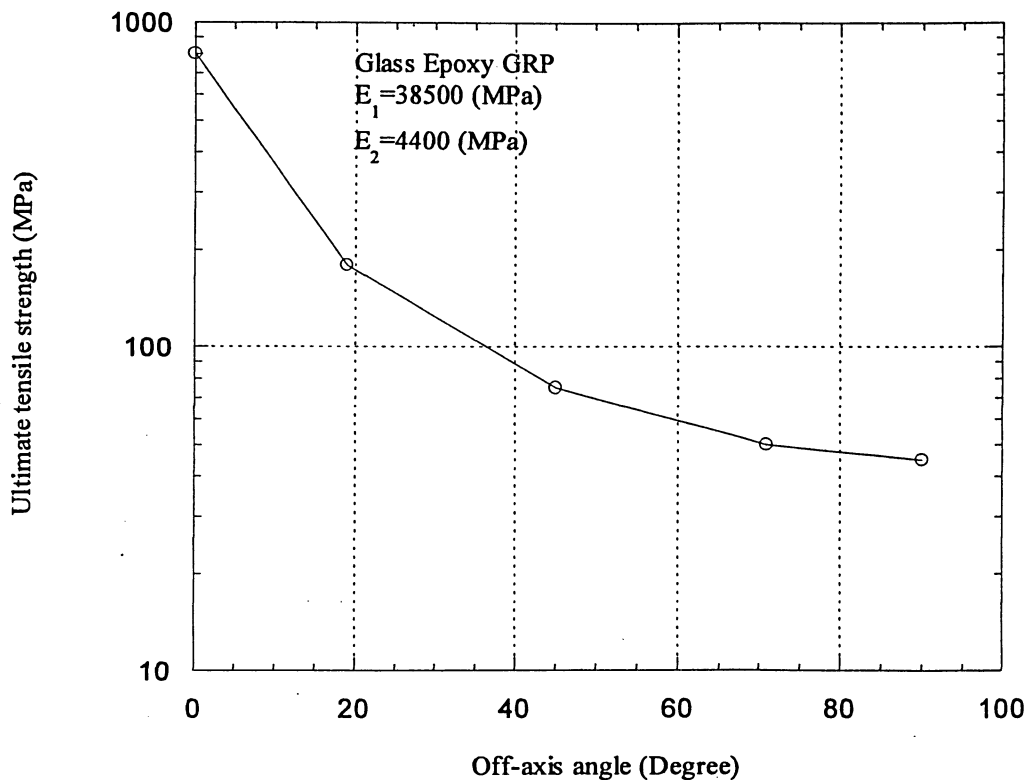


Figure 2.6 Variation of Tensile strength versus off-axis angles for GRP [6].

2.2.4 Effect of Polyester Resin Properties

Laminates fabricated from general purpose polyester resins from a variety of sources seem to suffer very similar damage. It has been suggested that damage could be partially or completely eliminated by using a more flexible or tougher resin, i.e., one with greater strain to failure [21]. Polyester resins are formulated to provide greater strain against failure having a lower initial modulus, non linear stress-strain curves, and sufficient toughness as a function of the area under the stress-strain curve.

2.3 Glass Fiber-Reinforced Polymers

Glass fibres or filaments of 8-15 μm in diameter are produced by drawing molten glass through a suitable orifice [23]. Most fibres for plastics reinforcement are made of a special low alkaline glass (alkali content of less than 1%, termed E glass), which draws well and has good strength,

stiffness, and electrical and weathering properties. Of many other types of glass fibres which are available, the main ones are: A glass, which has an alkali content of 10-15 %, is inferior to E glass, but cheaper; S glass, which is stronger and more temperature resistant than E glass, but more expensive. In this thesis, GRP composites with E glass fibres which are widely used as reinforcing fibers in polymeric matrix, have been studied. Some typical properties of E glass fibres are given in table 2.1.

Table 2.1: E-glass fibers properties [23]

Properties	Value	Properties	Value
Specific weight	2.56 g/cm ³	Coefficient of thermal expansion	$4.7 \times 10^{-6} / ^\circ \text{C}$
Tensile strength	1.4- 3.5 GN/ m ²	Dielectric constant at 1 MHZ	6.4
Extension at break	2.5 %	Thermal conductivity	1.04 w/m° k
Young's modulus	65-75 GN/ m ²	Sound velocity	5680 m/s
Poisson ratio	0.2	Hardness (Vickers 50g-15s)	5.6

The tensile test on polyester resin, glass fiber and GRP composite are presented in Figures 2.3 a, b, and c, respectively. The stress-strain curves presented in these figures show that the glass fiber is a brittle material and has linear behavior until final failure but the polyester resin is ductile and has a nonlinear stress-strain curve.

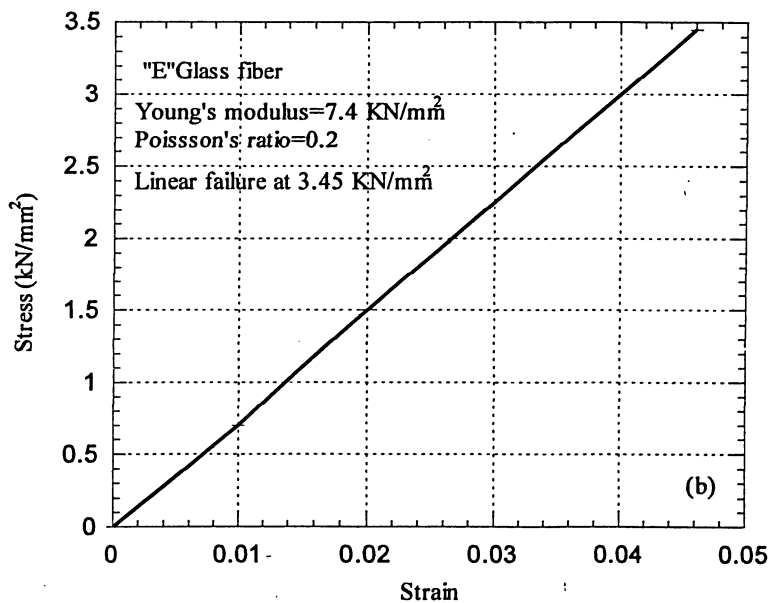
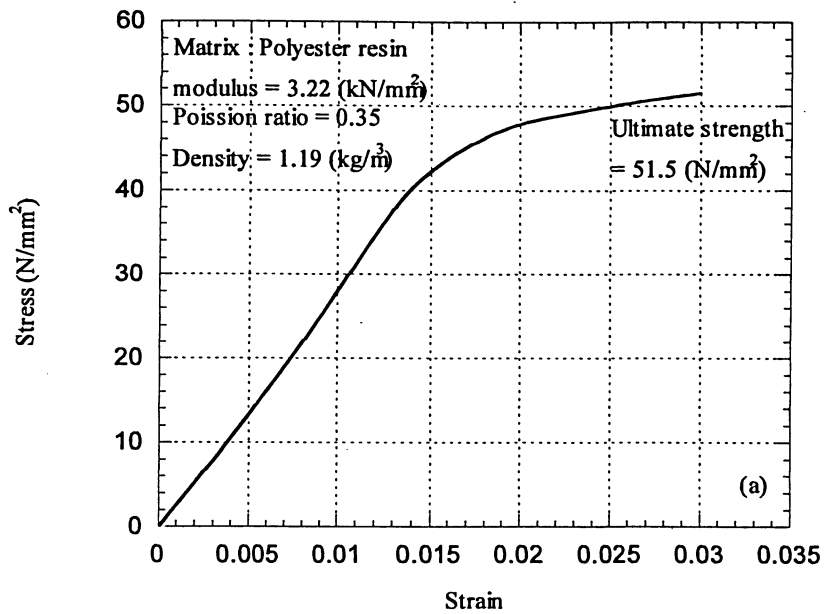


Figure 2.7: Stress-strain curves of glass fiber and polyester resin and GRP [27].

(a) Matrix: Polyester, (b) Fiber: Glass fiber.

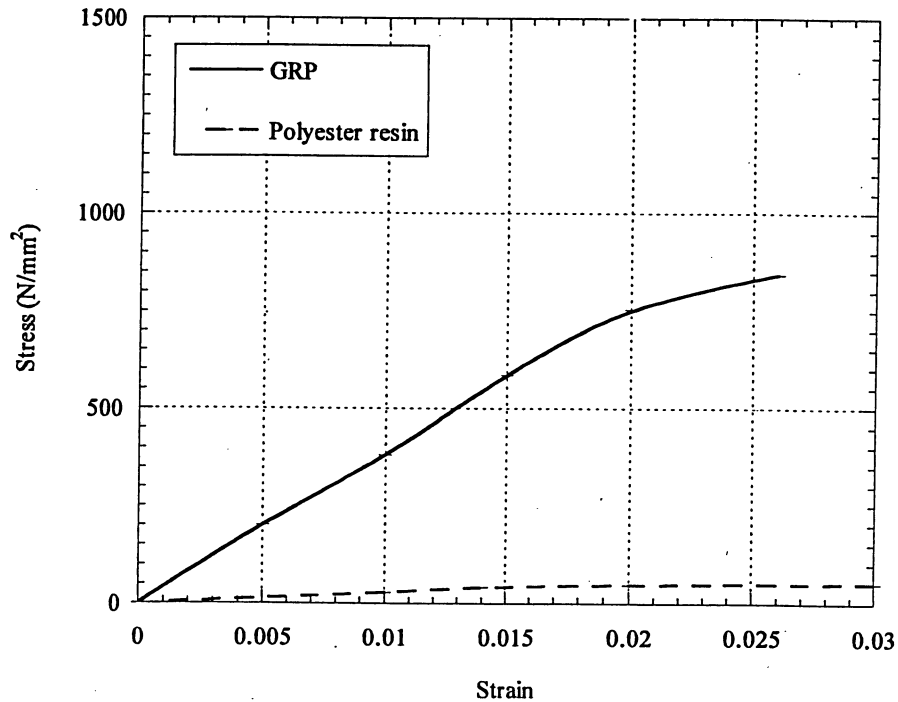


Figure 2.7 (Cont.): Stress-strain curves of glass fiber and polyester resin and GRP [27].

(c) Composite: GRP

2.4 Carbon Fiber-Reinforced Polymers

The advent of high-modulus carbon (graphite) fibers obtained from continuous polyacrylonitrile (PAN) filaments has caused considerable technical interest in recent years. Although a continuous spectrum of fiber strength and modulus values can be obtained by varying the process details, especially the maximum temperature at which the fibers are pyrolyzed, they are usually marked in the three basic forms often referred to as Types I, II, III fibers. The fiber properties are given in table 2.2. For practical purposes the fibers can only be used in conjunction with polymeric matrices such as epoxy and polyester resins. Typical properties of carbon fiber-epoxy resin unidirectional composites are given in Table 2.3.

Table 2.2: Typical properties of commercially produced Carbon Fibers [21]

Fiber	Filament diameter Mean(μm)	Average Density(g/cm^3)	Ultimate Tensile strength(GN/m^2)	Modulus (GN/m^2)
Grafil A or A-S	9.2	1.75	1.9-2.6	180-220
Grafil HT or HT-S	8.9	1.8	2.1-2.8	225-280
Grafil HM-S	8.2	1.95	1.8-2.4	350-410

Table 2.3 Properties of a unidirectional composite containing 60% fiber by volume [21]

Fiber	Tensile strength (GN/m^2)	Tensile modulus (GN/m^2)	Flexural Strength (GN/m^2)	Flexural modulus (GN/m^2)	Interlaminar Shear strength (MN/m^2)
Grafil A ¹	1.55	101	1.48	104	71
Grafil A-S ¹	1.45	104	1.42	107	81
Grafil HT-S ¹	1.37	140	1.4	123	78
Grafil HM-S ¹	1.14	211	.93	192	53
Grafil A ²	1.55	99	1.49	101	72
Grafil A-S ²	1.51	108	1.59	102	100
Grafil HT-S ²	1.43	120	1.65	122	97
Grafil HM-S ²	1.28	178	1.17	165	88
Grafil A ³	1.61	103	1.64	104	78
Grafil A-S ³	1.64	99	1.72	107	110
Grafil HT-S ³	1.62	121	1.7	127	100
Grafil HM-S ³	1.45	179	1.26	174	91

(1) Resin system: Shell Epikote 828/MNA/BDMA.

(2) Resin system: ERLA 4617/DDM, Cycloaliphatic epoxy resin.

(3) Resin system: 4617/MPD.

It should be noted that the high modulus of carbon fibers causes more anisotropy in strength, modulus, and thermal expansion coefficients than similar composites incorporating glass fibers. For a given type of fiber, the axial tensile strength and modulus of a composite depend on the volume fraction of fibers and only to a slight extent on the resin system employed. The axial compressive strength is substantially lower than the tensile strength. Figure (2.8 a) presents the tensile stress-strain curve which is almost linear until failure, so fiber properties are dominant. Figure (2.8 b) presents the shear stress-strain curve of CFRP composite which is non-linear and this nonlinearity is due to matrix ductility.

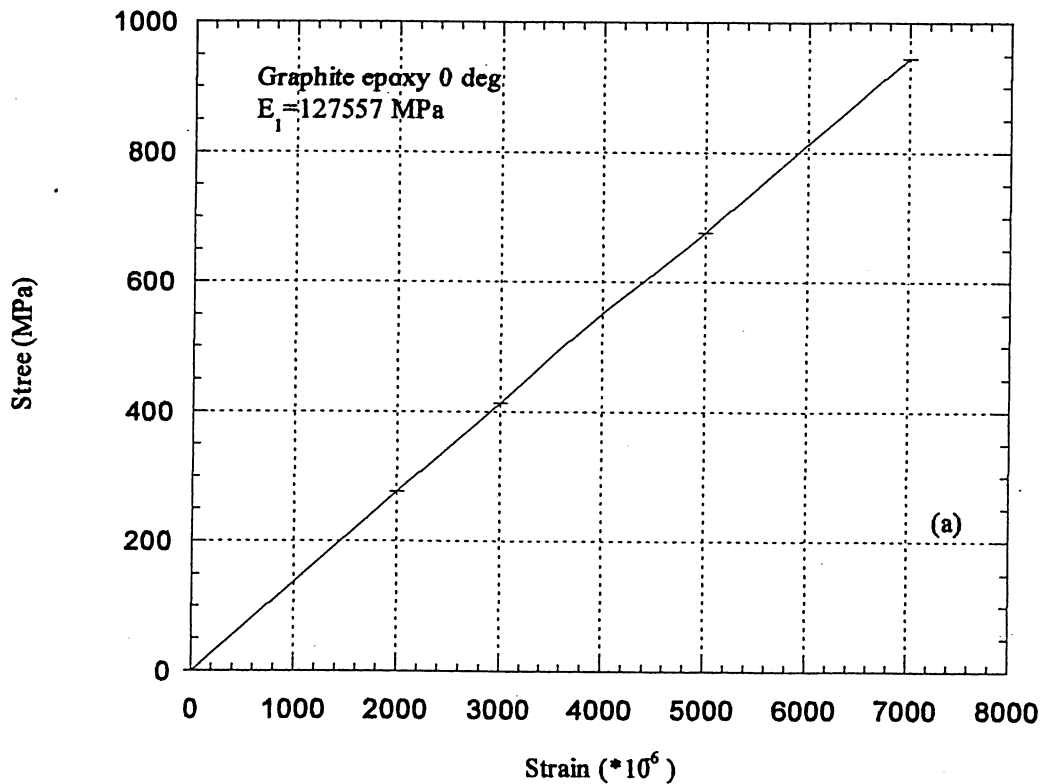


Figure 2.8: Stress-Strain response for Graphite Epoxy, (a) tensile test.

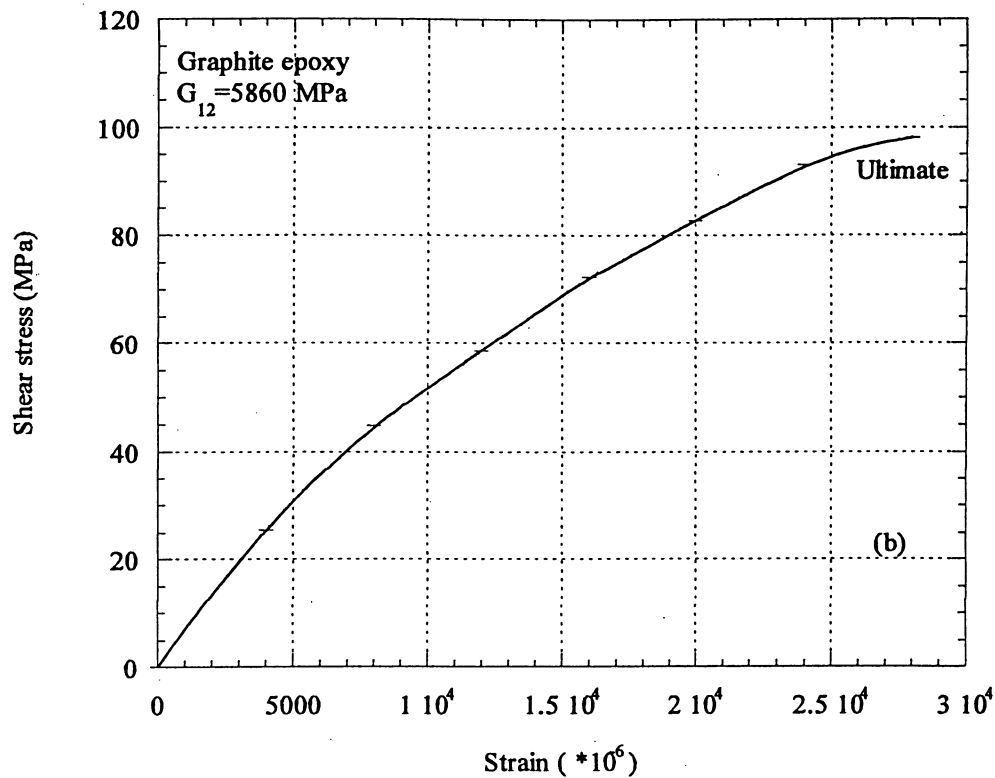


Figure 2.8 (Cont.): Stress-Strain response for Graphite Epoxy (b) shear test [28].

2.5 Applications

2.5.1 Aerospace and Military Applications

In the 1980s and the 1990s, major advancements in composite materials technology evolved. New developments in polymer resin formulations, fiber reinforcements, and processing technology led to increasing use of advanced composite materials, especially in aerospace applications. Designers of aerospace systems continued to exploit the principal advantages of composites, namely, their high strength-to-weight ratios (specific strength), high modulus-to-weight ratios (specific modulus), and fatigue resistance [29].

2.5.1.1 Composite Materials in U.S. Army Applications

Advanced composite materials are used on U.S. Army helicopters, such as the UH-60 Black Hawk, AH-64 Apache, and CH-47D Chinook. A helicopter, known as LHX, is expected to consist of at least 60 to 80 wt% composites. Composite materials will probably become the primary structural materials in future helicopters [30-31-32]. Composite materials are used for the helicopter rotor blades and spars, fuselage structure, crew seat armor, and a variety of other helicopter components, where strength, stiffness, and fatigue resistance are critical.

The FMC Corporation [33] has built a prototype composite hull Infantry Fighting Vehicle under U.S. Army contract. The hull is manufactured from glass fiber reinforced polymer composites. The use of composites reduces the weight at an equivalent ballistic protection level as compared to conventional metal, enhances crew survivability due to the lack of metal spall, improves damage tolerance, reduces crew space noise by 5 to 10 dB, provides greater hull fatigue and corrosion resistance, improves the vehicle thermal insulation, and reduces both the acoustic and infrared vehicle signatures.

2.5.1.2 Seawater Ball Valves

The U.S. Navy has evaluated commercially available composite ball valves in the 1-6 inches size range. The composite ball valves, made of glass- and graphite-reinforced thermosetting vinylester resin, have been subjected to full-scale fire tests, flammability, smoke, and toxicity tests, hydrostatic pressure tests, bending and torsion, tension and compression, high-impact shock, vibration, low-cycle fatigue, and ball valve actuation. Results of the investigation indicate that the composite valves are good candidates for shipboard applications [29].

2.5.1.3 Aero-Engine Applications

The introduction of carbon fibre in the 60s found Rolls Royce's first major exercise in incorporating composites into engines, with the Hyfil fan blade for the RB211. At that time, Rolls Royce's confidence in using a relatively new and, in hindsight, unproven material for a major rotating component was based on the fact that it had a thorough understanding of the material at the laminate level. A good example of this evolutionary process is the way in which FRP composites have been increasingly used in engine nacelles. Driven by the need to reduce weight in relation to existing aluminium designs, composites were first applied to relatively simple parts

such as the RB211 524 cowl doors. Applications spread progressively in this region of the engine to the extent that FRP composites now dominate the nacelle. A logical extension of the technology has occurred in by-pass ducts for both military (General Electric F414) and civil (Rolls-Royce Tay) engines [34].

Step change engine designs, which are the optimum vehicles to target for application of new materials technology, occur relatively infrequently. For example, both Rolls Royce's Trent and General Electric's GE90 were launched in the early 90s only after their previous engines, the RB211 524 and CF6, respectively, had served them well for over 15 years in their various marques. This issue is typified by the glass-reinforced epoxy fan nose spinner now used on all Rolls Royce civil engines. Although this appears to be a relatively straightforward component in terms of materials and manufacturing process, entry into service and the realisation of the cost and weight benefits had to wait until the costs of the certification test programme cyclic fatigue and bird impact could be borne by the launch of the next variants of the RB211 engine [34].

2.5.2 Offshore Application

Composite materials also provide a multitude of services in offshore hydrocarbon production, where they usually replace steel because of their lightness, corrosion resistance, and good mechanical performance. It has been proposed that submarine pipelines could be constructed with circumferential carbon fibers for resistant to external pressure and longitudinal glass fibers for lengthwise flexibility. Drilling risers for use at greater water depth are subject to compression and possible failure because the longitudinal resonant period of the disconnected rising is close to that of typical wave periods. The mass reduction on changing from steel to composites materials significantly reduces the dynamic stress and therefore increases either the fatigue resistance or the safety for deep-water drilling. It has been reported that 15 m lines manufactured from carbon and glass fibers have a burst pressure of 168 MPa. Self-righting, totally enclosed, motor - propelled survival craft and open lifeboats are manufactured in glass-reinforced plastic using fire-retardant resins [34].

2.5.3 Wind Power Plant Application

The revival of wind power began in the 1980's in America, Germany and Denmark, countries that depended mainly on fossil fuels but wished to lower production related pollution. Wind energy exploits local and inexhaustible resources without emitting greenhouse gases. It also has a limited and controllable impact on the environment. In less than 15 years, wind turbines have evolved from small, simple machines into a technology that can compete with established power generation sources such as coal, nuclear, gas and oil. Since 1995, world wind-generating capacity has increased by nearly 500% and the use of coal, the principal alternative, has declined by 9%. Europe now forms the fastest growing market for this type of energy [35].

The use of FRP composite materials in the turbines is an important technical element. Components must exhibit excellent fatigue strength, resist random loading and corrosion, require minimal maintenance and serve for 30+ years. Uncertainties over the performance of initial experiments with steel and aluminum have been overcome with the use of composite members, on which production is now almost entirely based. The blades are the main components, and the performance of the turbine is ultimately dictated by their efficiency. The use of lighter weight FRP materials means that the turbines can produce more power per unit volume, minimizing impact on the landscape.

2.5.4 Highway Infrastructure Application

Fiber reinforced polymer (FRP) composite materials show great potential for integration into the highway infrastructure. Typically, these materials have long and useful lives; are light in weight and easy to construct; provide excellent strength-to-weight characteristics; and can be fabricated for “made-to-order” strength, stiffness, geometry, and other properties. FRP composite materials may be the most cost-effective solution for repair, rehabilitation, and construction of portions of the highway infrastructure.

They can strengthen bridges without reduction of vertical clearance, and they can be applied in severe exposure environments that may have resulted in the deterioration of the original structure. FRP composite decks may be used to extend the life of girder-system bridges because their low dead weight allows for an increase in live-load carrying capacity [36].

CHAPTER THREE

Stress and Strain Constitutive Relationship in FRP Composites

3.1 Displacements, Strains, and Stresses

Fiber Reinforced Polymer (FRP) composites consist of continuous or discontinuous brittle fibers embedded in a matrix. Such a composite is heterogeneous, and the properties vary from point to point. On a scale that is large with respect to the fiber diameter, the fiber and matrix properties may be averaged, and the material may be treated as homogeneous. The material is considered to be quasi-homogeneous, which implies that the properties are taken to be the same at every point. These properties are not the same as the properties of either the fiber or the matrix but are a combination of the properties of the constituents.

In this chapter, equations are presented for calculating the displacements, stresses, and strains when the structure undergoes only small deformations and the material behaves in a linearly elastic manner. A unidirectional FRP composite consists of fibers reinforced within the matrix phase with an off-axis angle θ with respect to the applied loading axis. It is therefore convenient to employ two coordinate systems: a local coordinate system aligned, at a point, either with the fibers, and a global coordinate system attached to a fixed reference point. Figure 3.1 presents global and local coordinate systems used for fibrous composites. The local and global Cartesian coordinate systems are designated respectively by 1, 2, 3, and the x, y, z axes. In the x, y, z coordinate system the normal stresses are denoted by $\sigma_{xx}, \sigma_{yy}, \sigma_{zz}$ and the shear stresses by $\tau_{yz}, \tau_{xz}, \tau_{xy}$. The corresponding normal and shear strains are $\epsilon_{xx}, \epsilon_{yy}, \epsilon_{zz}$ and $\gamma_{yz}, \gamma_{xz}, \gamma_{xy}$, respectively. In the 1, 2, 3 coordinate system the normal stresses are denoted by $\sigma_{11}, \sigma_{22}, \sigma_{33}$ and the shear stresses are denoted by $\tau_{23}, \tau_{13}, \tau_{12}$. The corresponding normal and shear strains are $\epsilon_{11}, \epsilon_{22}, \epsilon_{33}$, and $\gamma_{23}, \gamma_{13}, \gamma_{12}$, respectively. The symbol γ represents engineering shear strain. Figure 3.2 presents all tensorial stresses in x, y, z and 1, 2, 3 coordinates.

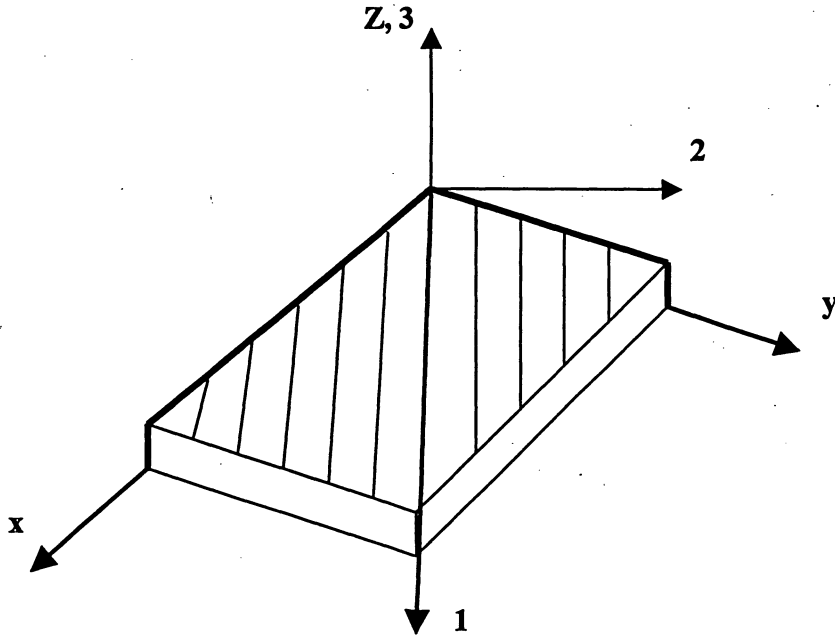


Figure 3.1: The global x, y, z and local 1, 2, 3 coordinate systems.

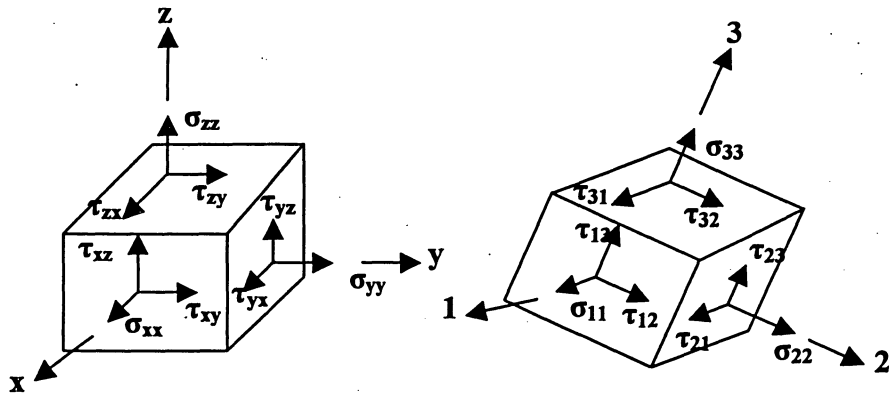


Figure 3.2: The stresses in the global x, y, z and the local 1, 2, 3 coordinate systems.

3.2 Stress-Strain Relationships

In a composite material the fibers may be oriented in an arbitrary manner. Depending on the arrangements of the fibers, the material may behave differently in different directions. According to their behavior, composites may be characterized as generally anisotropic, monoclinic, orthotropic, transversely isotropic, or isotropic. In the following, the stress-strain relationships for these types of materials under linear elastic conditions are presented.

3.2.1 Generally Anisotropic Material

When there are no symmetry planes with respect to the alignment of the fibers, the material is referred to as generally anisotropic. A fiber-reinforced composite material is generally anisotropic when the fibers are aligned in three non-orthogonal directions. For a generally anisotropic linear material in the x, y, z global coordinates the stress-strain relationships are presented in Eq 3.1 [37]:

$$\begin{Bmatrix} \sigma_{xx} \\ \sigma_{yy} \\ \sigma_{zz} \\ \tau_{yz} \\ \tau_{xz} \\ \tau_{xy} \end{Bmatrix} = \begin{bmatrix} \bar{C}_{11} & \bar{C}_{12} & \bar{C}_{13} & \bar{C}_{14} & \bar{C}_{15} & \bar{C}_{16} \\ \bar{C}_{21} & \bar{C}_{22} & \bar{C}_{23} & \bar{C}_{24} & \bar{C}_{25} & \bar{C}_{26} \\ \bar{C}_{31} & \bar{C}_{32} & \bar{C}_{33} & \bar{C}_{34} & \bar{C}_{35} & \bar{C}_{36} \\ \bar{C}_{41} & \bar{C}_{42} & \bar{C}_{43} & \bar{C}_{44} & \bar{C}_{45} & \bar{C}_{46} \\ \bar{C}_{51} & \bar{C}_{52} & \bar{C}_{53} & \bar{C}_{54} & \bar{C}_{55} & \bar{C}_{56} \\ \bar{C}_{61} & \bar{C}_{62} & \bar{C}_{63} & \bar{C}_{64} & \bar{C}_{65} & \bar{C}_{66} \end{bmatrix} \begin{Bmatrix} \varepsilon_{xx} \\ \varepsilon_{yy} \\ \varepsilon_{zz} \\ \gamma_{yz} \\ \gamma_{xz} \\ \gamma_{xy} \end{Bmatrix} \quad (3.1)$$

Where \bar{C}_{ij} are the elements of the stiffness matrix $[\bar{C}]$ in the x, y, z coordinate system. Inversion of Eq 3.1 results in the following strain-stress relationship in Eq 3.2:

$$\begin{Bmatrix} \varepsilon_{xx} \\ \varepsilon_{yy} \\ \varepsilon_{zz} \\ \gamma_{yz} \\ \gamma_{xz} \\ \gamma_{xy} \end{Bmatrix} = \begin{bmatrix} \bar{S}_{11} & \bar{S}_{12} & \bar{S}_{13} & \bar{S}_{14} & \bar{S}_{15} & \bar{S}_{16} \\ \bar{S}_{21} & \bar{S}_{22} & \bar{S}_{23} & \bar{S}_{24} & \bar{S}_{25} & \bar{S}_{26} \\ \bar{S}_{31} & \bar{S}_{32} & \bar{S}_{33} & \bar{S}_{34} & \bar{S}_{35} & \bar{S}_{36} \\ \bar{S}_{41} & \bar{S}_{42} & \bar{S}_{43} & \bar{S}_{44} & \bar{S}_{45} & \bar{S}_{46} \\ \bar{S}_{51} & \bar{S}_{52} & \bar{S}_{53} & \bar{S}_{54} & \bar{S}_{55} & \bar{S}_{56} \\ \bar{S}_{61} & \bar{S}_{62} & \bar{S}_{63} & \bar{S}_{64} & \bar{S}_{65} & \bar{S}_{66} \end{bmatrix} \begin{Bmatrix} \sigma_{xx} \\ \sigma_{yy} \\ \sigma_{zz} \\ \tau_{yz} \\ \tau_{xz} \\ \tau_{xy} \end{Bmatrix} \quad (3.2)$$

where \bar{S}_{ij} are the elements of the compliance matrix $[\bar{S}]$ in the x, y, z coordinate system and are

defined in Table 3.1. In the 1, 2, 3 coordinate system the stress-strain relationships can be defined by Eq 3.3:

$$\begin{Bmatrix} \sigma_{11} \\ \sigma_{22} \\ \sigma_{33} \\ \tau_{23} \\ \tau_{13} \\ \tau_{12} \end{Bmatrix} = \begin{bmatrix} C_{11} & C_{12} & C_{13} & C_{14} & C_{15} & C_{16} \\ C_{21} & C_{22} & C_{23} & C_{24} & C_{25} & C_{26} \\ C_{31} & C_{32} & C_{33} & C_{34} & C_{35} & C_{36} \\ C_{41} & C_{42} & C_{43} & C_{44} & C_{45} & C_{46} \\ C_{51} & C_{52} & C_{53} & C_{54} & C_{55} & C_{56} \\ C_{61} & C_{62} & C_{63} & C_{64} & C_{65} & C_{66} \end{bmatrix} \begin{Bmatrix} \epsilon_{11} \\ \epsilon_{22} \\ \epsilon_{33} \\ \gamma_{23} \\ \gamma_{13} \\ \gamma_{12} \end{Bmatrix} \quad (3.3)$$

Where C_{ij} are the elements of the stiffness matrix $[C]$ in the 1,2,3 coordinate system. By inverting Eq. (3.3), the following strain-stress relationships are obtained:

$$\begin{Bmatrix} \epsilon_{11} \\ \epsilon_{22} \\ \epsilon_{33} \\ \gamma_{23} \\ \gamma_{13} \\ \gamma_{12} \end{Bmatrix} = \begin{bmatrix} \bar{S}_{11} & \bar{S}_{12} & \bar{S}_{13} & \bar{S}_{14} & \bar{S}_{15} & \bar{S}_{16} \\ \bar{S}_{21} & \bar{S}_{22} & \bar{S}_{23} & \bar{S}_{24} & \bar{S}_{25} & \bar{S}_{26} \\ \bar{S}_{31} & \bar{S}_{32} & \bar{S}_{33} & \bar{S}_{34} & \bar{S}_{35} & \bar{S}_{36} \\ \bar{S}_{41} & \bar{S}_{42} & \bar{S}_{43} & \bar{S}_{44} & \bar{S}_{45} & \bar{S}_{46} \\ \bar{S}_{51} & \bar{S}_{52} & \bar{S}_{53} & \bar{S}_{54} & \bar{S}_{55} & \bar{S}_{56} \\ \bar{S}_{61} & \bar{S}_{62} & \bar{S}_{63} & \bar{S}_{64} & \bar{S}_{65} & \bar{S}_{66} \end{bmatrix} \begin{Bmatrix} \sigma_{11} \\ \sigma_{22} \\ \sigma_{33} \\ \tau_{23} \\ \tau_{13} \\ \tau_{12} \end{Bmatrix} \quad (3.4)$$

where S_{ij} are the elements of the compliance matrix $[S]$ in the 1, 2, 3 coordinate system (table 3.1).

It is evident from Eqs (3.2)-(3.3) that the compliance matrix $[S]$ is the inverse of the stiffness matrix $[C]$:

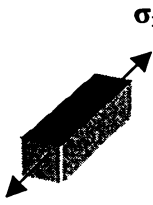


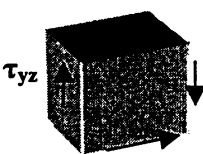

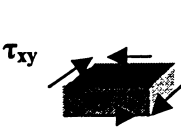
$$[\bar{S}] = [\bar{C}]^{-1} \quad [S] = [C]^{-1} \quad (3.5)$$

It can be shown that for an elastic material the stiffness and compliance matrices are symmetrical in the x, y, z and 1, 2, 3 coordinate systems as Eq 3.6:

$$\bar{S}_{ij} = \bar{S}_{ji}, S_{ij} = S_{ji} \quad \bar{C}_{ij} = \bar{C}_{ji} \quad C_{ij} = C_{ji} \quad i, j = 1, 2, \dots, 6 \quad (3.6)$$

Because of symmetry, in $[\bar{S}]$ and $[\bar{C}]$ matrices only 21 of the 36 elements are independent.

Table 3.1: The elements of the compliance matrix in the x, y, z systems

	$\begin{aligned} S_{11} &= \epsilon_{xx} / \sigma_{xx} & S_{41} &= \gamma_{yz} / \sigma_{xx} \\ S_{21} &= \epsilon_{yy} / \sigma_{xx} & S_{51} &= \gamma_{xz} / \sigma_{xx} \\ S_{31} &= \epsilon_{xz} / \sigma_{xx} & S_{61} &= \gamma_{xy} / \sigma_{xx} \end{aligned}$
	$\begin{aligned} S_{12} &= \epsilon_x / \sigma_{yy} & S_{42} &= \gamma_{yz} / \sigma_{yy} \\ S_{22} &= \epsilon_y / \sigma_{yy} & S_{52} &= \gamma_{xz} / \sigma_{yy} \\ S_{32} &= \epsilon_x / \sigma_{yy} & S_{62} &= \gamma_{xy} / \sigma_{yy} \end{aligned}$
	$\begin{aligned} S_{13} &= \epsilon_x / \sigma_{zz} & S_{43} &= \gamma_{yz} / \sigma_{zz} \\ S_{23} &= \epsilon_y / \sigma_{zz} & S_{53} &= \gamma_{xz} / \sigma_{zz} \\ S_{33} &= \epsilon_z / \sigma_{zz} & S_{63} &= \gamma_{xy} / \sigma_{zz} \end{aligned}$
	$\begin{aligned} S_{14} &= \epsilon_{xx} / \tau_{yz} & S_{44} &= \gamma_{yz} / \tau_{yz} \\ S_{24} &= \epsilon_{yy} / \tau_{yz} & S_{54} &= \gamma_{xz} / \tau_{yz} \\ S_{34} &= \epsilon_{zz} / \tau_{yz} & S_{64} &= \gamma_{xy} / \tau_{yz} \end{aligned}$
	$\begin{aligned} S_{15} &= \epsilon_{xx} / \tau_{xz} & S_{45} &= \gamma_{yz} / \tau_{xz} \\ S_{25} &= \epsilon_{yy} / \tau_{xz} & S_{55} &= \gamma_{xz} / \tau_{xz} \\ S_{35} &= \epsilon_{zz} / \tau_{xz} & S_{65} &= \gamma_{xy} / \tau_{xz} \end{aligned}$
	$\begin{aligned} S_{16} &= \epsilon_{xx} / \tau_{xy} & S_{46} &= \gamma_{yz} / \tau_{xy} \\ S_{26} &= \epsilon_{yy} / \tau_{xy} & S_{56} &= \gamma_{xz} / \tau_{xy} \\ S_{36} &= \epsilon_{xz} / \tau_{xy} & S_{66} &= \gamma_{xy} / \tau_{xy} \end{aligned}$

3.2.2 Transversely Isotropic Material

A transversely isotropic material has three planes of symmetry. These planes are illustrated in figure 3.3 a and b. In one of the planes of symmetry the material is treated as isotropic. An example of transversely isotropic material is a composite reinforced with continuous unidirectional fibers with all the fibers aligned in the direction 1 (See Figure 3.3 b). In this case the material in the plane perpendicular to the fibers (2-3 plane) is treated as isotropic. For a transversely isotropic material the stiffness and compliance matrices in an 1, 2, 3 coordinate system chosen in such a way that the axes are perpendicular to the planes of symmetry and the material properties in this system are:

$$E_3=E_2 \quad G_{13}=G_{12} \quad \nu_{13}=\nu_{12} \quad (3.7)$$

For an isotropic material the shear modulus is defined by Eq 3.8:

$$G = \frac{E}{2(1+\nu)} \quad (3.8)$$

Correspondingly, for a material that is isotropic in the 2-3 plane, the relation between Young's module and shear module can be presented by Eq 3.9:

$$G_{23} = \frac{E_2}{2(1+\nu_{23})} \quad (3.9)$$

Equations (3.7) and (3.9), together with the expressions in Table 3.2, yield the compliance matrix in terms of the engineering constants. The results are given in Eq 3.12-3.15. The zero and nonzero elements of the compliance matrix are given in Eq 3.10 [34]:

$$[S] = \begin{bmatrix} S_{11} & S_{12} & S_{13} & 0 & 0 & 0 \\ S_{12} & S_{22} & S_{23} & 0 & 0 & 0 \\ S_{12} & S_{23} & S_{22} & 0 & 0 & 0 \\ 0 & 0 & 0 & 2(S_{22} - S_{23}) & 0 & 0 \\ 0 & 0 & 0 & 0 & S_{66} & 0 \\ 0 & 0 & 0 & 0 & 0 & S_{66} \end{bmatrix} \quad (3.10)$$

The stiffness matrix is obtained by inverting the compliance matrix. The zero and nonzero elements of the stiffness matrix are defined by Eq 3.11:

$$[C] = \begin{bmatrix} C_{11} & C_{12} & C_{12} & 0 & 0 & 0 \\ C_{12} & C_{22} & C_{23} & 0 & 0 & 0 \\ C_{12} & C_{23} & C_{22} & 0 & 0 & 0 \\ 0 & 0 & 0 & \frac{C_{22} - C_{23}}{2} & 0 & 0 \\ 0 & 0 & 0 & 0 & C_{66} & 0 \\ 0 & 0 & 0 & 0 & 0 & C_{66} \end{bmatrix} \quad (3.11)$$

The compliance matrices in terms of the engineering constants for monoclinic, orthotropic, transversely isotropic, and isotropic materials can be shown as follows:

When there is a symmetry plane with respect to the alignment of the fibers, the monoclinic compliance matrix is defined by Eq 3.12.

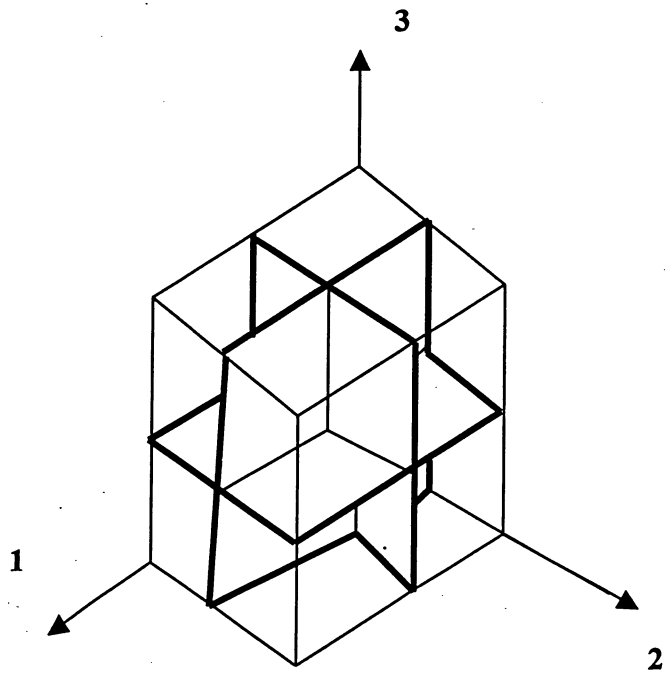


Figure 3.3a: Orthotropic material with three planes of symmetry.

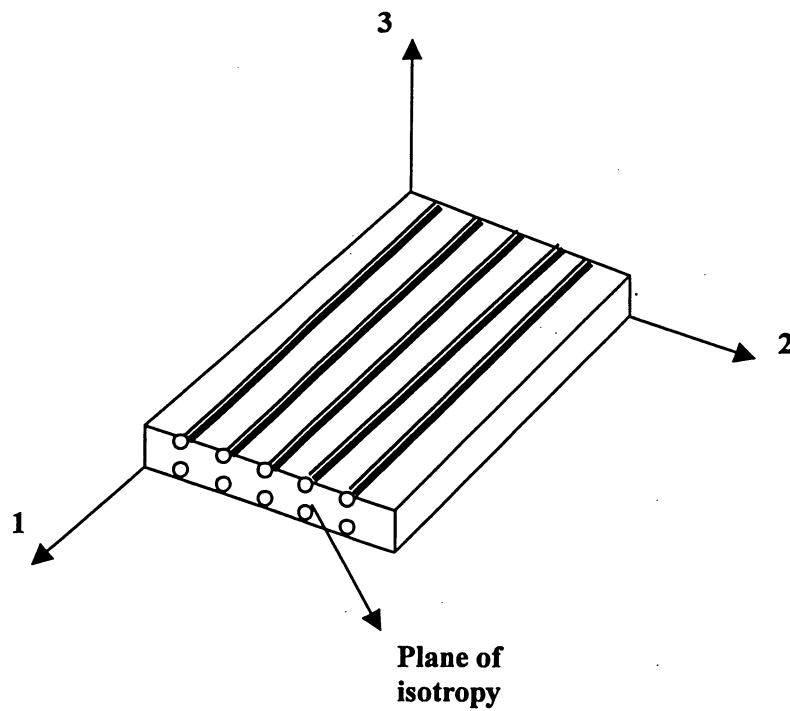


Figure 3.3b: Example of a fiber-reinforced, transversely isotropic composite.

Table 3.2: Elements of the compliance matrix in terms of the engineering constants

$S_{11}=\epsilon_{11}/\sigma_{11}=\epsilon_{11}/\epsilon_{11}E_1=1/E_1$	$S_{12}=\epsilon_{11}/\sigma_{22}=\epsilon_{22}/(E_2\epsilon_{22})=-\nu_{21}/E_2$	$S_{13}=\epsilon_{11}/\sigma_{33}=\epsilon_{33}/(E_3\epsilon_{33})=-\nu_{31}/E_3$	$S_{14}=0$	$S_{15}=0$	$S_{16}=\epsilon_{11}/\tau_{12}=\epsilon_{11}/(G_{12}\gamma_{12})=\nu_{61}/G_{12}$
$S_{21}=\epsilon_{22}/\sigma_{11}=\epsilon_{22}/(E_1\epsilon_{11})=-\nu_{12}/E_1$	$S_{22}=\epsilon_{22}/\sigma_{22}=\epsilon_{22}/(E_2\epsilon_{22})=1/E_2$	$S_{23}=\epsilon_{22}/\sigma_{33}=\epsilon_{33}/(E_3\epsilon_{33})=-\nu_{22}/E_3$	$S_{24}=0$	$S_{25}=0$	$S_{26}=\epsilon_{22}/\tau_{12}=\epsilon_{22}/(G_{12}\gamma_{12})=\nu_{62}/G_{12}$
$S_{31}=\epsilon_{33}/\sigma_{11}=\epsilon_{33}/(E_1\epsilon_{11})=-\nu_{13}/E_1$	$S_{32}=\epsilon_{33}/\sigma_{22}=\epsilon_{33}/(E_2\epsilon_{22})=-\nu_{23}/E_2$	$S_{33}=\epsilon_{33}/\sigma_{33}=\epsilon_{33}/(E_3\epsilon_{33})=1/E_3$	$S_{34}=0$	$S_{35}=0$	$S_{36}=\epsilon_{33}/\tau_{12}=\epsilon_{33}/(G_{12}\gamma_{12})=\nu_{63}/G_{12}$
$S_{41}=0$	$S_{42}=0$	$S_{43}=0$	$S_{44}=\gamma_{23}/\tau_{23}=\gamma_{23}/(G_{23}\gamma_{23})=1/G_{23}$	$S_{45}=\gamma_{23}/\tau_{13}=\gamma_{23}/(G_{13}\gamma_{13})=\nu_{54}/G_{13}$	$S_{46}=0$
$S_{51}=0$	$S_{52}=0$	$S_{53}=0$	$S_{54}=\gamma_{13}/\tau_{23}=\gamma_{13}/(G_{23}\gamma_{23})=\nu_{45}/G_{23}$	$S_{55}=\gamma_{13}/\tau_{13}=\gamma_{13}/(G_{13}\gamma_{13})=1/G_{13}$	$S_{56}=0$
$S_{61}=\gamma_{12}/\sigma_{11}=\gamma_{12}/(E_1\epsilon_{11})=\nu_{16}/E_1$	$S_{62}=\gamma_{12}/\sigma_{22}=\gamma_{12}/(E_2\epsilon_{22})=\nu_{26}/E_2$	$S_{63}=\gamma_{12}/\sigma_{33}=\gamma_{12}/(E_3\epsilon_{33})=\nu_{36}/E_3$	$S_{64}=0$	$S_{65}=0$	$S_{66}=\gamma_{12}/\tau_{12}=\gamma_{12}/(G_{12}\gamma_{12})=1/G_{12}$

The above table is also valid for orthotropic, transversely isotropic, and isotropic materials with $S_{16}=S_{61}=0$, $S_{26}=S_{62}=0$, $S_{36}=S_{63}=0$, $S_{45}=S_{54}=0$

$$[S] = \begin{bmatrix} \frac{1}{E_1} & -\frac{\nu_{21}}{E_2} & -\frac{\nu_{31}}{E_3} & 0 & 0 & \frac{\nu_{61}}{G_{12}} \\ -\frac{\nu_{12}}{E_1} & \frac{1}{E_2} & -\frac{\nu_{32}}{E_3} & 0 & 0 & \frac{\nu_{62}}{G_{12}} \\ -\frac{\nu_{13}}{E_1} & -\frac{\nu_{23}}{E_2} & \frac{1}{E_3} & 0 & 0 & \frac{\nu_{63}}{G_{12}} \\ 0 & 0 & 0 & \frac{1}{G_{23}} & \frac{\nu_{54}}{G_{13}} & 0 \\ 0 & 0 & 0 & \frac{\nu_{45}}{G_{23}} & \frac{1}{G_{13}} & 0 \\ -\frac{\nu_{16}}{E_1} & \frac{\nu_{26}}{E_2} & \frac{\nu_{36}}{E_3} & 0 & 0 & \frac{1}{G_{12}} \end{bmatrix} \quad (3.12)$$

When there are three mutually perpendicular symmetry planes with respect to the alignment of the fibers, the orthotropic compliance matrix is presented by Eq 3.13.

$$[S] = \begin{bmatrix} \frac{1}{E_1} & -\frac{\nu_{21}}{E_2} & -\frac{\nu_{31}}{E_3} & 0 & 0 & 0 \\ -\frac{\nu_{12}}{E_1} & \frac{1}{E_2} & -\frac{\nu_{32}}{E_3} & 0 & 0 & 0 \\ -\frac{\nu_{13}}{E_1} & -\frac{\nu_{23}}{E_2} & \frac{1}{E_3} & 0 & 0 & 0 \\ 0 & 0 & 0 & \frac{1}{G_{23}} & 0 & 0 \\ 0 & 0 & 0 & 0 & \frac{1}{G_{13}} & 0 \\ 0 & 0 & 0 & 0 & 0 & \frac{1}{G_{12}} \end{bmatrix} \quad (3.13)$$

When there are three planes of symmetry and in one of them the material is treated as isotropic materials, the transversely isotropic compliance matrix is presented by Eq 3.14.

$$[S] = \begin{bmatrix} \frac{1}{E_1} & -\frac{\nu_{21}}{E_2} & -\frac{\nu_{31}}{E_3} & 0 & 0 & 0 \\ -\frac{\nu_{12}}{E_1} & \frac{1}{E_2} & -\frac{\nu_{32}}{E_3} & 0 & 0 & 0 \\ -\frac{\nu_{13}}{E_1} & -\frac{\nu_{23}}{E_2} & \frac{1}{E_3} & 0 & 0 & 0 \\ 0 & 0 & 0 & \frac{2(1+\nu_{23})}{E_2} & 0 & 0 \\ 0 & 0 & 0 & 0 & \frac{1}{G_{13}} & 0 \\ 0 & 0 & 0 & 0 & 0 & \frac{1}{G_{12}} \end{bmatrix} \quad (3.14)$$

There are no preferred directions and every plane is a plane of symmetry in an isotropic material and its compliance matrix is given by Eq 3.15.

$$[S] = \begin{bmatrix} \frac{1}{E_1} & -\frac{\nu}{E} & -\frac{\nu}{E} & 0 & 0 & 0 \\ -\frac{\nu}{E} & \frac{1}{E} & -\frac{\nu}{E} & 0 & 0 & 0 \\ -\frac{\nu}{E} & -\frac{\nu}{E} & \frac{1}{E} & 0 & 0 & 0 \\ 0 & 0 & 0 & \frac{2(1+\nu)}{E} & 0 & 0 \\ 0 & 0 & 0 & 0 & \frac{2(1+\nu)}{E} & 0 \\ 0 & 0 & 0 & 0 & 0 & \frac{2(1+\nu)}{E} \end{bmatrix} \quad (3.15)$$

3.3 Macro-mechanical Analysis of a Unidirectional Lamina

The unidirectional composite ply can be considered as a transversely isotropic material and the elastic moduli for an angle lamina (See Figure3.3 b) are derived by compliance matrix in x-y coordination.

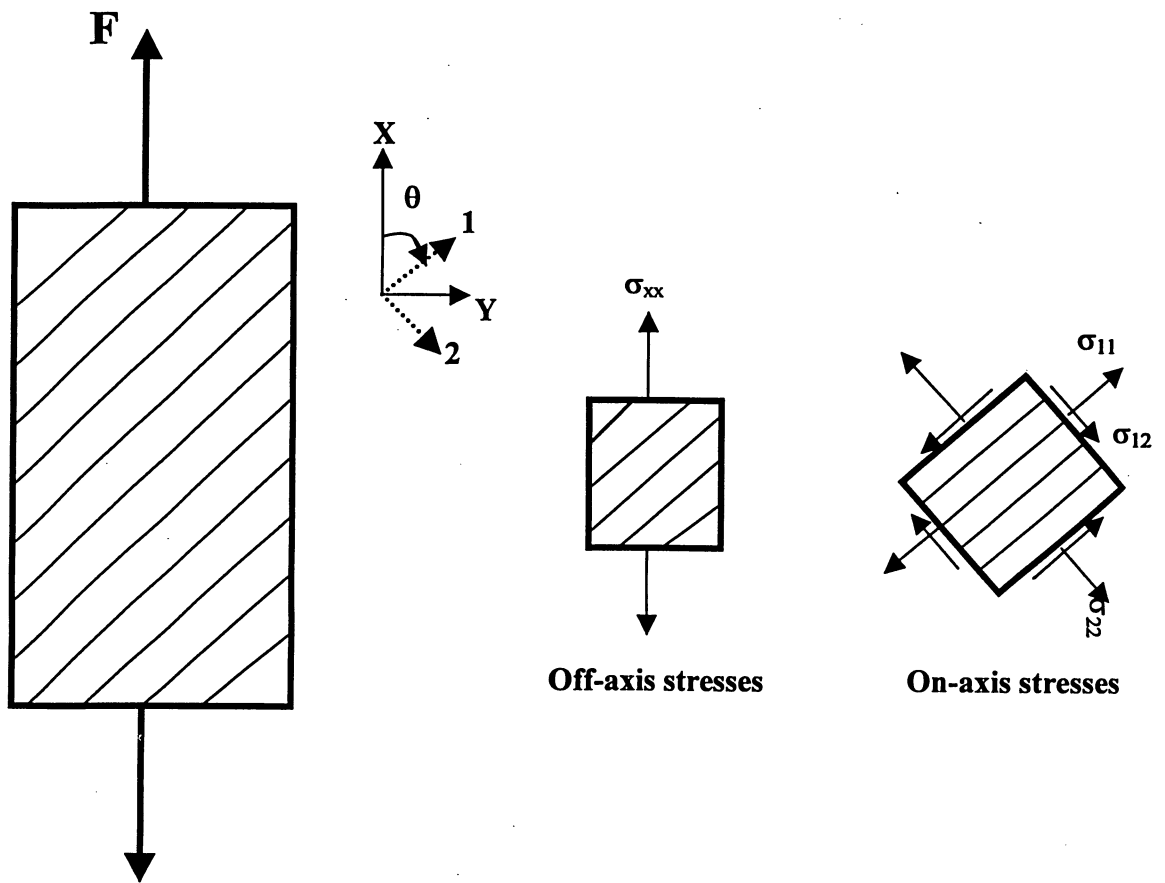


Figure 3.4: For an off-axis unidirectional specimen under uniaxial tension, the on-axis stresses are found by transforming the off-axis stress from the off-axis to on-axis directions [39].

The relationships between stresses and strains in the x, y coordinate system are written in Eq 3.16.

$$\begin{bmatrix} \varepsilon_{xx} \\ \varepsilon_{yy} \\ \varepsilon_{zz} \end{bmatrix} = \begin{bmatrix} \bar{S}_{11} & \bar{S}_{12} & \bar{S}_{13} \\ \bar{S}_{21} & \bar{S}_{22} & \bar{S}_{23} \\ \bar{S}_{31} & \bar{S}_{32} & \bar{S}_{33} \end{bmatrix} \begin{bmatrix} \sigma_{xx} \\ \sigma_{yy} \\ \sigma_{zz} \end{bmatrix} \quad (3.16)$$

Where the transformation matrix S_{ij} in 1-2 coordination can be define as Eq 3.17 [27]:

$$[S_{ij}]_{\theta} = \begin{bmatrix} \cos^2 \theta & \sin^2 \theta & -\sin \theta \cos \theta \\ \sin^2 \theta & \cos^2 \theta & \sin \theta \cos \theta \\ 2\sin \theta \cos \theta & -2\sin \theta \cos \theta & \cos^2 \theta - \sin^2 \theta \end{bmatrix} \quad (3.17)$$

From equations 3.16 and 3.17 the relationships between the stresses and strains in the arbitrary x-y coordinate system can be derived from $[\bar{S}_{ij}]_{\theta}$ elements through following transformations:

$$\begin{aligned} \bar{S}_{11} &= S_{11} \cos^4 \theta + S_{22} \sin^4 \theta + (2S_{12} + S_{33}) \sin^2 \theta \cos^2 \theta \\ \bar{S}_{12} = \bar{S}_{21} &= S_{12} (\sin \theta + \cos \theta) + (S_{11} + S_{22} - S_{33}) \sin^2 \theta \cos^2 \theta \\ \bar{S}_{13} &= S_{31} + (2S_{11} - 2S_{12} - S_{33}) \sin \theta \cos^3 \theta \\ \bar{S}_{22} &= S_{11} \sin^4 \theta + S_{22} \cos^4 \theta + (2S_{12} + S_{33}) \sin^2 \theta \cos^2 \theta \\ \bar{S}_{32} = \bar{S}_{23} &= (2S_{11} - 2S_{12} - S_{33}) \sin^3 \theta \cos \theta - (2S_{22} - 2S_{12} - S_{33}) \sin \theta \cos^3 \theta \\ \bar{S}_{33} &= 2(2S_{11} + 2S_{22} - 4S_{12} - S_{33}) \sin^2 \theta \cos^2 \theta + S_{33} (\sin^4 \theta + \cos^4 \theta) \end{aligned} \quad (3.17a-g)$$

$$S_{11} = \frac{1}{E_1}, S_{22} = \frac{1}{E_2}, S_{12} = -\frac{\nu_{21}}{E_2} = -\frac{\nu_{12}}{E_1}, S_{33} = \frac{1}{G_{12}}$$

Thus, the relationships between material properties in x-y and 1-2 coordinates can be calculated by equations 3.18, 19, 20, and 21.

$$1/E_x = \cos^4 \theta / E_1 + (1/G_{12} - 2\nu_{12}/E_1) \sin^2 \theta \cos^2 \theta + \sin^4 \theta / E_2 \quad (3.18)$$

$$\nu_{xy} = E_x [\nu_{12} (\sin^4 \theta + \cos^4 \theta) / E_1 - (1/E_1 + 1/E_2 - 1/G_{12}) \sin^2 \theta \cos^2 \theta] \quad (3.19)$$

$$1/E_y = \sin^4 \theta / E_1 + (1/G_{12} - 2\nu_{12}/E_1) \sin^2 \theta \cos^2 \theta + \cos^4 \theta / E_2 \quad (3.20)$$

$$1/G_{xy} = 2(2/E_1 + 2/E_2 + 4\nu_{12}/E_1 - 1/G_{12}) \sin^2 \theta \cos^2 \theta + (\cos^4 \theta + \sin^4 \theta)/G_{12} \quad (3.21)$$

Transformation of stress components in Eq 3.22 is expressed as:

$$\begin{bmatrix} \sigma_{11} \\ \sigma_{22} \\ \sigma_{12} \end{bmatrix} = \begin{bmatrix} \cos^2 \theta & \sin^2 \theta & 2 \sin \theta \cos \theta \\ \sin^2 \theta & \cos^2 \theta & -2 \sin \theta \cos \theta \\ -\sin \theta \cos \theta & \sin \theta \cos \theta & (\cos^2 \theta - \sin^2 \theta) \end{bmatrix} \begin{bmatrix} \sigma_{xx} \\ \sigma_{yy} \\ \sigma_{xy} \end{bmatrix} \quad (3.22)$$

The off-axis and on-axis stress components demonstrated in figure 3.4 are calculated from transformation matrix (Eq 3.22) as:

$$\begin{aligned} \sigma_{11} &= \sigma_{xx} \cos^2 \theta \\ \sigma_{22} &= \sigma_{xx} \sin^2 \theta \\ \tau_{12} &= -\sigma_{xx} \sin \theta \cos \theta \end{aligned} \quad (3.23)$$

Figures 3.5-3.8 represent the variations of the shear modulus and elastic modulus of GRP and CFRP composites as the off-axis angle increases. These variations were calculated using equations 3.18-3.21. As figures 3.5 and 3.7 show, the elastic modulus initially possesses the highest value at 0° off-axis angle where the fibers are oriented along the loading axis. The magnitude of the elastic modulus decreases as off-axis angle increases. Figures 3.6 and 3.8 represent an initial increase of the shear modulus as off-axis angle increases from zero to a maximum value of 45°. Beyond off-axis 45°: the shear modulus keeps decreasing as off-axis angle increases from 45° to 90°. At 90° off-axis angle the shear modulus becomes as small as the shear modulus achieved at 0° off-axis.

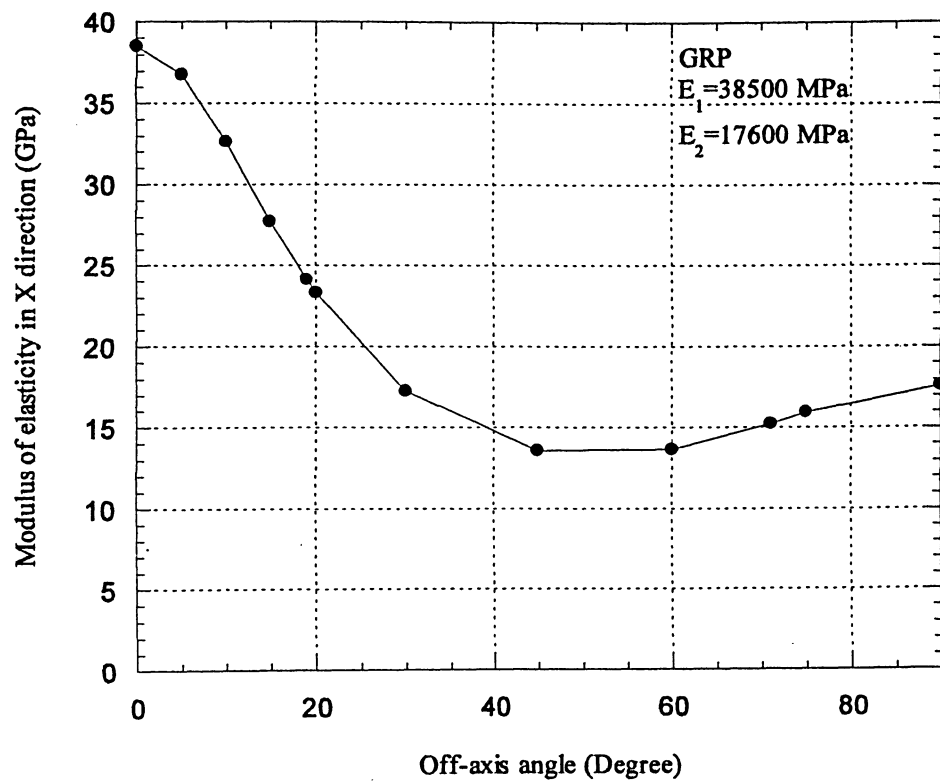


Figure 3.5: The elastic modulus response as off-axis angle changes for a typical unidirectional GRP

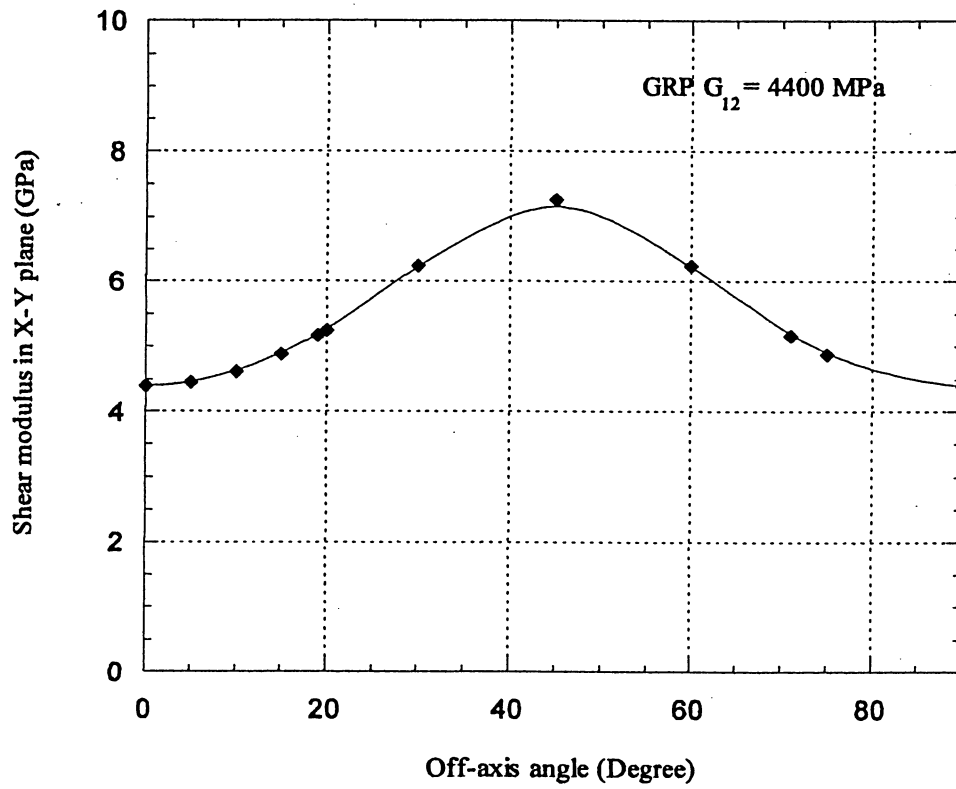


Figure 3.6: The shear modulus response as off-axis angle changes for a typical unidirectional GRP

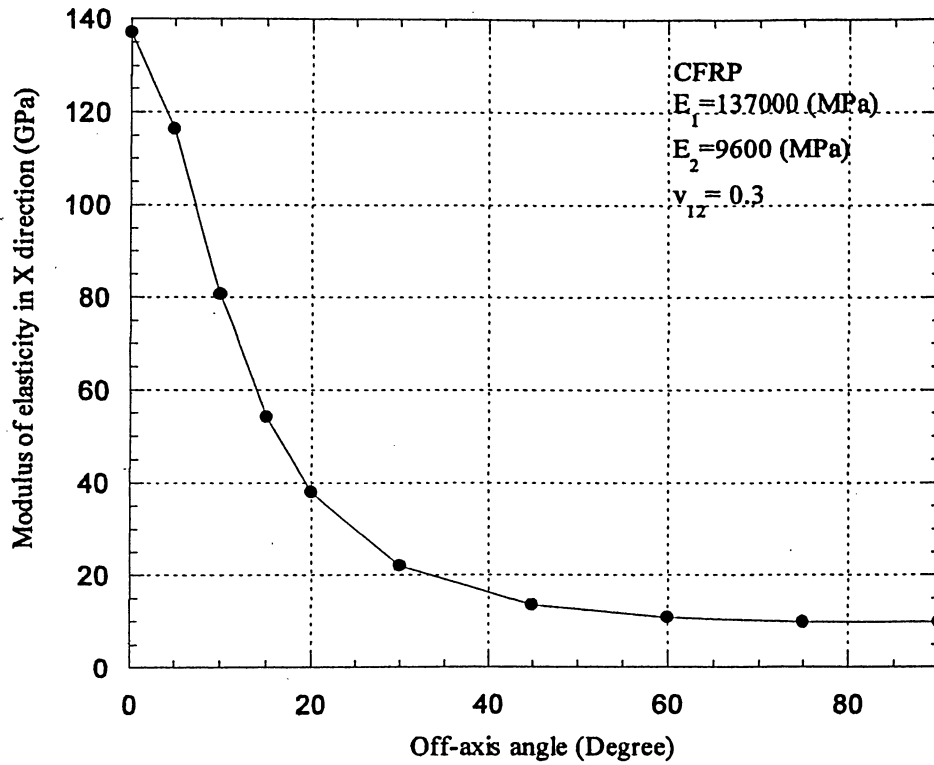


Figure 3.7: The elastic modulus response as off-axis angle changes for a typical unidirectional CFRP

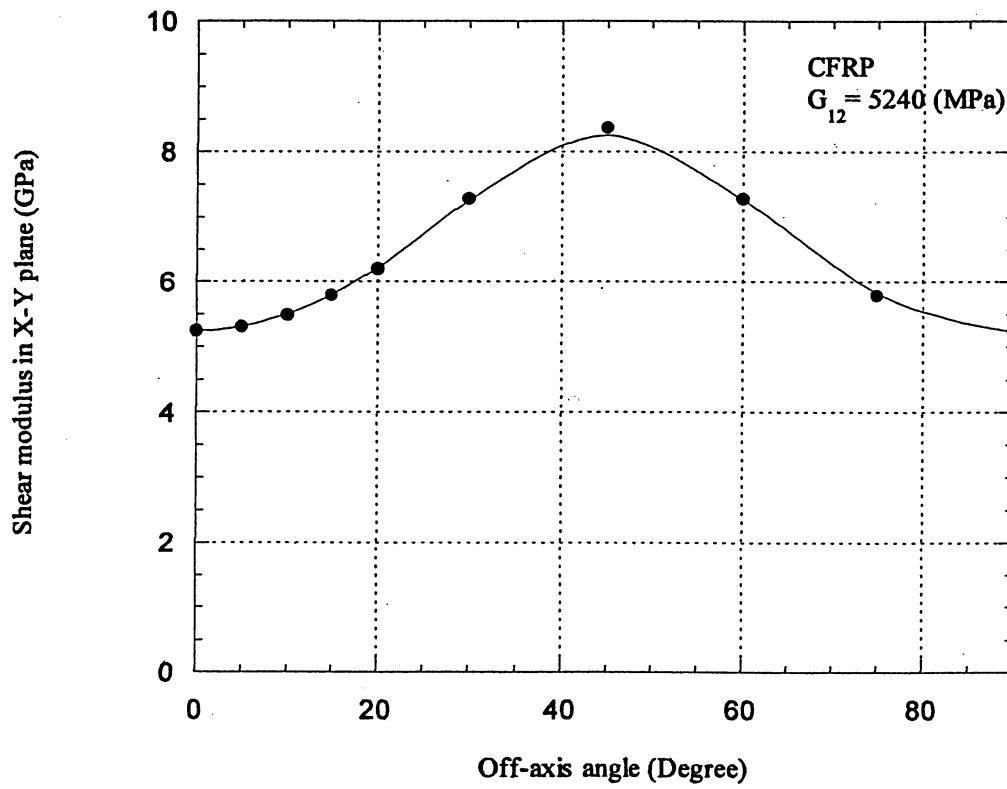


Figure 3.8: The Shear modulus response as off-axis angle changes for a typical unidirectional CFRP

CHAPTER FOUR

Fatigue Damage Analysis and modeling for GRP and CFRP composites

4.1 Fatigue Damage Mechanism in FRP Composites

Under cyclic loading, damage will accumulate in composite materials and cause the fracture or functional failure of structures. For homogeneous or monolithic materials with isotropic material properties, damage is accumulated at a low growth rate in the beginning, and a single crack propagates in a direction perpendicular to the cyclic loading axis. On the other hand, in composite materials, especially for those structures with multiple plies and laminates, the fracture behavior is characterized by multiple damage modes of crazing and cracking of the matrix, fiber/matrix decohesion, and fiber fracture. The mechanisms of crack initiation and crack growth are quite complex for composite materials. For a unidirectional laminate under cyclic loading the damage mechanisms can be divided into three regions as shown in figure 4.1. Since inter-fiber fracture is caused by normal and shear components only, considering these two terms is sufficient. In the region I cracks initiate in the matrix when shear component is dominant. These cracks propagate in the same plane and direction (direction 2) perpendicular to the fiber alignments. In the region II, when the crack is blocked by the fiber, the crack grows in the direction 1 (parallel to the fiber) and fiber/matrix interaction must be accounted (shear and normal stress components). The third region or fiber cracking occurs when the normal stress component is dominant.

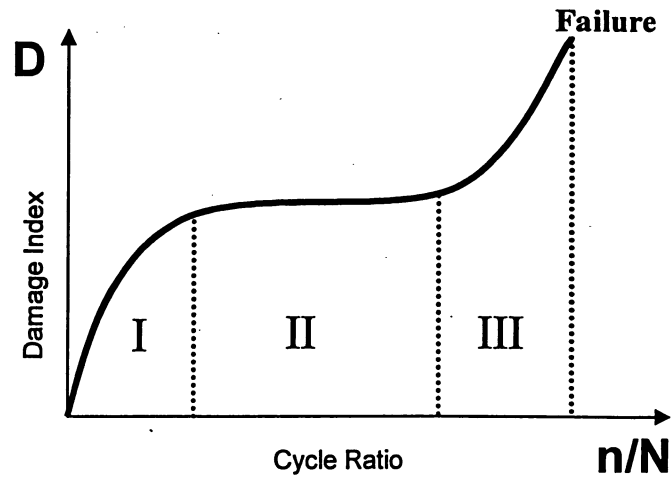


Figure 4.1: Three regions of cracking in unidirectional FRP composites: (I) matrix cracking, (II) matrix-fiber cracking, and (III) fiber failure [25].

4.2 The Proposed Fatigue Damage Model in this Thesis

This study develops a fatigue damage criterion based on the physics and the mechanism of cracking in three regions of matrix, matrix-fiber interface, and fiber (see Figure 4.1). The proposed model characterizes the damage progress in described regions based on the strain energy criterion developed earlier by Varvani-Farahani [40] and a criterion by Plumtree-Cheng [7]. The elements of the fatigue damage model in this study for the three main cracking regions are described as follow:

Region I damage:

Fatigue damage progress in region I involves cracks initiating in the matrix where the shear components are dominant. These cracks propagate in direction 2 (perpendicular to the fiber direction). Varvnai [40] described fatigue analysis using the concept of critical plane of maximum shear strain and stress based on the fracture mode or the initiation mechanism of cracks. The parameter is given by the sum of the normal energy range and the shear energy range calculated for the critical plane at which the stress and the strain Mohr's circles are the largest during the loading and unloading parts of a cycle. Matrix failure is dominant in Region I can be represented by Eq 4.1.

$$\Delta W_I = \left[\frac{\Delta \tau_{\max} \Delta \frac{\gamma_{\max}}{2}}{\tau_{ULT} \left(\frac{\tau_{ULT}}{G_m} \right)} \right] \quad (4.1)$$

where $\Delta \tau_{\max}$ and $\Delta \gamma_{\max}/2$ are the range of maximum shear stress and shear strain obtained from the largest stress and strain Mohr's circles during the loading and unloading parts of a cycle and ΔW_I is the proposed fatigue damage parameter in region I.(see region III)

Region III damage:

Fatigue damage progress in region III involves fiber cracking when the normal stress component is dominant. Normal stress and strain components in direction 1 are responsible for brittle fiber failure. Similarly in region III, The corresponding normal stress range $\Delta \sigma_n$ and normal strain range $\Delta \varepsilon_n$ obtained from the largest stress and strain Mohr's circles using Varvani's [40] approach and can be represented by Eq 4.2:

$$\Delta W_{III} = \left[\frac{\Delta \sigma_n \Delta \varepsilon_n}{\sigma_{ULT} \left(\frac{\sigma_{ULT}}{E_f} \right)} \right] \quad (4.2)$$

where ΔW_{III} is the proposed fatigue damage parameter in region III and the range of maximum shear strain and the corresponding normal stress and strain range on the critical plane at which both strain and stress Mohr's cycles are the largest during loading (at the angle θ_1) and unloading (at the angle θ_2) of a circle are shown in figure 4.2 and calculated by Eq 4.3 and 4.4 [52].

$$\Delta \left(\frac{\gamma_{\max}}{2} \right) = \left(\frac{\varepsilon_1 - \varepsilon_3}{2} \right)_{\theta_1} - \left(\frac{\varepsilon_1 - \varepsilon_3}{2} \right)_{\theta_2} \quad (4.3)$$

$$\Delta \varepsilon_n = \left(\frac{\varepsilon_1 + \varepsilon_2}{2} \right)_{\theta_1} - \left(\frac{\varepsilon_1 + \varepsilon_3}{2} \right)_{\theta_2} \quad (4.4)$$

ε_1 , ε_2 , and ε_3 are the principal strain values ($\varepsilon_1 > \varepsilon_2 > \varepsilon_3$) which are calculated from Mohr's circle (see figure 4.2) in equations 4.5, 4.6, and 4.7:

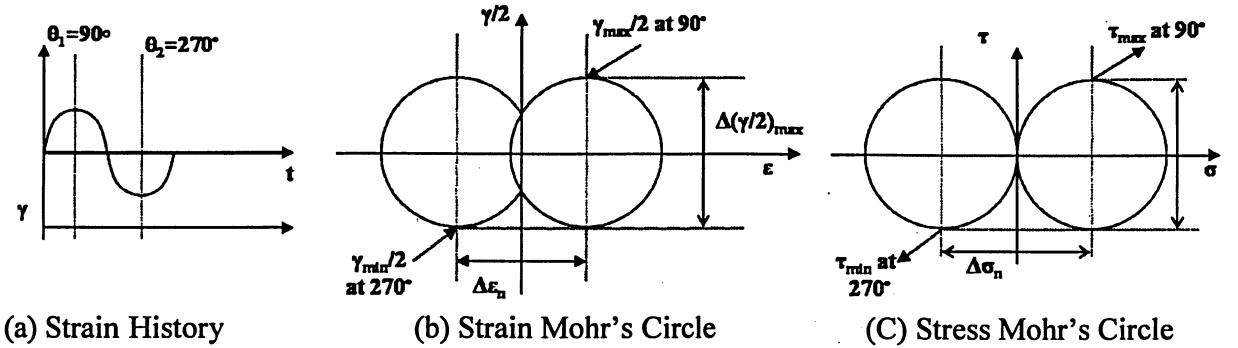


Figure 4.2: Strain history, strain Mohr's circles, and stress Mohr's circles for uniaxial loading condition [40].

$$\varepsilon_1 = (1 - \nu_{eff}) \frac{\varepsilon_{ap}}{2} + \frac{1}{2} \left[\varepsilon_{ap}^2 (1 + \nu_{eff})^2 + \left(\frac{\gamma_{ap}}{2} \right)^2 \right]^{1/2} \quad (4.5)$$

$$\varepsilon_2 = -\nu_{eff} \varepsilon_{ap} \quad (4.6)$$

$$\varepsilon_3 = (1 - \nu_{eff}) \frac{\varepsilon_{ap}}{2} - \frac{1}{2} \left[\varepsilon_{ap}^2 (1 + \nu_{eff})^2 + \left(\frac{\gamma_{ap}}{2} \right)^2 \right]^{1/2} \quad (4.7)$$

Similarly, the range of maximum shear stress and the corresponding normal stress Mohr's circle during loading (at the angle θ_1) and unloading (at the angle θ_2) of a cycle are given in equations 4.8 and 4.9 :

$$\Delta\tau_{\max} = \left(\frac{\sigma_1 - \sigma_3}{2} \right)_{\theta_1} - \left(\frac{\sigma_1 - \sigma_3}{2} \right)_{\theta_2} \quad (4.8)$$

$$\Delta\sigma_n = \left(\frac{\sigma_1 + \sigma_2}{2} \right)_{\theta_1} - \left(\frac{\sigma_1 + \sigma_3}{2} \right)_{\theta_2} \quad (4.9)$$

where σ_1 , σ_2 , and σ_3 are the principal stress values ($\sigma_1 > \sigma_2 > \sigma_3$) and they calculated from the stress Mohr's circle (see figure 4.2) in equations 4.10 and 4.11:

$$\sigma_1 = \frac{\sigma_a}{2} + \frac{1}{2} [\sigma_a^2 + 4\tau_a^2]^{1/2} \quad (4.10)$$

$$\sigma_2 = 0 \text{ (Plane stress condition)}$$

$$\sigma_3 = \frac{\sigma_a}{2} - \frac{1}{2} [\sigma_a^2 + 4\tau_a^2]^{1/2} \quad (4.11)$$

In this approach both the shear and normal strain energies are weighted by the ultimate shear strength (τ_{ULT})_m and the shear modulus (G_m) of the matrix in region I and the ultimate tensile strength (σ_{UTL})_f and the Young's modulus of the fiber (E_f) in region III.

Region II damage:

Fatigue damage progress in region II involves shear cracking along the interface of matrix –fiber. Stress and strain components normal to the fiber direction (direction 2) is responsible for the opening of the crack and the shear stress and strain components along 1-2 direction cause decohesion and crack progresses along the sliding direction. Plumtree and Cheng [7] described the damage progress based on energy concept for normal mode (direction 2) and sliding mode (direction 1-2). For region II, a modified Plumtree-Cheng model is expressed as:

$$\Delta W_{II} = \left[\frac{\Delta \tau_{12} \Delta \frac{\gamma_{12}}{2}}{\tau_{ULT} \left(\frac{\tau_{ULT}}{G_m} \right)} + \frac{\Delta \sigma_{22} \Delta \varepsilon_{22}}{\sigma_{ULT} \left(\frac{\sigma_{ULT}}{E_F} \right)} \right] \quad (4.12)$$

where $\Delta \sigma_{22}$, $\Delta \varepsilon_{22}$ and $\Delta \tau_{12}$, $\Delta \gamma_{12}$ are the range of normal stress and strain, and the range of shear stress and strain acting parallel to fibers in region II, respectively.

Three regions of cracking have been illustrated in figure 4.3. Shear and normal energies in the brackets of equations 4.1, 4.2 and 4.12 have been weighted for different off-axis angles θ and resulted in Eq 4.13 a, b and c (see Eq 3.23).

$$\Delta W_I = \sin \theta \cos \theta \left[\frac{\Delta \tau_{\max} \Delta \frac{\gamma_{\max}}{2}}{\tau_{ULT} \left(\frac{\tau_{ULT}}{G_m} \right)} \right] \quad (4.13 \text{ a})$$

$$\Delta W_{II} = \left[(\sin \theta \cos \theta) \frac{\Delta \tau_{12} \Delta \frac{\gamma_{12}}{2}}{\tau_{ULT} \left(\frac{\tau_{ULT}}{G_m} \right)} + (\cos^2 \theta) \frac{\Delta \sigma_{22} \Delta \varepsilon_{22}}{\sigma_{ULT} \left(\frac{\sigma_{ULT}}{E_f} \right)} \right] \quad (4.13 \text{ b})$$

$$\Delta W_{III} = \cos^2 \theta \left[\frac{\Delta \sigma_n \Delta \varepsilon_n}{\sigma_{ULT} \left(\frac{\sigma_{ULT}}{E_f} \right)} \right] \quad (4.13 \text{ c})$$

The total fatigue damage in unidirectional GRP and CFRP composites is calculated by accumulating damage progress of above three regions represented in Eq 4.14:

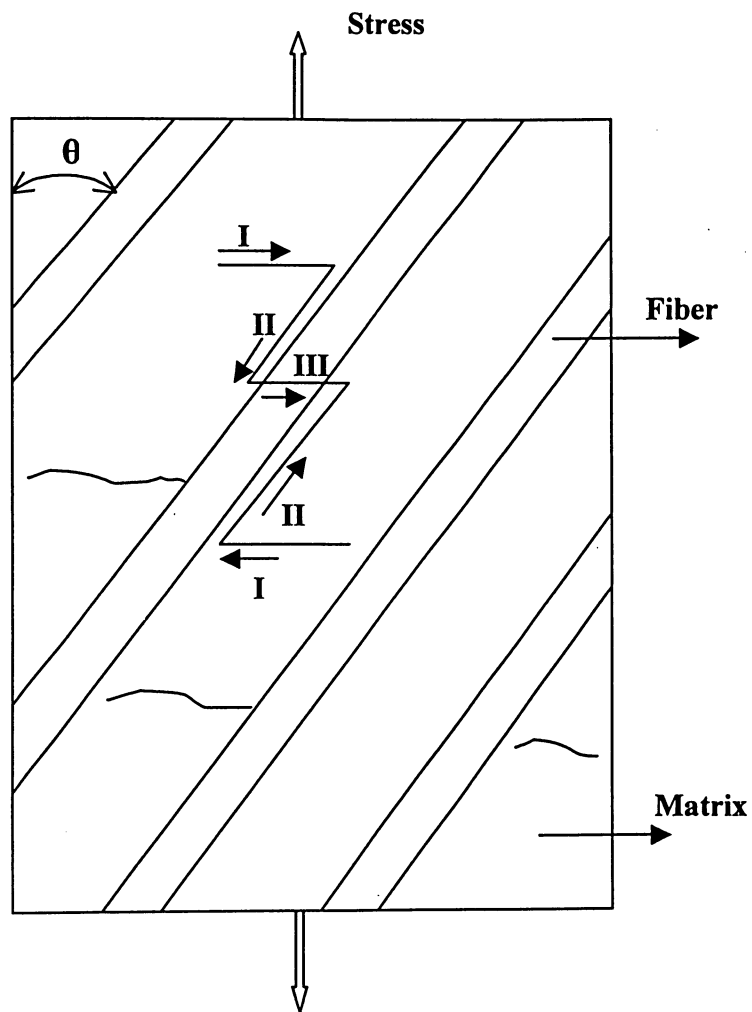


Figure 4.3: Three regions of cracking mechanism in unidirectional composites.

$$\Delta W = \Delta W_I + \Delta W_{II} + \Delta W_{III} \quad (4.14)$$

The proposed fatigue damage model (see Eqs 4.13 a, b, and c) was weighted for various off-axis angles by normalizing Eq 14.4 by $\cos^2\theta$. This further unified the damage magnitude at different off-axis angles in both GRP and CFRP composites studied in this thesis.

4.3 Fatigue Damage Analysis Procedures and Methodology

Figure 4.4 represents the procedures of fatigue damage analysis of unidirectional GRP and CFRP composites based on the proposed damage method in this thesis. Fatigue damage model developed in this study includes damage progress in three regions of the matrix, the matrix-fiber interface, and the fiber and reflects the cracking mechanisms within these regions from the early stage of growth to final failure. This figure shows the procedure of damage analysis in the following rational steps:

- (i) S-N curves and the material properties of unidirectional GRP and CFRP composites for various off-axis angles are required as the initial step of the analysis,
- (ii) Principal stress and strain components were calculated and the largest Mohr's circles were found to describe the damage within the matrix in region I and the fibers in region III based on Varvani's fatigue damage model,
- (iii) Fatigue damage in region II was calculated using the normal and in-plane stress and strain components based on Plumtree-Cheng,
- (iv) Fatigue damage was calculated from the accumulation of damage for region I, II, and III through stages (ii) and (iii),
- (v) The damage model developed in stage (iv) was weighted for various off-axis angles. This step unifies the fatigue ΔW -N data for different off-axis angles to enable more accurate life prediction results.

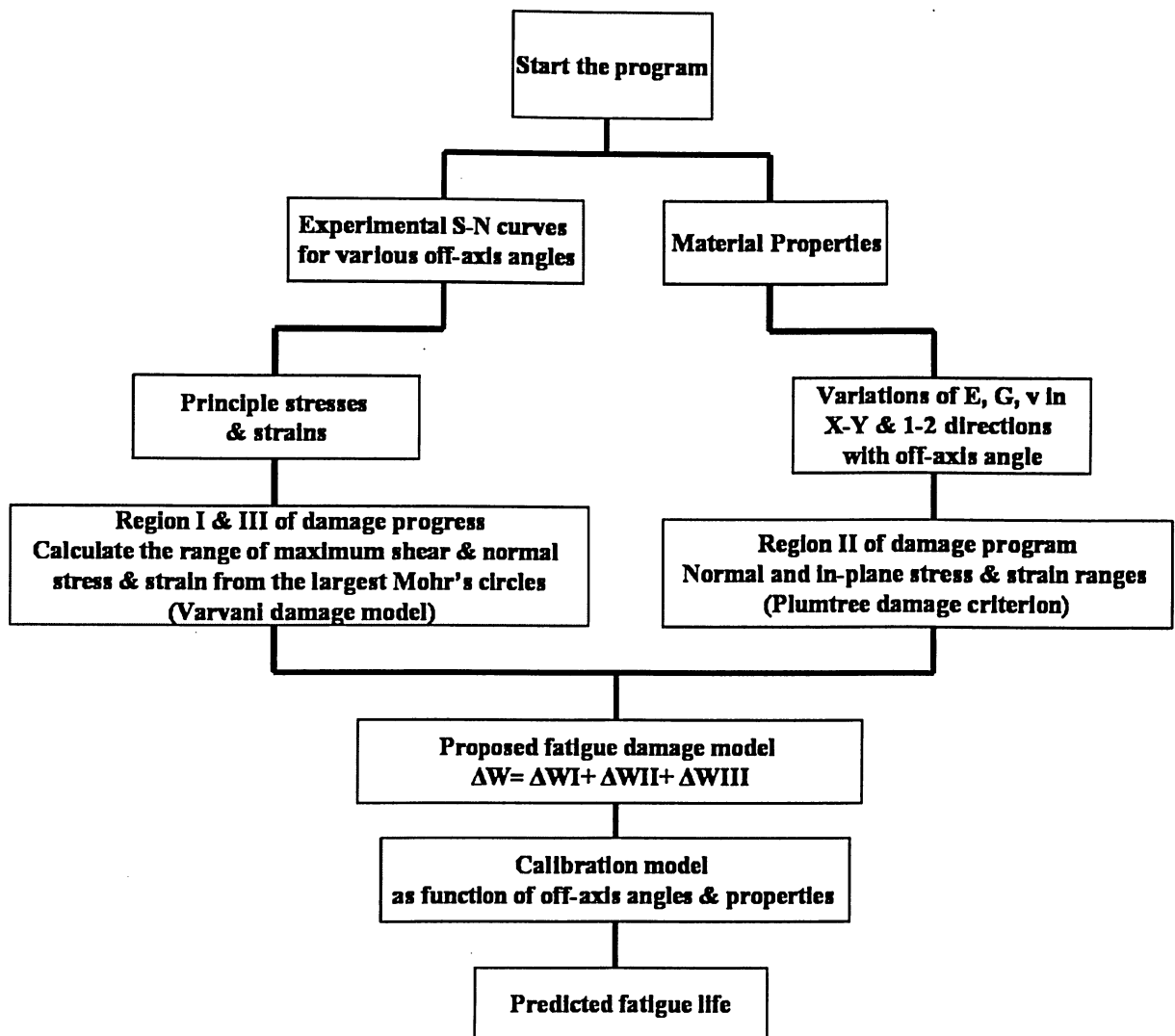


Figure 4.4: Procedure of fatigue damage analysis for unidirectional GRP and CFRP composites.

CHAPTER FIVE

Fatigue Damage Assessment Results of Unidirectional GRP and CFRP Composites

This chapter discusses results of fatigue damage assessment using the proposed model in this thesis. The available experimental data are first converted to terms required in the model and accordingly the values are substituted in the model. This chapter evaluates the model with unidirectional GRP and CFRP data obtained at different off-axis angles and (R) ratios.

5.1 GRP and CFRP Fatigue Data

To evaluate the fatigue damage model proposed in this thesis, fatigue data of unidirectional GRP and CFRP composites at various angles and R-ratios have been extracted through the literature. Appendix A consists of material properties, fatigue stress-life data at various off-axis angles tested at different R-ratios and by different laboratories.

5.1.1 Hashin and Rotem Data

The experimental program consisted of fatigue testing of off-axis fibers unidirectional reinforced polymers under uniaxial tension. The material tested was composed of E-glass fibers with the volume fraction of 0.6 and epoxy matrix. Single and roving of E-glass fibers (Gevetex Es 13-320X1-K921) and epoxy resin (Bakeelite ERL 2256 with 27 pbw of ZZL0820) were used to fabricate unidirectional plates. To obtain off-axis specimens rectangular strips of 19mm width were cut from the plates with a diamond wheel saw at different angles with respect to fiber direction. Aluminum tabs were glued to the specimens with epoxy resin in order to provide gripping surfaces for testing. The length of specimens was limited by the dimensions of the plates off which they were cut out. The free lengths of specimens between the extremities of the aluminum tabs were 100mm. The free length-to-width ratio was 5.26. Having obtained off-axis

static strengths at various fiber angles (5, 10, 15, 20, 30, 60 degree), specimens were tested to fatigue failure under stress amplitudes smaller than static strength. Specimens were tested up to 10^6 cycles for three different frequencies of cycling: 34, 19 and 1.8 Hz. The stress ratio in almost all of the tests was $R=0.1$ (ratio of minimum-to-maximum stress) [3].

5.1.2 Ellyin and El Kadi Data

Fatigue behavior of unidirectional glass fiber/epoxy composite laminate under tension-tension and tension-compression loading was investigated. Stress-Life experimental data were obtained for fiber orientation angle, θ , of 0, 19, 45, 71, and 90° where θ is the angle between the fiber direction and the direction of the applied load. The material used was Scotchly Reinforced Plastic Type 1003, a 3M product. This composite is a non-woven, glass fiber-reinforced epoxy resin material designed for high performance structural applications. ASTM D3039 is the only available standard to test fiber-reinforced composites under tension-tension fatigue loading. The thickness of the specimens with $\theta = 19, 45, 71, 71$, and 90° was 5mm (0.2 in) consisting 20 layers. The thickness of the 0° specimen was 12.5mm (0.5 in). The specimen length and width were 145mm and 12.5mm. Aluminum tabs were glued to the ends of the specimens for gripping purposes. Fatigue tests were conducted using a loading frequency of 3.3 Hz. These tests were performed under stress ratios of 0.5, 0, and -1 [6].

5.1.3 Xiao and Bathias Data

Fatigue behavior of non-woven glass fiber/epoxy composite laminate under tension-compression loading was investigated. Stress-Life experimental data were obtained for off-axis angles, θ , of 0, 19, 45, 71, and 90° where θ is the angle between the fiber direction and the direction of the applied load. The epoxy resin system was E51, and supplied by Hexcel-Genin in France. The volume fraction of E-Glass fibers was 60%. All specimens were cut from 600mm×600mm plates. The fatigue specimens had 300 mm length and 25 mm width and 3.3 mm thickness [44]. The ends of each specimen were bonded by E-Glass-fabric/epoxy plates. These plates had 1 mm thickness and 75 mm length. The fatigue tests were carried out with a sinusoidal loading frequency of 20Hz and a stress ratio of $R=-1$.

5.1.4 Zheng-Ming Data

Fatigue behavior of unidirectional graphite fiber/epoxy composite laminate under tension-tension loading was investigated. Stress-Life experimental data were obtained for off-axis angles, θ , of 0, 10, 20, 45, 60, and 90° [41]. The material used was graphite-epoxy (AS/350-5A) unidirectional lamina, with a fiber volume fraction of 0.7. These tests were performed under stress ratios of 0.1 and cycling frequencies of 18 Hz. Specimen dimensions were determined according to the specification of ASTM D3039-76. The 2.1 mm thick panels were cut by diamond blade cutting machine with water cooling into fatigue testing of specimens 240mm length by 25.4mm width. The 1.5 mm thick copper plate was used for the gripping parts of specimens.

5.1.5 Kawai Data

The unidirectional carbon-epoxy laminates used in this study were fabricated from prepreg tapes of P2053-17 (T800H/2500, TORAY). The lay-up of virgin laminates is 0 degree consisting of 12 layers. The volume fraction of fibers was 0.64. Six kinds of plain coupon specimens with different fiber orientations ($\theta=0, 10, 15, 30, 45$, and 90°) were cut from 400mm by 400mm panels. The shape and dimensions of the off-axis coupon specimens are based on the testing standards JIS K 7083 and ASTM D3479 [42], the specimen length, the gauge length, and the thickness were 200 mm, 100 mm, and 2 mm, respectively. The specimen width was 10mm for the fiber direction 0°, and 20mm for other orientations. Rectangular-shaped aluminum alloy tabs were bonded on both ends of the specimens using epoxy adhesive (Araldite). The thickness of the end-tabs was 1.0 mm.

Constant amplitude off-axis fatigue tests were performed in load-control condition under different stress ratios of 0.1, 0.5, and -1 at room temperature. The specimens were fatigue tested for up to 10^6 cycles. In principle, one specimen was tested at each fatigue stress level for every fiber orientation. Fatigue load was applied in a sinusoidal waveform with a frequency of 10 Hz. Tension-compression fatigue tests ($R<0$) were conducted using antibuckling guide fixtures based on JIS K7076. The ant buckling guide fixtures were made of Al alloy (2024-T3) and the dimensions were 94mm long, 44mm wide, and 5mm thick [14].

5.2 Evaluation of Proposed Fatigue Damage Model

The above experimental fatigue data for GRP and CFRP composites were extracted from the literature [6, 3, 41, 14, 43] and were applied to evaluate the proposed model in this thesis. Figures 5.1- 5.9 a, b show a comparison between the proposed model and S-N diagram in Log-Log scale, respectively. Comparison of part (a) and part (b) of these figures shows how successfully the proposed damage model can unify the fatigue data of GRP and CFRP composites with various off-axis angles and R-ratios.

To further discuss the width of the scatter range in fatigue strength of GRP and CFRP presented in figures 5.1- 5.9, at the given life of 10^5 cycles, the upper limit and the lower limit were denoted by y_U and y_L , respectively on the upper and lower bounds (see Figure 5.1). The ratio of $\frac{y_U}{y_L}$ for GRP and CFRP composites are presented in Table 5.1. The smaller ratios achieved using the proposed damage model in this thesis resulted in a better fatigue data correlation for both unidirectional GRP and CFRP composites at various off-axis angles. This ratio varies between 2.0-3.0 for GRP data and 1.9-3.4 for CFRP data when correlated by the proposed damage model which successfully correlated fatigue lives of GRP and CFRP composites. The proposed damage model capability in correlating fatigue data is noticeable when the stress-life curve (part (a)) is compared with the proposed model correlation results (Part (b)) in figures 5.1- 5.9.

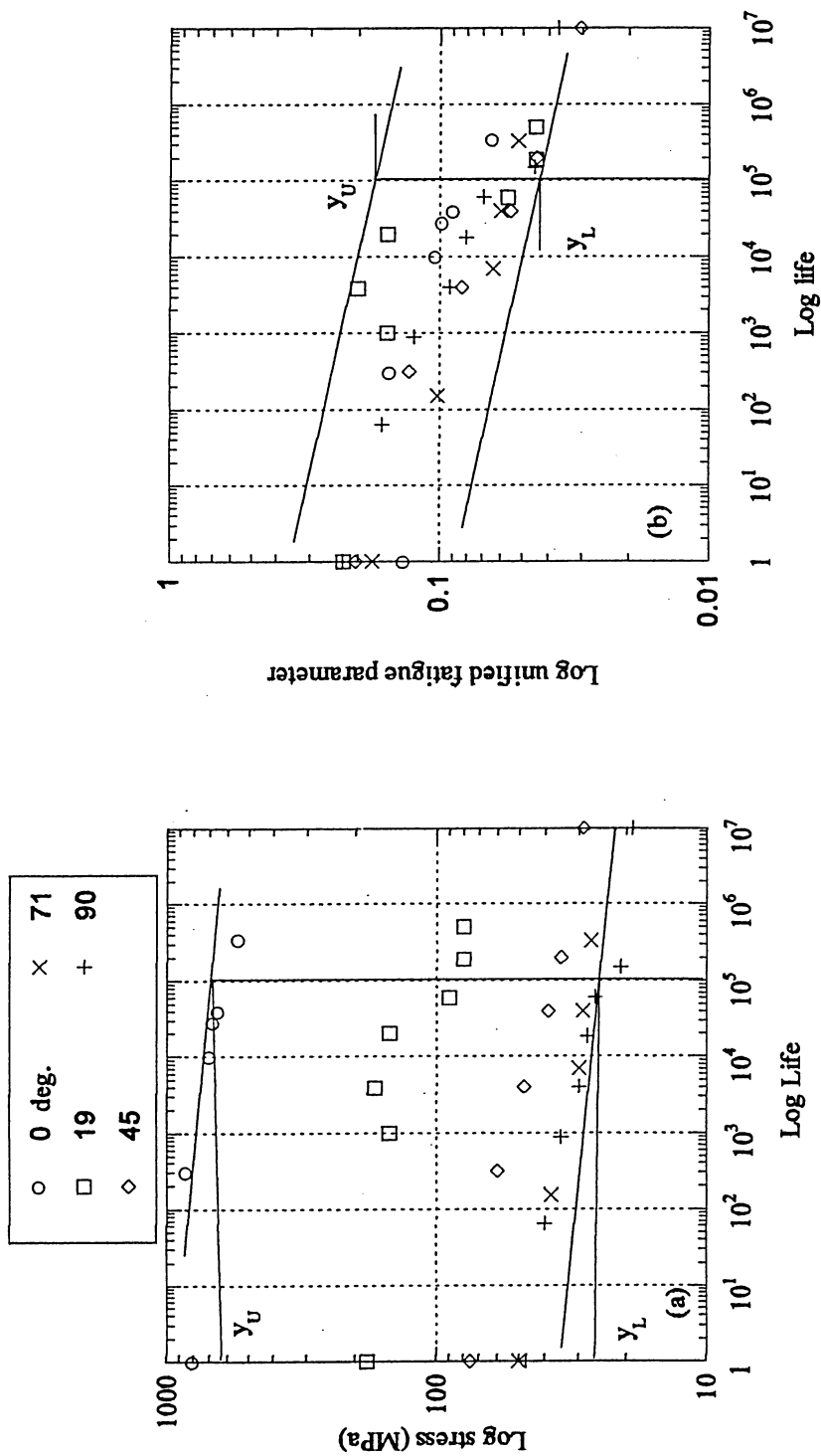


Figure 5.1: Experimentally obtained fatigue lives of GRP composite of Ellyin-El Kadi [6] at various off-axis angles and $R = 0$: (a) stress-fatigue life, and (b) the proposed fatigue damage parameter versus life.

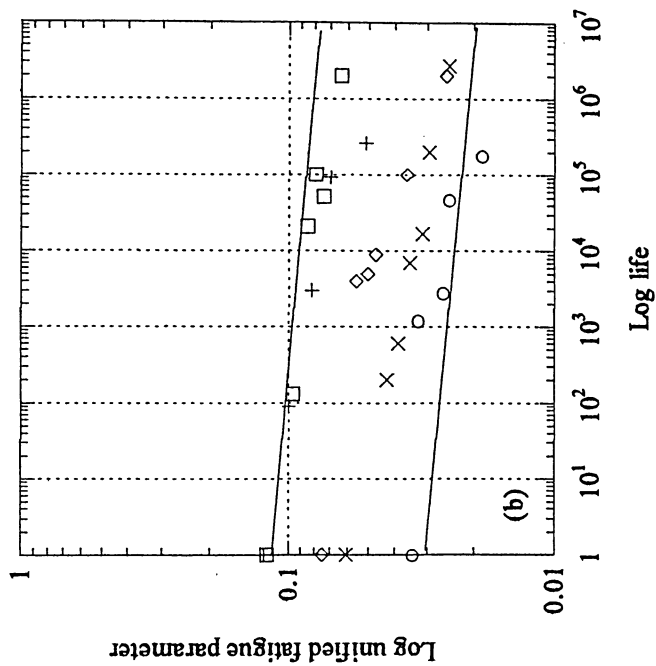
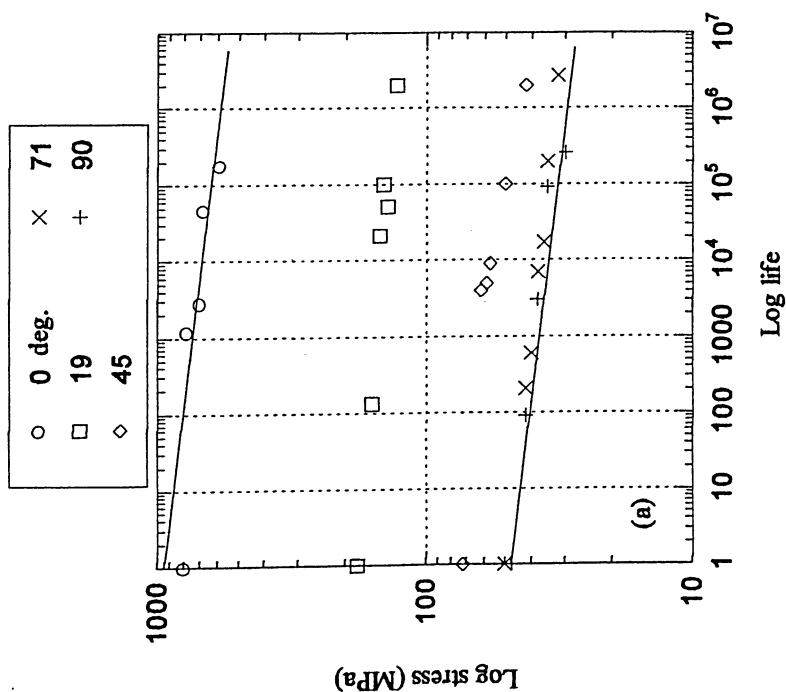


Figure 5.2: Experimentally obtained fatigue lives of GRP composite of Ellyin-El Kadi [6] at various off-axis angles and $R = 0.5$: (a) stress-fatigue life, and (b) the proposed fatigue damage parameter versus life.

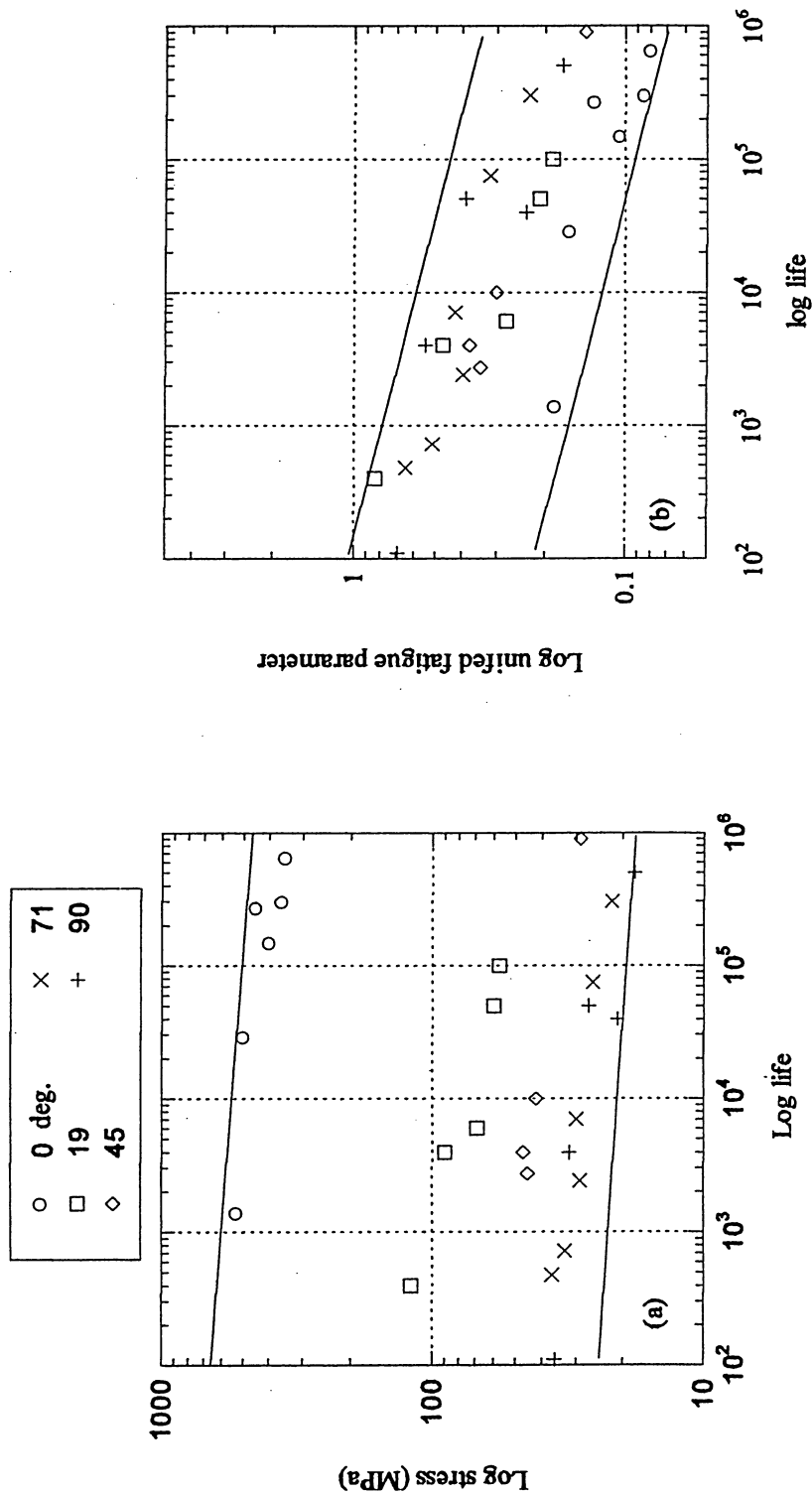


Figure 5.3: Experimentally obtained fatigue lives of GRP composite of Ellyin-El Kadi [6] at various off-axis angles and $R = -1$: (a) stress-fatigue life, and (b) the proposed fatigue damage parameter versus life.

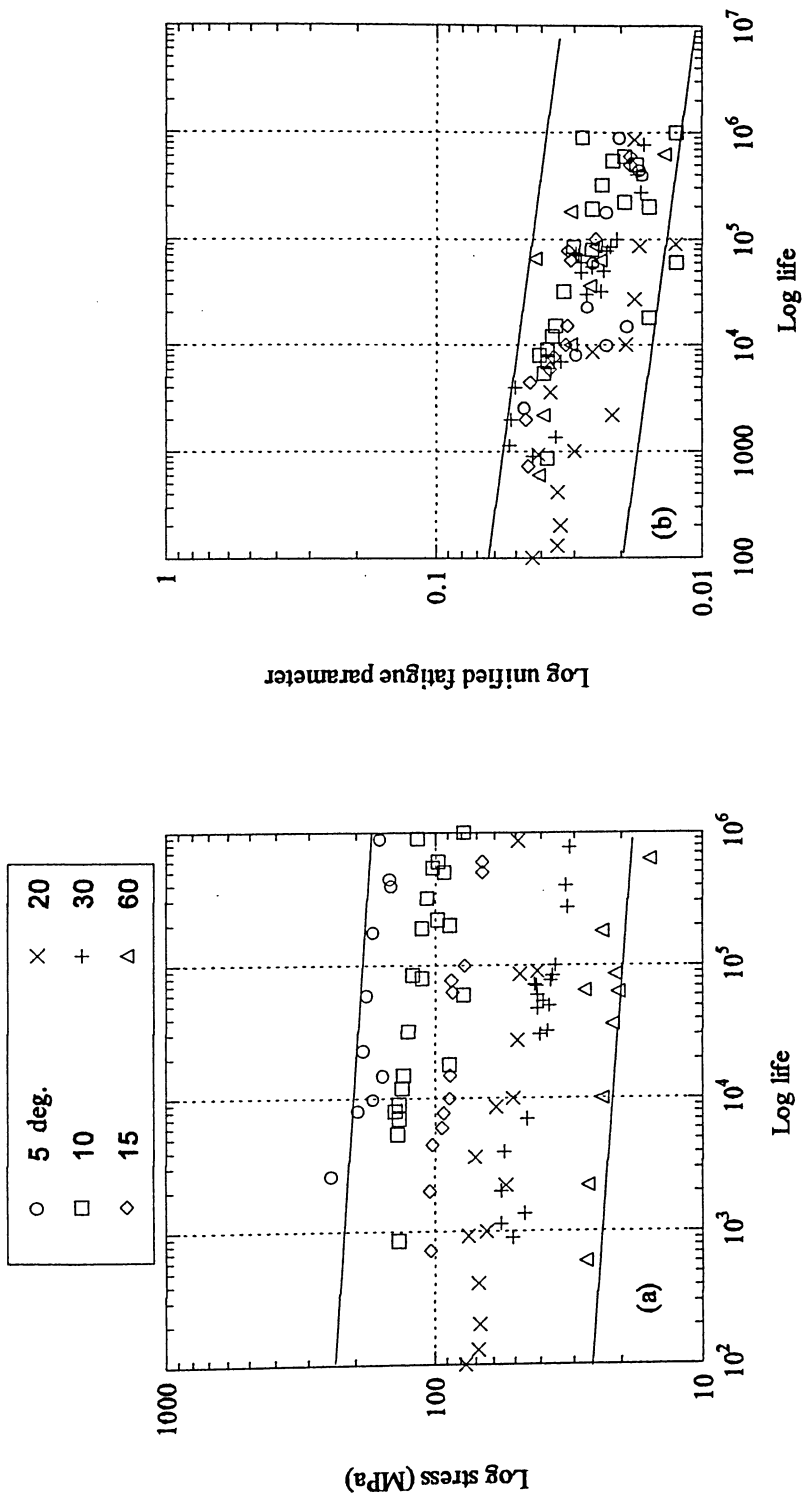


Figure 5.4: Experimentally obtained fatigue lives of GRP composite of Hashin-Rotem [3] at various off-axis angles and $R = 0.1$: (a) stress-fatigue life, and (b) the proposed fatigue damage parameter versus life.

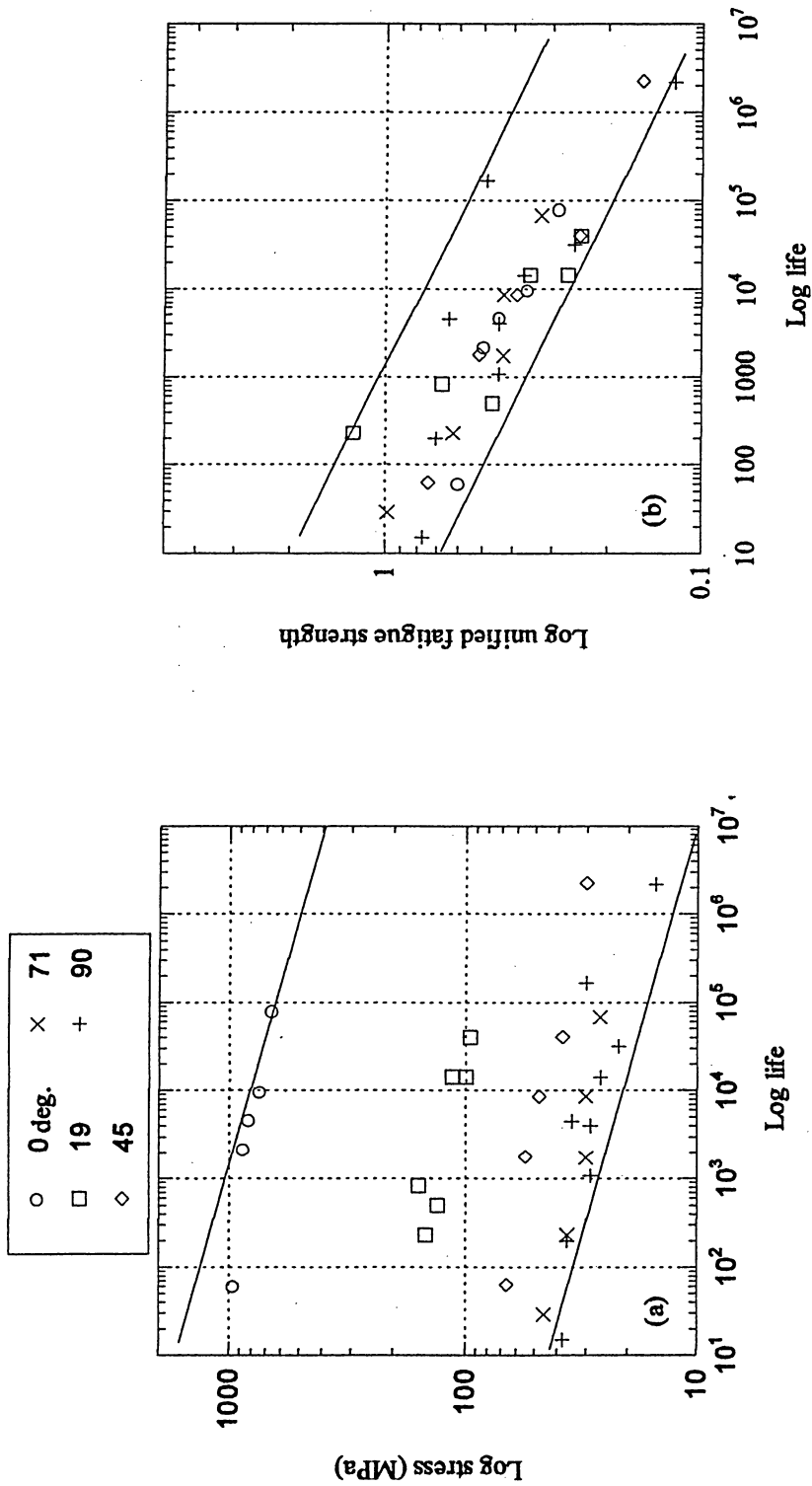


Figure 5.5: Experimentally obtained fatigue lives of GRP composite of Xiao-Bathias [33] at various off-axis angles and $R = -1$: (a) stress-fatigue life, and (b) the proposed fatigue damage parameter versus life.

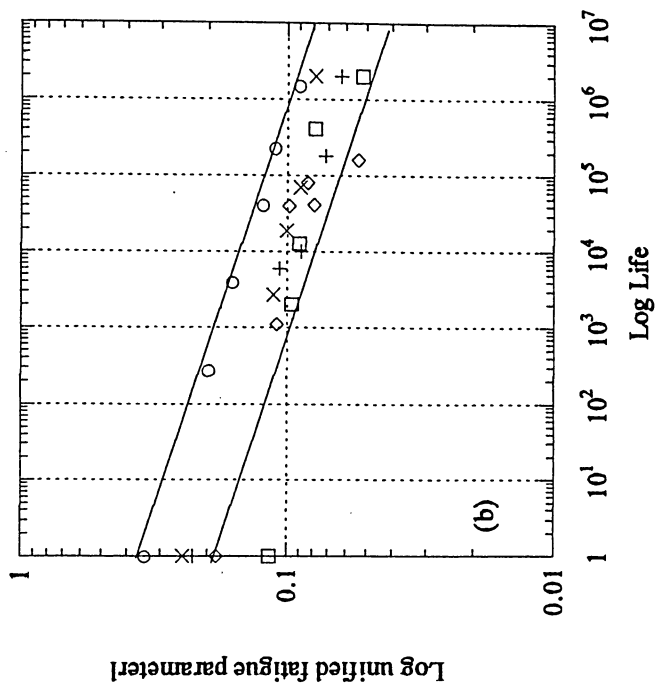
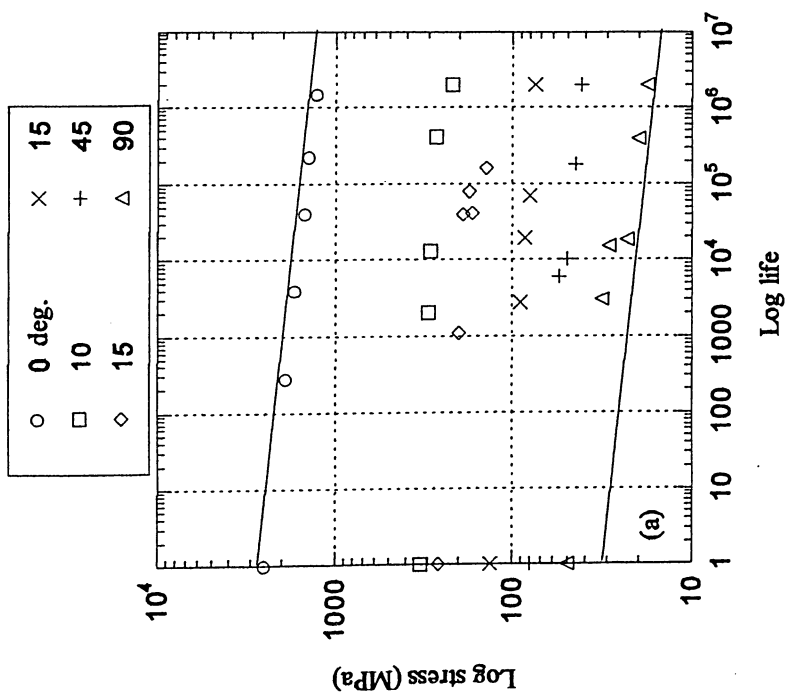


Figure 5.6: Experimentally obtained fatigue lives of CFRP composite of Kawai [14] at various off-axis angles and $R = 0.1$: (a) stress-fatigue life, and (b) the proposed fatigue damage parameter versus life.

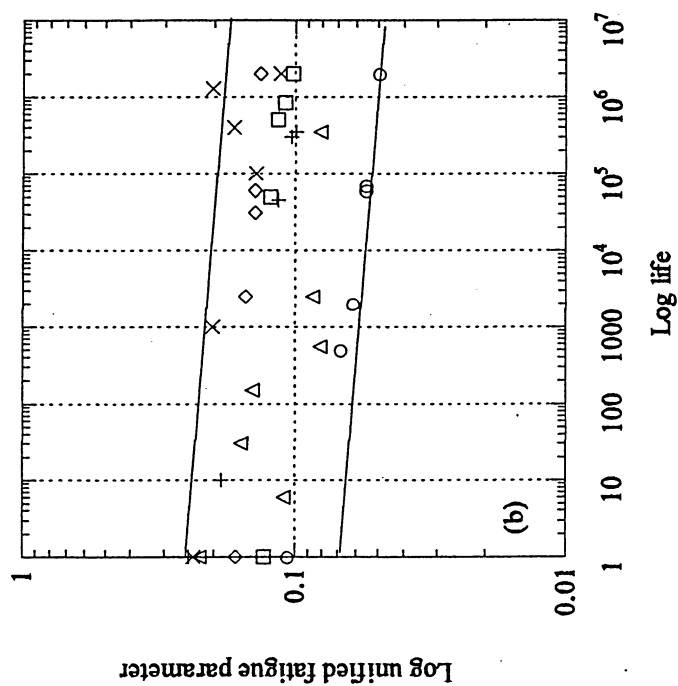
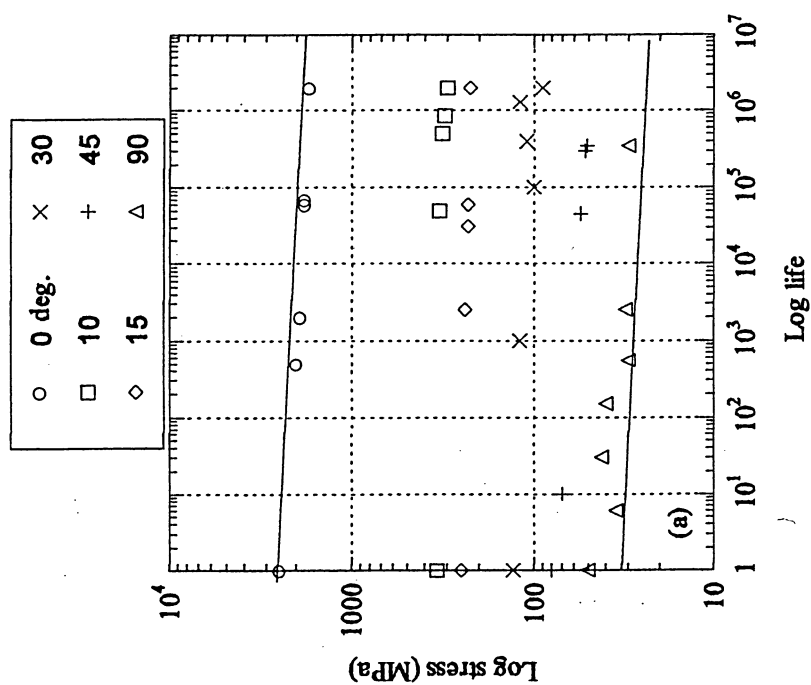


Figure 5.7: Experimentally obtained fatigue lives of CFRP composite of Kawai [14] at various off-axis angles and $R = 0.5$: (a) stress-fatigue life, and (b) the proposed fatigue damage parameter versus life.

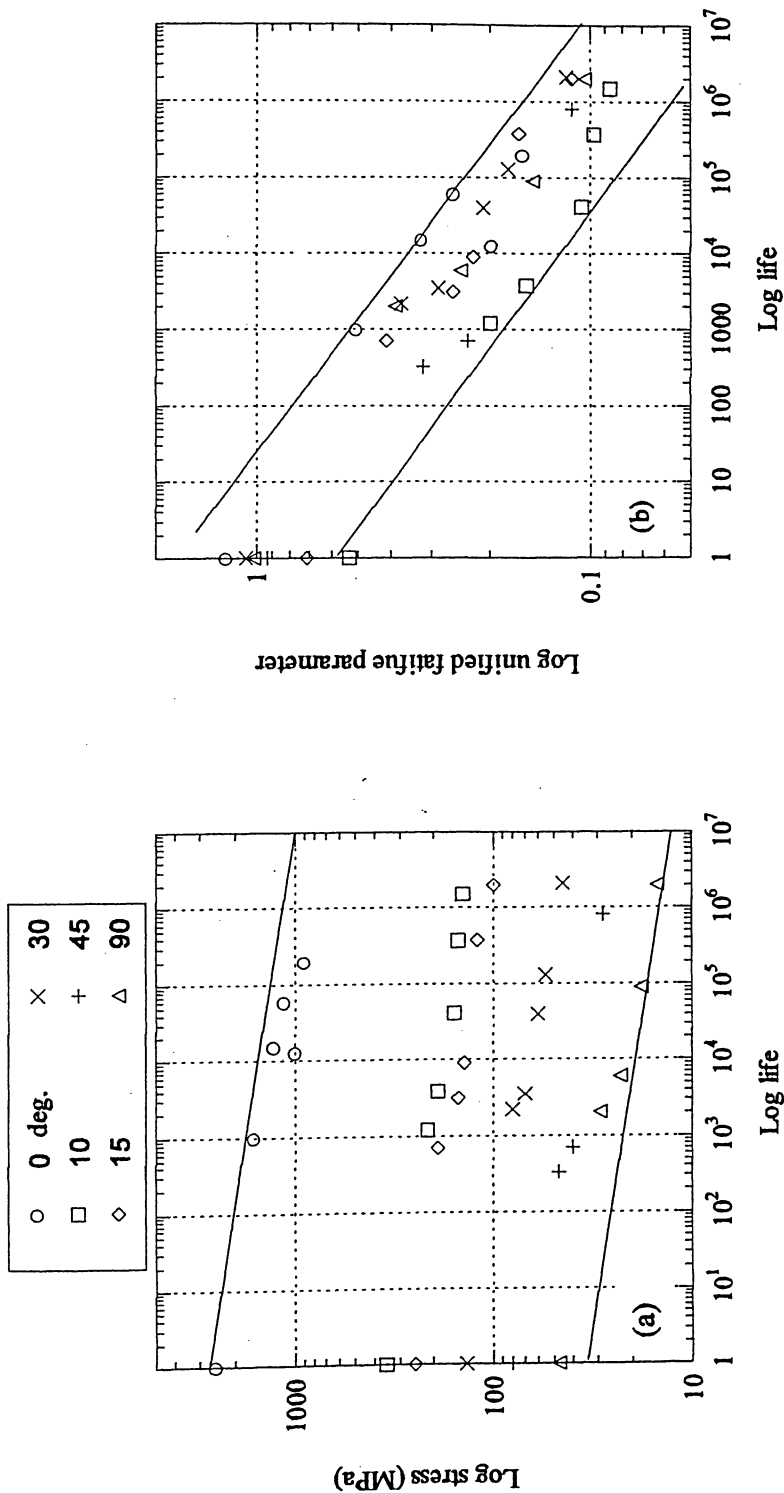


Figure 5.8: Experimentally obtained fatigue lives of CFRP composite of Kawai [14] at various off-axis angles and $R = -1$: (a) stress-fatigue life, and (b) the proposed fatigue damage parameter versus life.

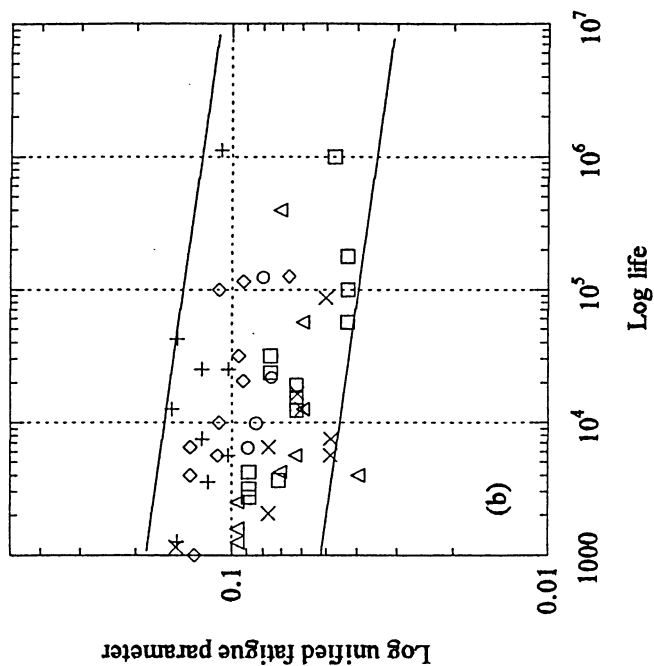
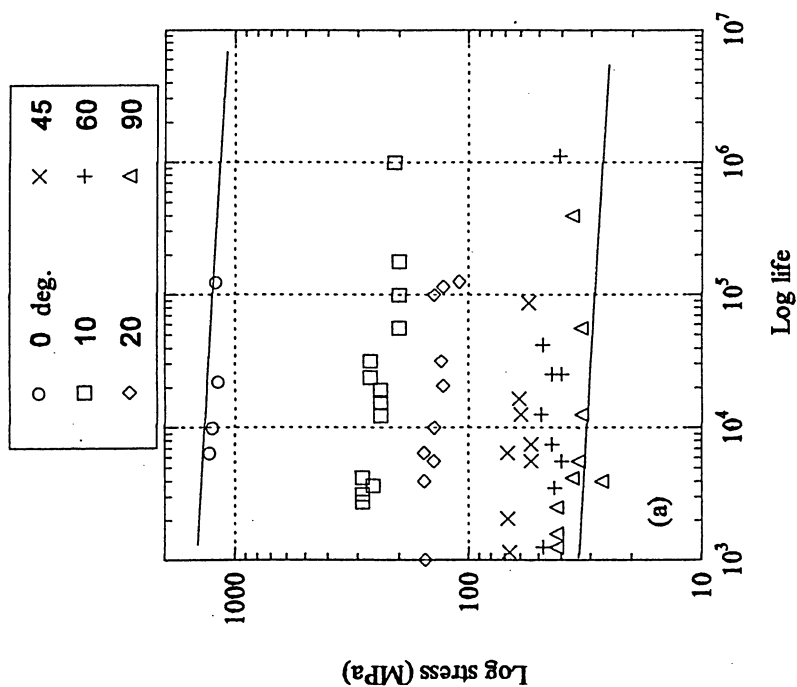


Figure 5.9: Experimentally obtained fatigue lives of CFRP composite of Zheng-Ming [4] at various off-axis angles and $R = 0.1$: (a) stress-fatigue life, and (b) the proposed fatigue damage parameter versus life.

Table 5.1: Table of evaluation of the proposed model in fatigue data correlation of unidirectional GRP and CFRP composites

Fatigue damage model	$\frac{\gamma_U}{\gamma_L}$ for GRP					$\frac{\gamma_U}{\gamma_L}$ for CFRP			GRP			CFRP	
	Ellyin data R=0	Ellyin data R=0.5	Ellyin data R=-1	Hashin data R=0.1	Xiao data R=-1	Kawai data R=0.1	Kawai data R=0.5	Kawai data R=-1	Zheng data R=0.1	Mean value	Standard deviation error%	Mean value	Standard deviation error%
Proposed model	2.9	2.8	2	3	2.6	1.9	3.1	2	3.4	2.66	0.18	2.6	0.38
S-N data	25.7	20.2	25.7	9.3	39	86	77.25	77.27	44.5	23.98	10.74	71.25	18.3

$$\text{Mean Value} = \bar{x} = \frac{\sum_i^n x_i}{n}, \text{Standard Deviation} = \sqrt{\frac{\sum_i^n (x_i - \bar{x})^2}{n-1}}$$

$$\text{Standard Deviation Error} = \frac{\text{Standard Deviation}}{\sqrt{n}}$$

CHAPTER SIX

Evaluation of Proposed Damage Model and Discussion

There have been many attempts to develop life-prediction methods for FRP composites, but the complexity of the response of these materials to stress makes it very difficult to develop universally applicable models.

Fatigue analysis using the concept of critical plane of maximum shear strain is [45- 48] very effective because the critical plane concept is based on the fracture mode or the initiation mechanism of cracks. In the critical plane concept, after determining the maximum shear strain plane, many researchers define fatigue parameters as combinations of the maximum shear strain (or stress) and normal strain (or stress) and on that plane to explain fatigue behavior.

Based on a fatigue damage model developed by Varvani-Farahani [40] the fatigue damage of materials was evaluated by incorporating the critical plane where the cracking starts from this most damaging plane and the amount of normal and shear energies calculated from stress and strain components acting on the critical plane. The parameter is given by the sum of the normal energy range and the shear energy range calculated for the critical plane at which the stress and the strain Mohr's circles are the largest during the loading and unloading parts of a cycle. The normal and shear energies in this parameter have been weighted by the tensile and shear fatigue properties.

The proposed damage analysis in this thesis takes into account the three regions of the damage development based on physics and mechanism of cracking in matrix, matrix-fiber interface, and fiber. This model characterizes the damage progress in regions I and III based on strain energy criterion developed earlier by Varvani-Farahani [40] and region II based on a criterion by Plumtree and Cheng [7]. The developed damage analysis method is capable of damage assessment in GRP and CFRP composites due to its important damage variables. The proposed damage parameter

- Accounts for the energy rather than stress or strain as both stress and strain based damage models lack a rigorous continuum mechanics basis and include possible strain hardening in the analysis.
- Incorporates the stress and strain analysis through the largest Mohr's circles. This will correspond to the maximum energy required for damage and cracking of materials as the number of fatigue cycles increases.
- Unifies the different off-axis angles through equivalent modulus of elasticity in x or y directions.
- Accounts for the matrix and fiber properties and their cracking responses.

6.1 Evaluation of Proposed Damage Assessment Model

This chapter aims to evaluate and compare the proposed damage model with previously developed fatigue damage theories for FRP composites. To achieve a quantitative damage assessment, a few well-known damage theories are described initially. Comparison of fatigue damage assessment based on these theories and the one proposed in this thesis over several sets of fatigue data on unidirectional GRP and CFRP composites with various off-axis angle and R-ratios, will show how capable is the proposed model in fatigue life correlation of unidirectional fibrous composites.

6.2 Fatigue Damage Theories for Fibrous Composites

6.2.1 Kawai Damage Model

Kawai [14] developed a phenomenological fatigue model for the off-axis fatigue behavior of a class of unidirectional FRP composites subjected to constant-amplitude loading with non-negative mean stresses. This non-dimensional damage approach considers the effects of both the stress ratio, and the state of stress on fatigue behavior of unidirectional FRP composites. The parameter is the ratio of the maximum fatigue stress σ_{\max} and is expressed as:

$$\Psi = \frac{\sigma_{\max}}{\sigma_B} \quad (6.1)$$

The fatigue strength ratio Ψ is a quantitative measure of tendency to static failure. The alternating stress σ_a , and the mean stress σ_m are defined as: $\sigma_a = \frac{1}{2}(1 - R)\sigma_{\max}$ and $\sigma_m = \frac{1}{2}(1 + R)\sigma_{\max}$, respectively, where $\sigma_{\max} = \sigma_a + \sigma_m$ and stress ratio $R = \frac{\sigma_{\min}}{\sigma_{\max}}$.

Using σ_a and σ_m it can be confirmed that the static failure condition ($\sigma_{\max} = \sigma_B$) is expressed as $\sigma_a / (\sigma_B - \sigma_m) = 1$. Similarly, the non-dimensional scalar quantity, ψ can be expressed as:

$$\psi = \frac{\sigma_a}{\sigma_B - \sigma_m} \quad (6.2)$$

Kawai's damage parameter is a stress-based damage theory. Although it is convenient to use for fatigue life assessment particularly for long lives, this parameter lacks holding strain components for fatigue life assessment in the low-cycle fatigue regime where materials experience plastic deformation. This shortcoming can be compensated by applying energy based damage theories.

6.2.2 Ellyin and El Kadi Strain Energy Model

Ellin and El Kadi [6] showed that the strain energy can be used as a fatigue failure criterion for fiber-reinforced laminate. Based on this criterion, when a material is loaded externally, a part of the supplied energy is dissipated into heat and the remaining part is stored in the material. Damage is caused by the irrecoverable part of the stored energy, i.e.,

$$dW_{\text{damage}} = dW_{\text{supplied}} - (dW_{\text{recoverable}}) \quad (6.3)$$

A material possesses a certain capacity to absorb energy and damage is accumulated over stress-strain hysteresis until failure takes place. It is generally assumed that the damage is proportional to absorbed energy, i.e.,

$$dW_{\text{damage}} \propto dW_{\text{supplied}} \quad (6.4)$$

The damage caused in the material can therefore be related to the input energy through a functional relationship, $\Delta W = f(N_f)$. For positive stress ratios ($R > 0$) the strain energy, ΔW^* , is calculated from the area under stress-strain curves presented in as shown in figure 6.1.

$$\Delta W^* = 1/2 (\sigma_{\max} \epsilon_{\max} - \sigma_{\min} \epsilon_{\min}) \quad (6.5a)$$

For $R=0$ Equation 6.5a reduces to

$$\Delta W^* = \frac{1}{2} (\sigma_{\max} \epsilon_{\max}) \quad (6.5b)$$

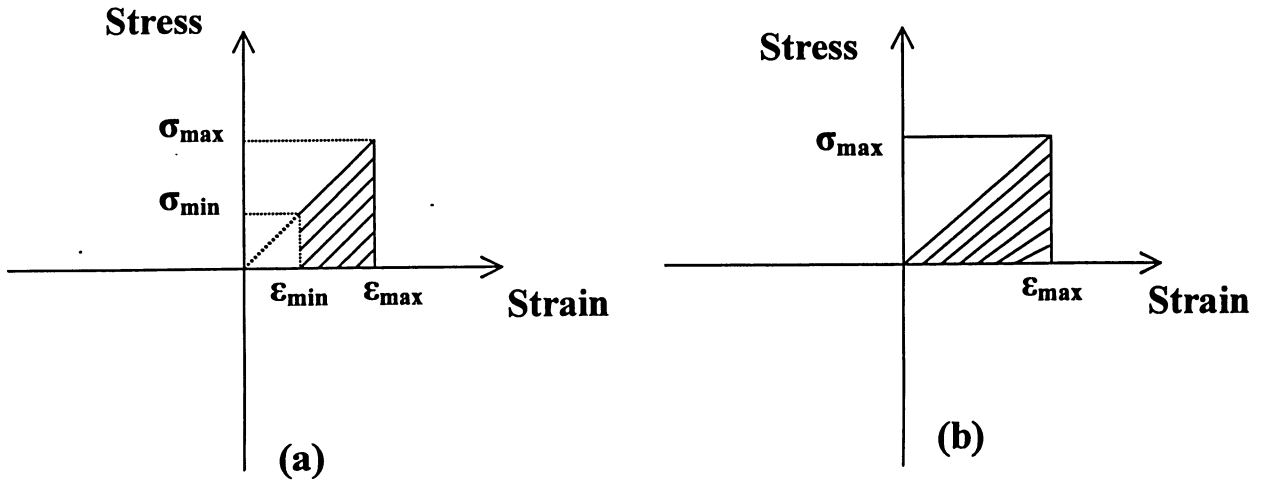


Figure 6.1: The strain energy for different values of stress ratio. (a) $R=0$ (b) $R>0$ [5].

6.2.3 Plumtree and Cheng Energy-Based Model

Plumtree and Cheng [7] investigated a unified fatigue criterion based on micro-mechanics related to the fracture plane. In this model, the failure criterion incorporates both stresses and strains.

Critical plane concepts are based on the observation that fatigue cracks initiate and propagate along critical planes. Figure 6.2 shows the deformation of a unidirectional lamina under cyclic loading [41]. This damage model incorporates the amount of energy calculated from stress and strain components acting normal to the unidirectional fibers (direction 2) and the amount of shear energy calculated from stress and strain components acting along the fiber-matrix interface (direction 1) to the total damage causing failure of GRP composites.

$$W_1 = \frac{1}{2}(\sigma_{22}^{\max} \epsilon_{22}^{\max} - \sigma_{22}^{\min} \epsilon_{22}^{\min}) = \frac{1}{2}(1 - R^2)\sigma_{22}^{\max} \epsilon_{22}^{\max} \quad (6.6)$$

Similarly, the shear strain energy density was given by:

$$W_2 = \frac{1}{2}(\tau_{12}^{\max} \gamma_{12}^{\max} - \tau_{12}^{\min} \gamma_{12}^{\min}) = \frac{1}{2}(1 - R^2)\tau_{12}^{\max} \gamma_{12}^{\max} \quad (6.7)$$

The total fatigue parameter then was expressed as:

$$W = W_1 + W_2 = \lambda(\sigma_{22}^{\max} \epsilon_{22}^{\max} + \tau_{12}^{\max} \gamma_{12}^{\max}) \quad (6.8)$$

where

$$\lambda = \frac{1 - R^2}{2} \quad (5.9)$$

It should be mentioned that Eqs 6.7 and 6.9 were derived for tension-tension fatigue loading conditions ($R > 0$). Equation (6.8) takes into account the effects of mean stress and fiber orientations in damage analysis.

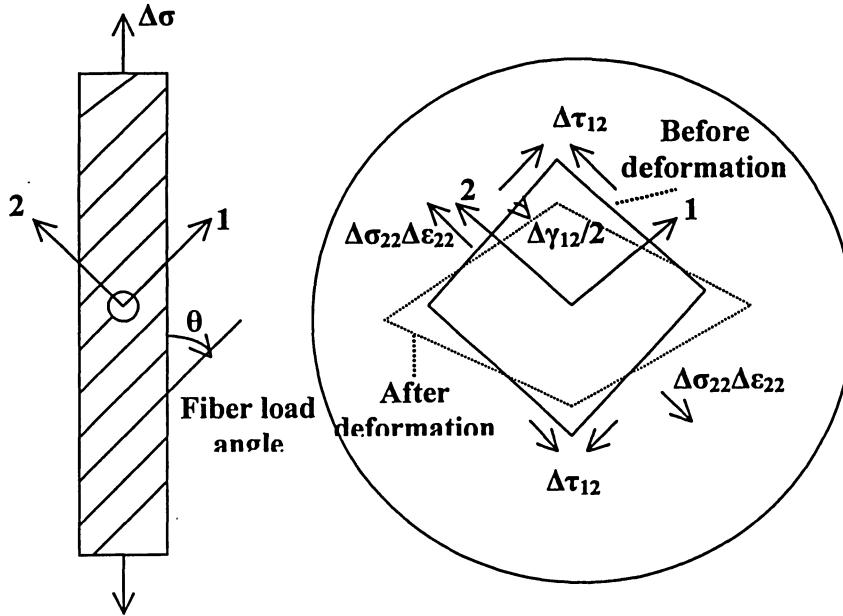


Figure 6.2: Deformations in fracture plane.

6.3 Comparison of Results of Proposed Model with other Models

A few well-known fatigue damage models were compared with the proposed model in this thesis to evaluate the degree of capability of the proposed damage model in life assessment of unidirectional GRP and CFRP composites with various off-axis angles subjected to fatigue loading conditions. Table 6.1 briefly lists these approaches. To assess these models, five sets of fatigue life data for unidirectional GRP and CFRP composites of various R-ratios were extracted from the literature [3, 6, 14, 43, 41].

Figures 6.3-6.11 present experimentally fatigue obtained lives of unidirectional GRP and CFRP composites by different laboratories plotted versus fatigue damage models of (a) Kawai [14], (b) Ellyin and El Kadi [6], (c) Plumtree and cheng [7], and finally, the proposed damage model in this thesis. In these figures two straight thin lines are the upper bound and the lower bound which represents the range of fatigue strength estimated at a given life of 10^5 cycles. This range shows how successfully these models correlate the fatigue data of various off-axis angles for both GRP and CFRP composites.

Figure 6.3 shows a higher degree of success of the proposed damage parameter in damage assessment of GRP composites ($R=0$) for various θ , over Kawai's, Ellyin's, and Plumtree's damage models. The factor of fatigue correlation at 10^5 cycles for Kawai, Ellyin-El Kadi, Plumtree-Cheng, and the proposed damage model are found respectively to be $\frac{y_U}{y_L} = 3.7, 574,$

15.5, and 2.9. The ratio of $\frac{y_U}{y_L}$ at 10^5 cycles for all GRP and CFRP composites evaluated by fatigue damage models of (a) Ellyin-El Kadi, (b) Kawai, (c) Plumtree-Cheng and (d) the proposed study have been tabulated in Table 6.2. The proposed damage parameter in this thesis, shows much better fatigue life correlations for both unidirectional GRP and CFRP composites as compared with other damage models. Damage analysis based on the proposed model, results in fatigue life correlation ratios varying within a factor of 2.0 to 3.0 for GRP composite and 1.9 to 3.4 for CFRP composite specimens tested at various R ratios and off-axis angles θ . From figures 6.3-6.11, it is also noticeable that the proposed damage model correlates various fatigue data for GRP and CFRP composites with a steeper decreasing trend, which unifies the fatigue life data within a smaller range factor at a given value of the proposed model. This shows how accurate the proposed damage model predicts fatigue life of these materials.

It is noticed that a higher degree of scatter in fatigue life correlation by Ellyin-El Kadi model is mainly due to only one set of fatigue data possessing a fiber orientation of $\theta=0$ in GRP and CFRP composites. Excluding fatigue data of 0° off-axis from fatigue life evaluation curves by Ellyin-El Kadi, reduces the $\frac{y_U}{y_L}$ ratios and unifies the fatigue data of GRP and CFRP composites significantly. For the Ellyin-El Kadi life correction diagrams, the upper bound is presented by a dashed line and y_U^* has been selected from the dashed line at 10^5 cycles and tabulated in Table 6.2.

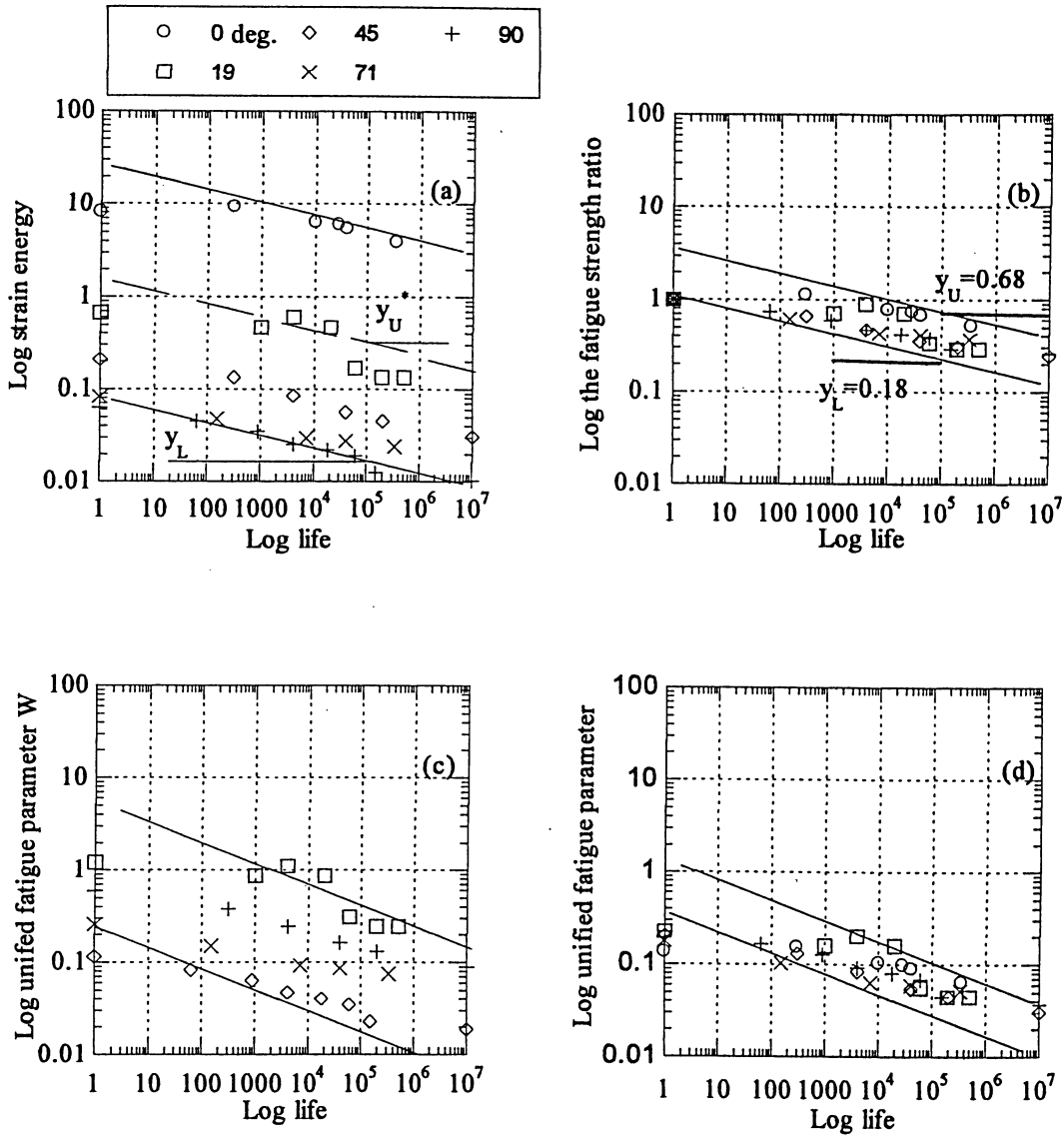


Figure 6.3: Fatigue life correlation of unidirectional GRP composites at different off-axis angles and at a stress ratio of $R=0$ [6] using (a) Ellyin-El Kadi model , (b) Kawai model, (c) Plumtree-Cheng model, (d) the proposed model.

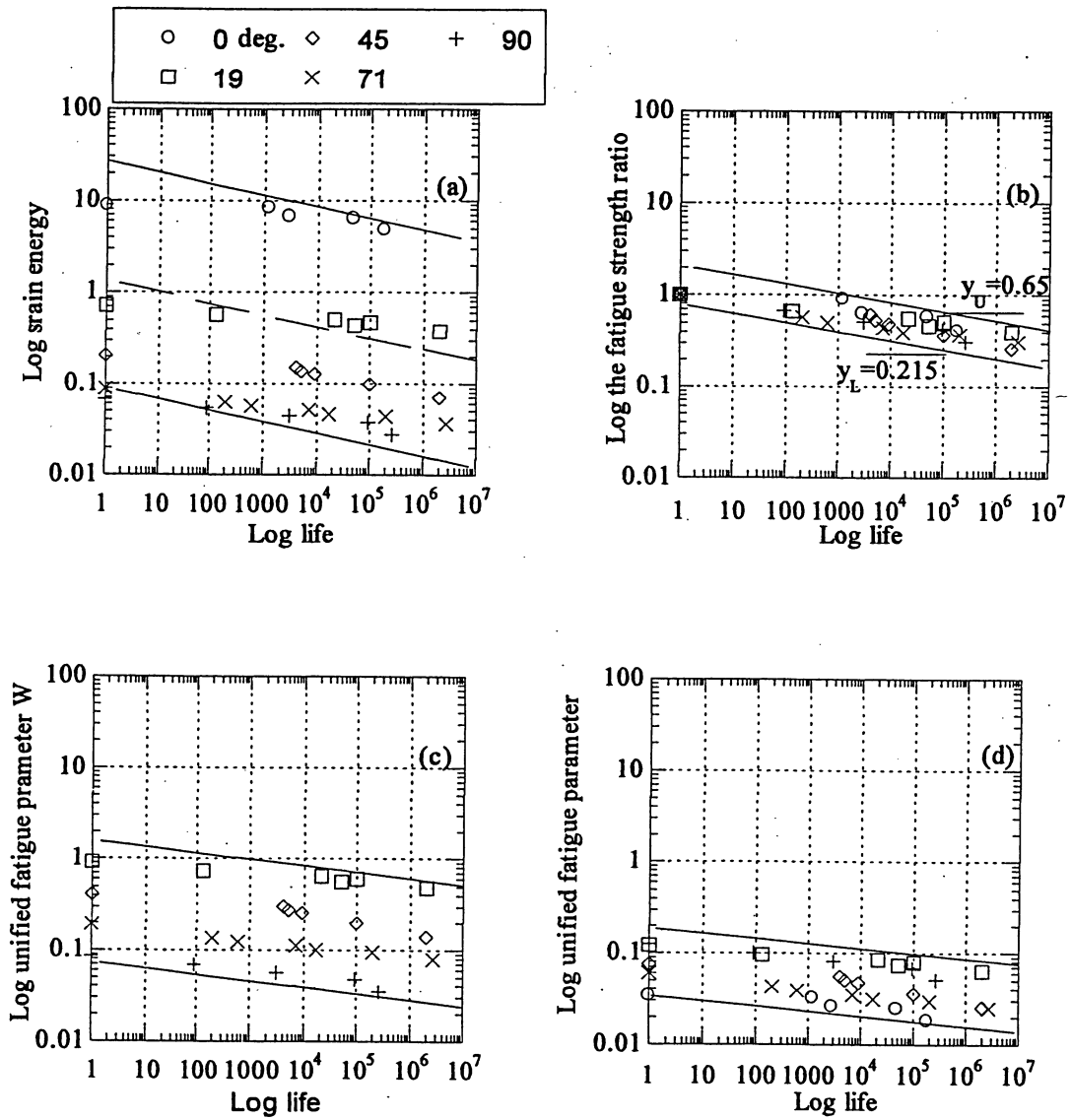


Figure 6.4: Fatigue life correlation of unidirectional GRP composites at different off-axis angles and at a stress ratio of $R = 0.5$ [6] using (a) Ellyin-El Kadi model, (b) Kawai model, (c) Plumtree-Cheng model, (d) the proposed model.

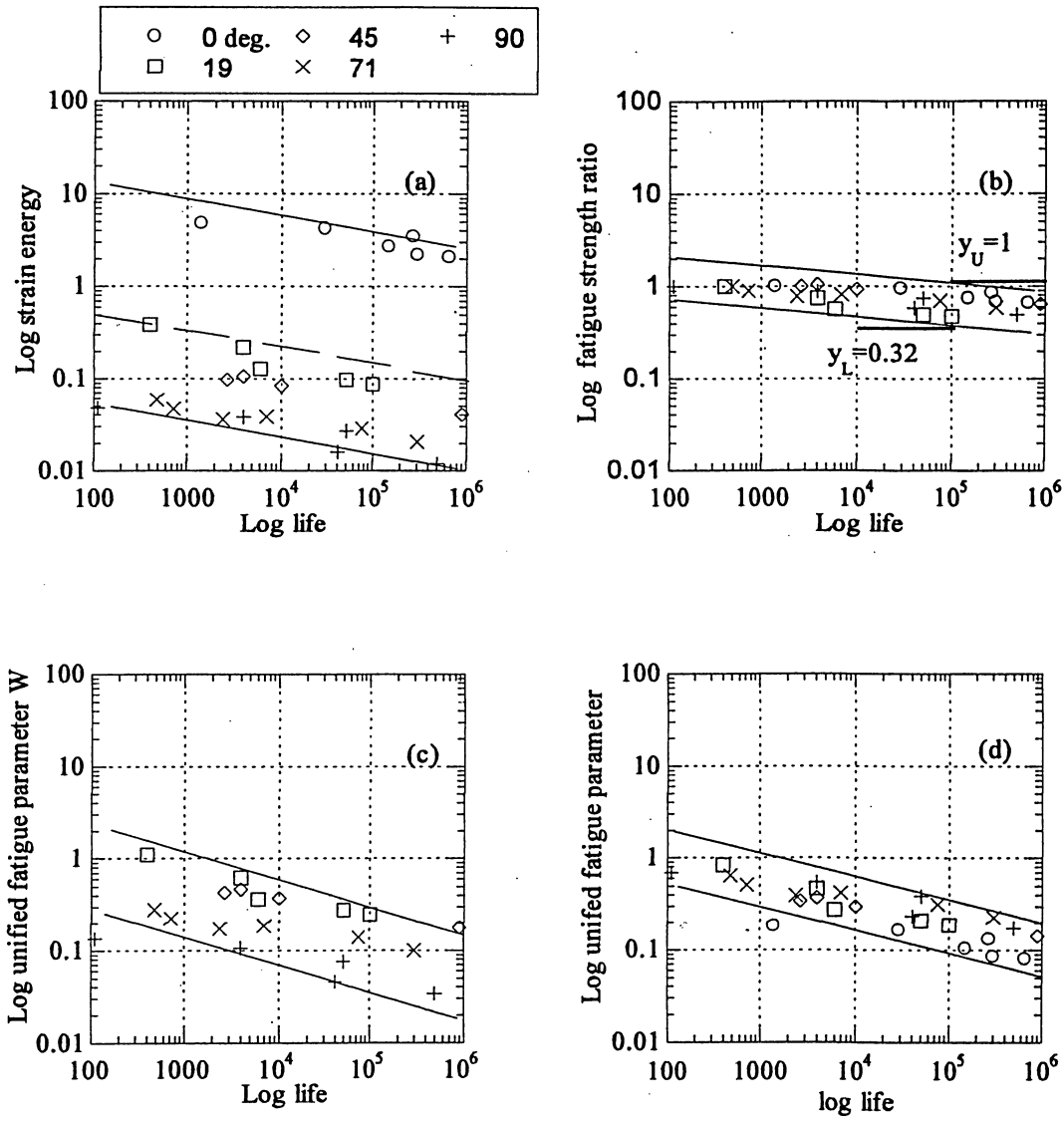


Figure 6.5: Fatigue life correlation of unidirectional GRP composites at different off-axis angles and at a stress ratio of $R = -1$ [6] using (a) Ellyin-El Kadi model, (b) Kawai model, (c) Plumtree-Cheng model, (d) the proposed model.

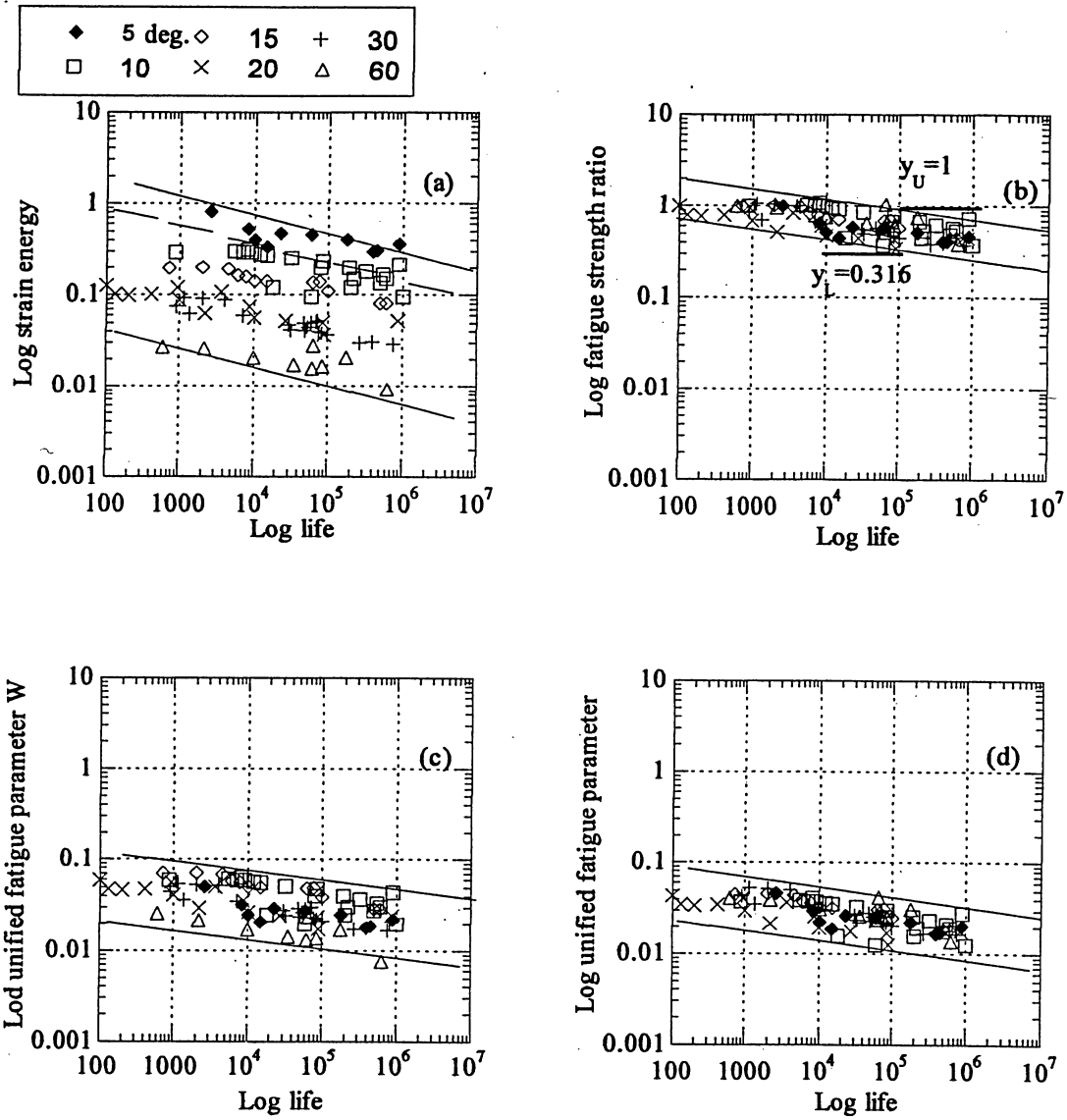


Figure 6.6: Fatigue life correlation of unidirectional GRP composites at different off-axis angles and at a stress ratio of $R = 0.1$ [3] using (a) Ellyin-El Kadi model, (b) Kawai model, (c) Plumtree-Cheng model, (d) the proposed model.

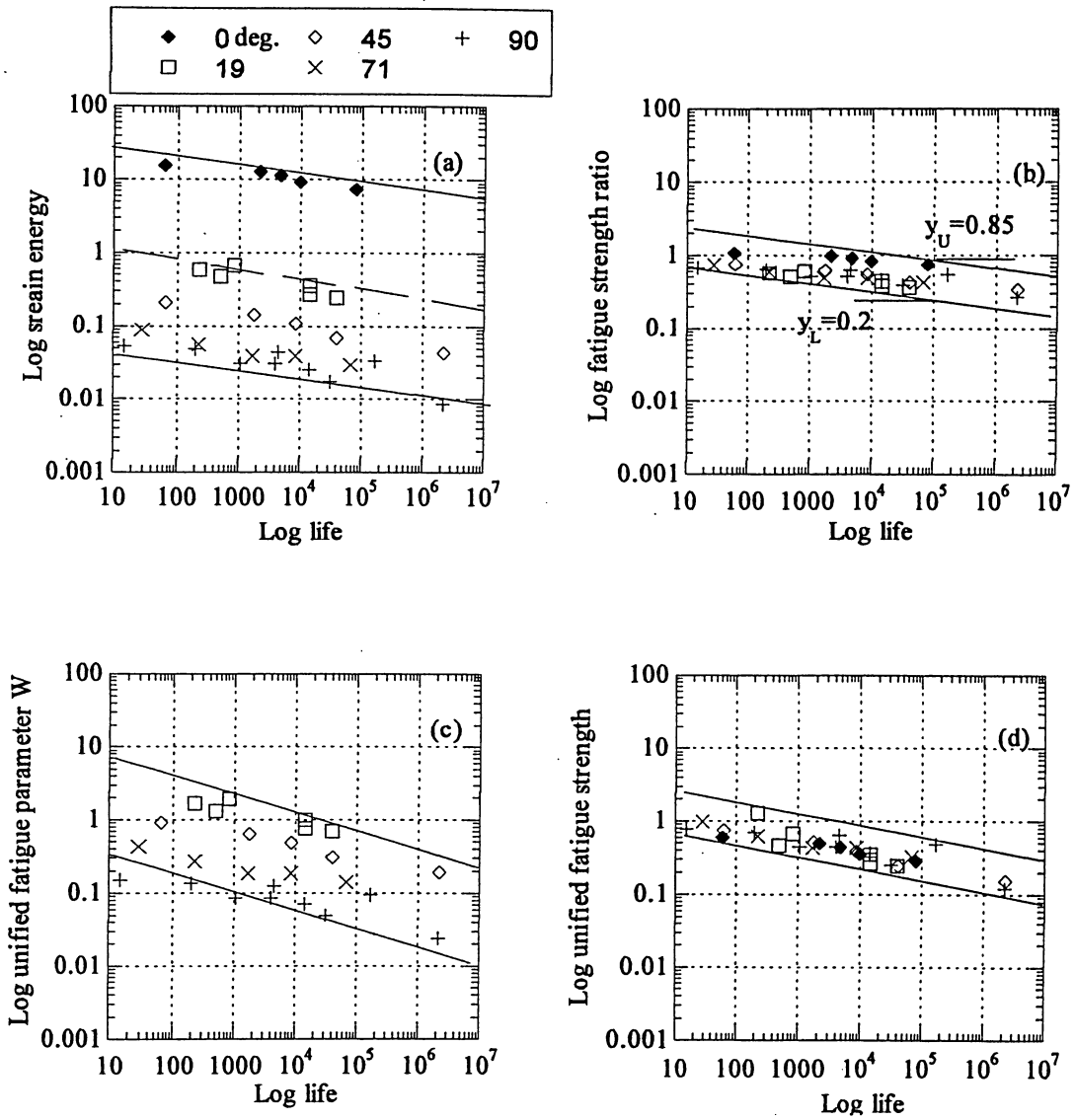


Figure 6.7: Fatigue life correlation of unidirectional GRP composites at different off-axis angles and at a stress ratio of $R = -1$ [43] using (a) Ellyin-El Kadi model, (b) Kawai model, (c) Plumtree-Cheng model, (d) the proposed model.

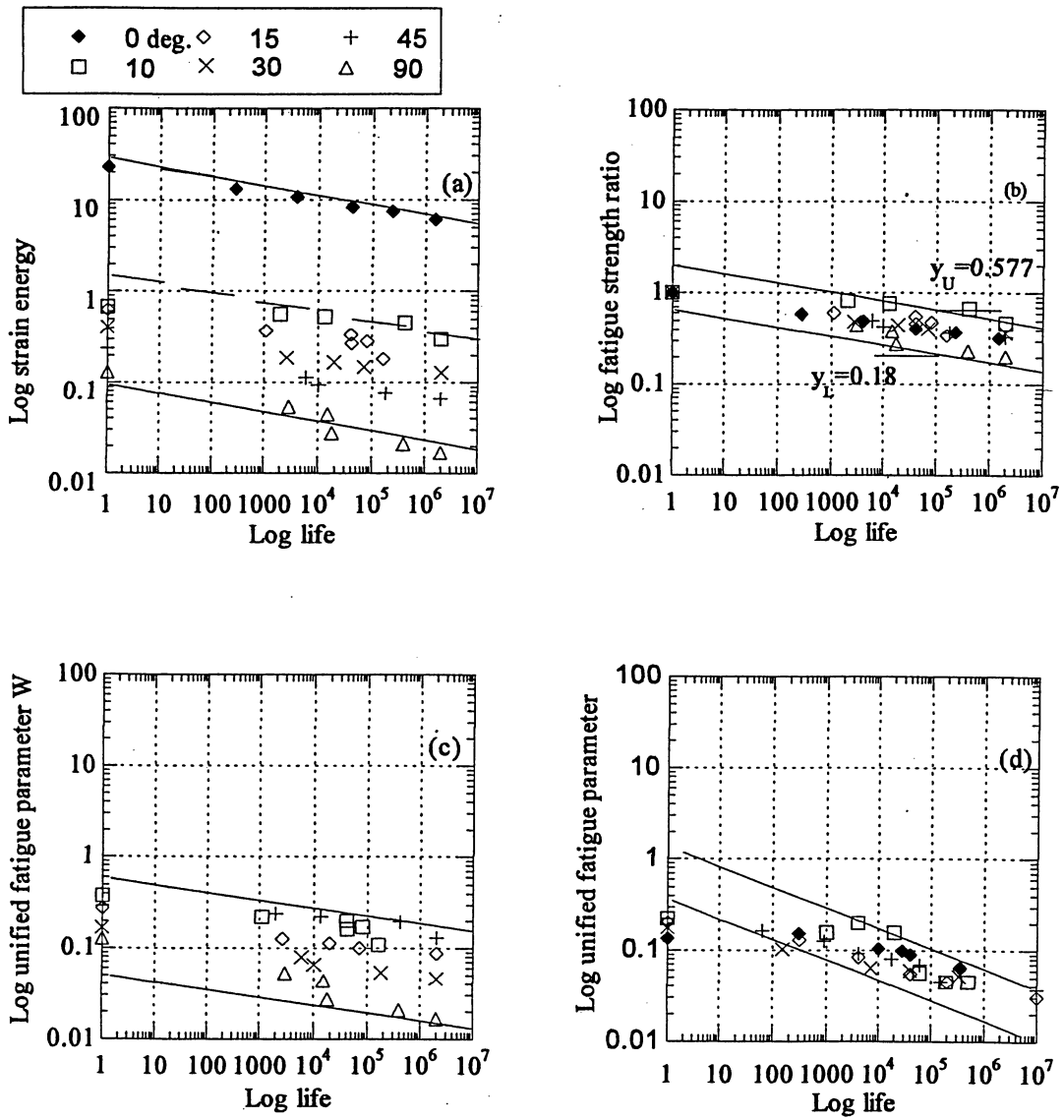


Figure 6.8: Fatigue life correlation of unidirectional CFRP composites at different off-axis angles and at a stress ratio of $R = 0.1$ [14] using (a) Ellyin-El Kadi model, (b) Kawai model, (c) Plumtree-Cheng model, (d) the proposed model.

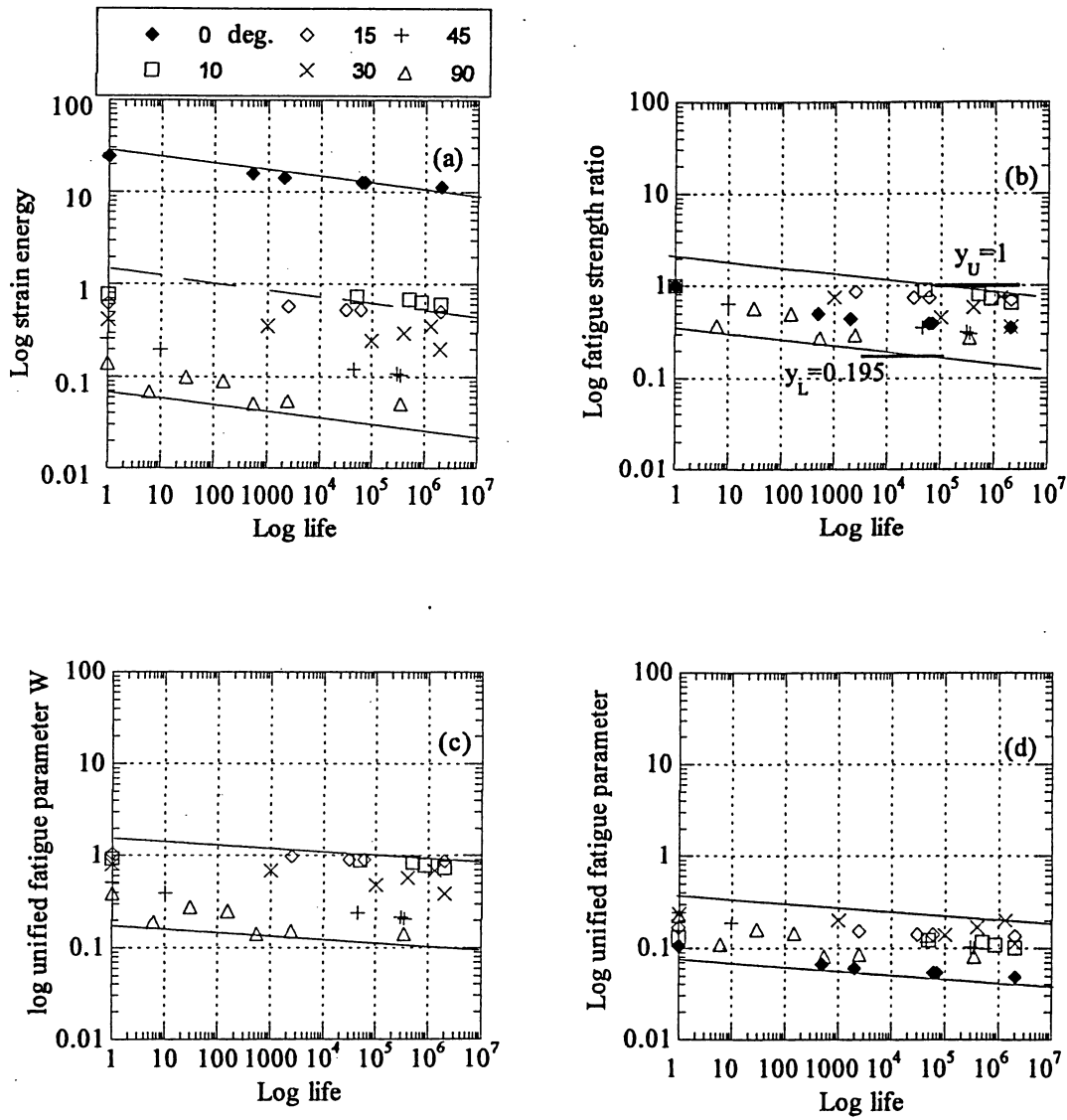


Figure 6.9: Fatigue life correlation of unidirectional CFRP composites at different off-axis angles and at a stress ratio of $R=0.5$ [14] using (a) Ellyin-El Kadi model, (b) Kawai model, (c) Plumtree-Cheng model, (d) the proposed model.

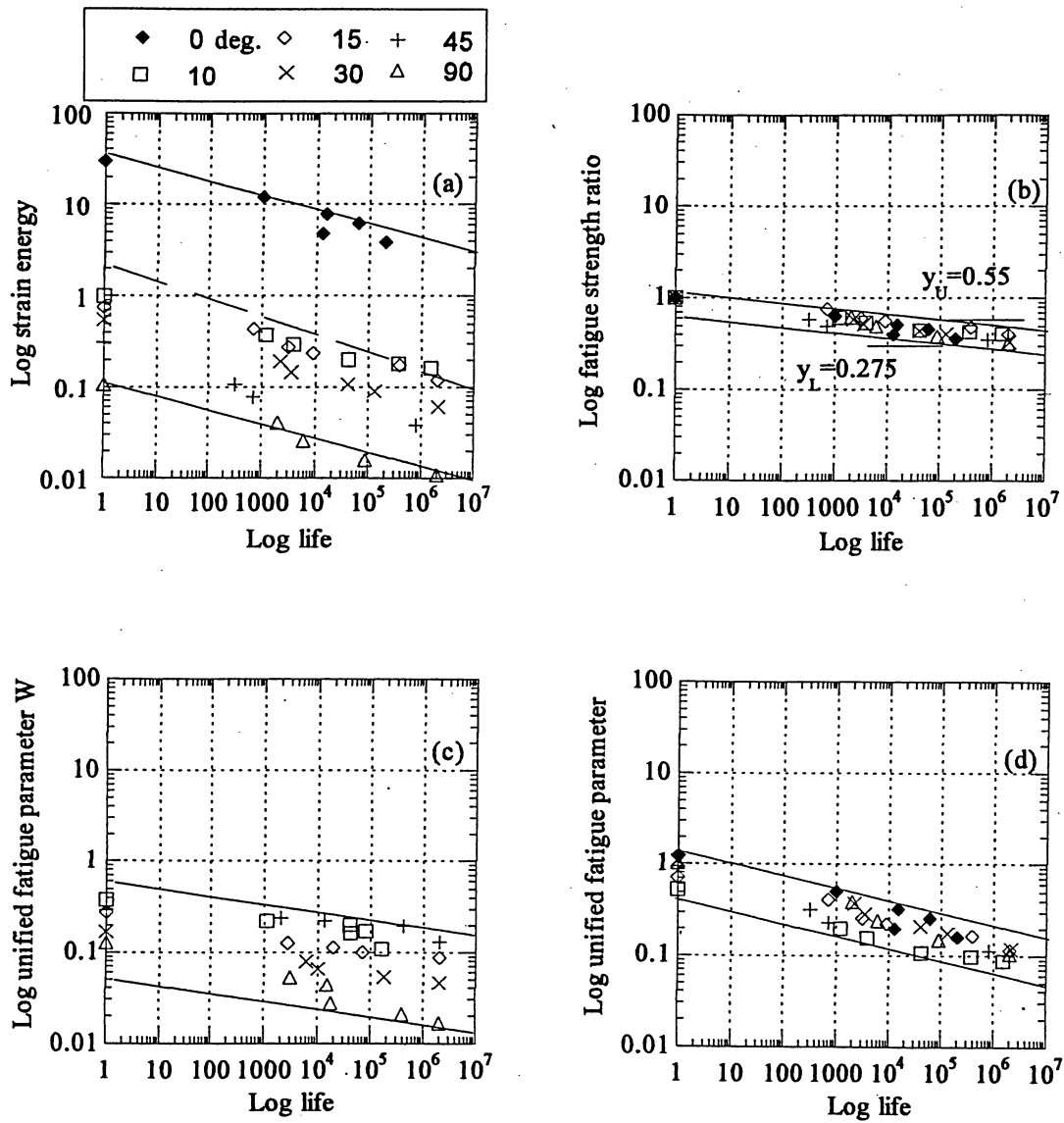


Figure 6.10: Fatigue life correlation of unidirectional CFRP composites at different off-axis angles and at a stress ratio of $R = -1$ [14] using (a) Ellyin-El Kadi model, (b) Kawai model, (c) Plumtree-Cheng model, (d) the proposed model.

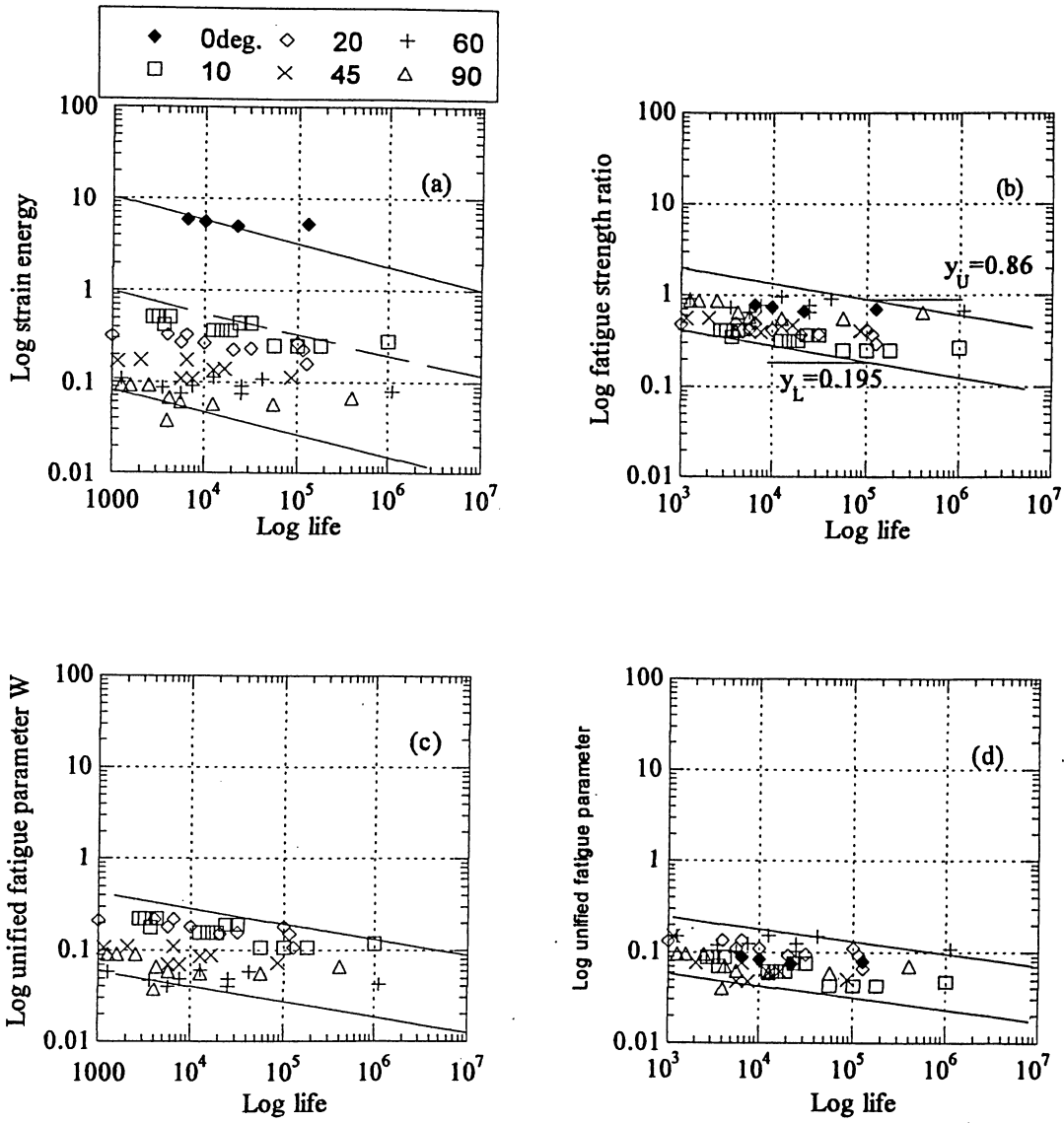


Figure 6.11: Fatigue life correlation of unidirectional CFRP composites at different off-axis angles and at a stress ratio of $R=0.1$ [41] using (a) Ellyin-El Kadi model, (b) Kawai model, (c) Plumtree-Cheng model, (d) the proposed model.

Table 6.1: Summary of fatigue damage models evaluated in this thesis

Models	Failure criterion	Damage equations	Materials and references
Kawai	The static failure mode	$\Psi = \frac{\sigma_{\max}}{\sigma_B}$	E-glass fibers Gevetex WS 13-320 Xi-K921 in epoxy resin [14]
Ellyin-EI Kadi	Matrix dominated failure at a direction parallel to the fibers	$\Delta W^* = 1/2 (\sigma_{\max} \epsilon_{\max} - \sigma_{\min} \epsilon_{\min})$	Scotchply Reinforced plastic type 1003, glass fiber-epoxy resin [6]
Plumtree- Cheng	Energy based damage along and normal to fiber direction	$W = W_1 + W_2 = \lambda (\sigma_{22}^{\max} \epsilon_{22}^{\max} + \tau_{12}^{\max} \gamma_{12}^{\max})$	E-glass fibers Gevetex WS 13-320 Xi-K921 in epoxy resin [3].
Proposed model	Energy based-critical plane within matrix and fibers, and damage progress along and normal to fiber orientation. Damage analysis is based on cracking on three regions as life cycles increases.	$\Delta W = \Delta W_I + \Delta W_{II} + \Delta W_{III}$ $\Delta W_I = \left[\frac{\Delta \tau_{\max} \Delta \frac{\gamma_{\max}}{2}}{\tau_{ULT} (\frac{\sigma_{ULT}}{G_m})} \right], \Delta W_{II} = \left[\frac{\Delta \tau_{12} \Delta \frac{\gamma_{12}}{2}}{\tau_{ULT} (\frac{\sigma_{ULT}}{G_m})} + \frac{\Delta \sigma_{22} \Delta \epsilon_{22}}{\sigma_{ULT} (\frac{\sigma_{ULT}}{E_f})} \right]$ $\Delta W_{III} = \left[\frac{\Delta \sigma_n \Delta \epsilon_n}{\sigma_{ULT} (\frac{\sigma_{ULT}}{E_f})} \right]$	GRP data and CFRP data T800H/2500 in epoxy resin [3, 6, 14, 41, 43].

Table 6.2: Table of evaluation of models in life correlation of GRP and CFRP composites at various θ_s and R ratios

Fatigue damage model	Factor of life correlation for GRP						Factor of life correlation for CFRP				GRP			CFRP		
	$\frac{y_U}{y_L}$						$\frac{y_U}{y_L}$									
	Ellyin data R=0	Ellyin data R=0.5	Ellyin data R=-1	Hashin data R=0.1	Xiao data R=-1	Kawai data R=0.1	Kawai data R=0.5	Kawai data R=-1	Zheng data R=0.1	Mean value	Standard deviation error %	Mean value	Standard deviation error %	Mean value	Standard deviation error %	
Kawai	3.7	2.9	3.2	3.2	4.22	3.2	4.4	2	4.4	3.44	0.23	3.2	0.23			
Ellyin	15*	15*	10*	42*	16*	14*	23*	11*	20*	19.6*	5.69*	17*	5.69*		2.73*	
Plumtree	15.5	14.5	8	5	19.5	9.1	8.5	5.5	5.8	12.5	2.63	7.22	2.63		0.91	
Present model	2.9	2.8	2	3	2.6	1.9	3.1	2.75	3.4	2.66	0.18	2.6	0.18		0.38	

(*) $\frac{y_U}{y_L}$, where y_U^* represents the upper bound of data at 10^5 cycles excluding 0° off-axis fatigue data.

$$\text{Mean Value} = \bar{x} = \frac{\sum_i x_i}{n}, \text{ Standard Deviation} = \sqrt{\frac{\sum_i (x_i - \bar{x})^2}{n-1}}$$

$$\text{Standard Deviation Error} = \frac{\text{Standard Deviation}}{\sqrt{n}}$$

CHAPTER SEVEN

Conclusion and Recommendation

7.1 Conclusion

Unidirectional GRP and CFRP composite materials have gained increased use in structural applications in the last few decades. Due to the inherent difference in microstructure, design with composite materials has to be treated differently compared to more conventional metallic materials. An investigation of fatigue damage mechanisms is prompted by the fact that most failures in service of load-carrying structures can be attributed to fatigue. To date, no model enjoys expensing a universal fatigue damage description in composite materials. This is mainly due to complex fatigue response of these materials. The present thesis has attempted to develop a fatigue damage model based on the physics and the mechanism of cracking in matrix, matrix-fiber interface, and fiber. The proposed model characterizes the damage progress in region I and III based on the strain energy criterion developed earlier by Varvani-Farahani and in a region II based on the criterion developed by Plumtree-Cheng. The total fatigue damage parameters in unidirectional GRP and CFRP were calculated by damage accumulation in the three regions I, II, III. In region I, cracks initiate in the matrix when shear cracking is dominant. These microcracks increase in numbers and size as the number of cycle progresses. As the matrix cracks approach fibers, fatigue damage further progress into region II along the interface of matrix-fiber. Stress and strain components normal to the fiber direction are responsible for decohesion and therefore cracks progress along the interface direction. In region III, fiber cracking is dominant due to the normal principal stress criterion. The proposed fatigue damage model successfully correlated fatigue lives of unidirectional GRP and CFRP composites at different θ and R . The results of fatigue damage assessment revealed that the proposed damage model correlated the data with a

higher degree of success as compared with fatigue damage models developed by Kawai, Ellyin-El Kadi and Plumtree-Cheng.

7.2 Recommendation

Further modeling of the fatigue damage accumulation is useful in several aspects. Parametric simulations can be undertaken to elucidate the interaction of constituent properties in fatigue degradation, which could provide valuable insight for microstructural tailoring for optimal fatigue performance. More specifically, the presented energy-critical plane parameter for fatigue life assessment could be generalized to embrace the behavior of the composite laminate under complicated fatigue load. Calibration of such a model by more experimental data would hopefully validate the model and characterize the microstructural properties and energy relations in a composite framework.

Finally, vigorous attempts to extend the models for service applications are endorsed. In a distant perspective, this should include multidirectional laminates, variable amplitude loading, elevated temperature, environmental fatigue, variable frequency which all influence the fatigue behavior of composite materials when used in real application.

REFERENCES

- [1] Degrieck J and Van Paepegem W (2001), Fatigue Damage Modeling of Fiber-Reinforced Composite Materials: Reviews. *Applied Mechanics Review*, 54 (4), pp.279-300.
- [2] Sendekyi GP (1981), Fitting models to composite materials fatigue data In : Chamis CC, Test methods and design allowable for fibrous composite. *ASTM STP 734*, American Society for Testing and Materials, pp.245-260.
- [3] Hashin.Z.and Rotem A (1973), A fatigue failure criterion for fiber reinforced composites. *Journal of composite materials*. 7, pp.448-64.
- [4] Refsnider KL and Gao Z (1991), A Micromachannmics Model for Composites under Fatigue, Loading, *International Journal of Fatigue* 13(2), pp.149-156.
- [5] Epaarachechi JA and Gluasen PD (2000), Anew approach to a fatigue damage model for glass-fiber reinforcement plastic composites, *Proceeding of the Seventh International Conference on Composites Engineering (ICCE/7)*, Denver, Colorado, 2-8 July 2000, pp.211-222.
- [6] Ellyin F and El-Kadi H (1990), A Fatigue Failure Criterion for Fiber Reinforcement Composite Laminates, *Composites Structure* 15, pp.61-74.
- [7] Plumtree A and Cheng GX (1999), A fatigue damage parameter for off-axis unidirectional fiber-reinforced composites, *International Journal of Fatigue* 21(8), pp.849-856.
- [8] Highsmith Al and Refsnider KL (1982), Stiffness-reduction mechanisms in composite laminates In: Refsnider KL, Damage in composite materials. *ASTM STP 775*, pp.103-117.

- [9] Hwang W and Han Ks (1986a), Cumulative damage models and multi-stress fatigue life prediction, *Journal of Composite Materials* 20, pp.125-153.
- [10] Hwang W and Han Ks (1986b), Fatigue of composites – Fatigue modulus concepts and life prediction, *Journal of Composite Materials* 20, pp.154-165.
- [11] Kam TY, Chu KH and Tsai SY (1998), Fatigue reliability evaluation for composite laminates via a direct numerical integration technique, *International Journal of Solids Structure* 35(13), pp.1411-23.
- [12] Kam TY, Tsai SY, and Chu KH (1997), Fatigue reliability analysis of composite laminates under spectrum stress, *International Journal of Solids Structure* 35(12), pp.1441-1461.
- [13] Sidoroff F and Subagio B (1987), Fatigue damage modeling of composite materials from bending tests In: Matthews FI, Buskell NCR, Hodgkinson IM, and Morton J, *Sixth International Conference on Composite Materials (ICCM-VI) and Second European Conference on Composite Materials (ECCM-II)* Volume 4, Proceedings, 20-24 July 1987, London UK, pp. 4.32-4.39.
- [14] Kawai M (2004), A phenomenological model for off-axis fatigue behavior of unidirectional polymer matrix composites under different stress ratios, *Composites: Part A* 35, pp.955-963.
- [15] Chou PC and Croman R (1978), Residual Strength in Fatigue Based on the Strength-Life Equal Rank Assumption, *Journal of Composite Materials* 12, pp.177-194.
- [16] Chou PC and Croman R (1979), Degredation and sudden-death models of fatigue of graphite/epoxy composites. In: Tsai SW, Composite materials: Testing and design, *AST STP 674*, Philadelphia, American Society for Testing and Materials, pp.431-454.
- [17] Hahn HT and Kim RY (1975), Proof testing of composite materials, *Journal of Composite Materials* 9, pp.279-311.

- [18] Haplin JC, Jerina KL, and Johnson TA (1973), Characterization of composites for the purpose of reliability evaluation. In: Analysis of test methods for high modulus fibers and composites. *ASTM STP 521*, pp. 5-64.
- [19] Caprino G , D'Amore A and Facciolo F (1998), Fatigue sensitivity of random glass fiber reinforced plastics, *Journal of composites materials* 32(12), pp.1203-1220.
- [20] Caprino G and Gioralco G (1999), Fatigue life time of glass fabric/epoxy composites, Composites Part A, *Applied Science and Manufacturing* 30(3), pp.299-304.
- [21] Owen MJ and Bishop PT (1974), Prediction of static and fatigue damage and crack propagation in composite materials. In: Advisory Group for Aerospace Research and Development (AGARD), Failure modes for composite materials with organic matrices and their consequences on design, *AGARD Conference Proceedings* No.163 (CP-163), pp. 1.1-1.12.
- [22] Feng X, Gilchirst MD, Kinloch AJ, and Mathews FL (1997), Development a method for predicting the fatigue life of CFRP composites. In: Degalliax S, Bathias C, and Fougères R, *International Conference on Fatigue of Composites. Proceedings*, 3-5 June 1997, Paris, France, pp.407-417.
- [23] Johnson A.F, Engineering Design Properties of GRP, British plastics Federation, 1978.
- [24] Haris, B., Engineering Composite Materials, IOM, 1999.
- [25] Refisnider KL., Fatigue of Composite Materials, Elsevier, Amsterdam, 1991.
- [26] Lee CH and Jen MHR (1998), Strength and life in thermoplastic composite laminates under static and fatigue loads. Part I: Experimental, *International Journal of Fatigue* 20, 9, pp. 605-615.
- [27] Holmes M and Just DJ, GRP in Structural Engineering, Applied Science Publishers, 1983.

- [28] Haplin JC , Primer on Composite Materials: ANALYSIS, Technomic Pub. Co, 1984.
- [29] Traceski FT., Specifications and Standards for Plastics and Composites, ASM International , U.S 1990.
- [30] Thermoplastic Application, Lower Leading Edge Fairing AH64 A Apache Helicopter, Philips 66 Company/Advanced Composites technical data sheet, (1986).
- [31] Composites: Helicopters Leading the Way (1989), *Aerospace Engineering*, Vol 9, pp. 19-26.
- [32] Caravasos N, McArdle F.H, and Swats F, (1985), CH-47D Composite Rotor Hub , Conference on Fibrous Composites in Structural Design, Denver June 17-20, 1985.
- [33] Gourley SR, (1989) FMS Shows Composite Hull Fighting Vehicle, Jane's Defense Weekly , 8 July 1989.
- [34] King J (1997), Advanced composite materials, *Material World*, Vol. 5, No 6, pp.324-327.
- [35] Polymer Composites as Construction Materials, (2000) Application summery sheet 27, British Wind Energy Association.
- [36] NCHRP Report 503 (2003) Application of Fiber Reinforced Polymer Composites to the High way Infrastructure, National Cooperative Highway Research Program.
- [37] Kollar L, Mechanics of Composite Structure, Cambridge University, Press, 2003.
- [38] Kaw AK , Mechanics of Composite Materials, CRC Press, Portland, 1997.
- [39] Shokrieh M and Lessard LB (1997), Multiaxial fatigue behavior of unidirectional plies based on uniaxial fatigue experiments, *International Journal of Fatigue* 19, 3, pp. 209-217.

- [40] Varvani-Farahani,A (2000), A new energy Plane parameter for fatigue life assessment of various metallic materials subjected to in-plane and out –of-phase multiaxial fatigue loading conditions. *International Journal of Fatigue* 22, pp. 295-305.
- [41] Huang ZM (2002), Micromechaical Modeling of fatigue strength of unidirectional fibrous composites. *International Journal of Fatigue* 24, pp.659-670.
- [42] ASTM standards, D 3090M.2000: Standard test method for tensile properties of polymer matrix composite materials, *ASTM standards, D 3479-96*: Standard test method for tension-tension fatigue of polymer matrix composite materials.
- [43] Xiao J, Bathias C, (1994) Fatigue behavior of un-notched and notched woven glass/epoxy laminates, *Composite science and Technology* Vol. 50, pp.141-148
- [44] Plumtree A and Petermann J (2001), A unified fatigue criterion for unidirectional laminates. *Composites Part A* 32, pp.107-118.
- [45] Garud YS A new approach to the evaluation of fatigue under multiaxial loadings. In: Ostergreen WJ, Whitehead JR, editors. Proceeding of the Symposium on Methods for Predicting Materials Life in Fatigue, New York, *ASTM* 1979, 247-63.
- [46] Brown MW, Miller KJ, A theory for fatigue under multiaxial stress-strain conditions. *Proc Inst Mech Eng* 1973, 187, 745-55.
- [47] Flavenot JF, Skalli N, (1989) A critical depth criterion for evaluation of long life fatigue strength under multiaxial loadings and stress gradient. In: Brown MW, Miller KJ, editors. Biaxial and multiaxial fatigue. London: *ESIS Publication no. EGF3*, 355-65.
- [48] Findley WN, A A theory for the effect of mean stress on fatigue of metals under combined torsion and axial load or bending . *J Eng Ind* 1959, 81, 301-6.

APPENDIX A

Appendix A tabulates the material properties and fatigue data for unidirectional GRP and CFRP composites tested at various off-axis angles θ and stress ratios R .

Table (A1-1) presents material properties of unidirectional GRP composites consist of the E-glass fibers and the epoxy resin as polymeric matrix phase. Table (A1-2) through Table (A1-6) list the fatigue life data of unidirectional GRP composites tested at various off-axis angles θ and stress ratios R .

Table (A2-1) lists material properties of unidirectional CFRP composites consist of the carbon fiber and the epoxy resin as polymeric matrix phase. Table (A2-2) through Table (A2-5) tabulate fatigue life versus the maximum applied stress to the unidirectional CFRP composites of various off-axis angles θ and stress ratios R .

All fatigue data listed in Tables A1 and A2 are experimental data reported in the literature from different laboratories.

Table A1-1: Material Properties of GRP

Material Properties of GRP	Values
Modulus of Elasticity in Direction 1	$E_1 = 38500 \text{ MPa}$
Modulus of Elasticity in Direction 2	$E_2 = 17600 \text{ MPa}$
Shear Modulus in Direction 1-2	$G_{12} = 4400 \text{ MPa}$
Ultimate Tensile Strength of E-Glass Fiber	$\sigma_{UTS} = 1726 \text{ MPa}$
Modulus of Elasticity of E-Glass Fiber	$E = 75000 \text{ MPa}$
Volume Fraction of E-Glass Fiber	$V_f = 60\%$
Shear Strength of Epoxy Resin	$\sigma_{UST} = 55 \text{ MPa}$
Shear Modulus of Epoxy Resin	$G = 1822 \text{ MPa}$

Table A1-2: Fatigue data of GRP composites tested by Ellyin-El Kadi [6] at various off-axis angles θ (degrees) at the stress ratio of $R=0$.

θ	σ_{\max} (MPa)	Life (Cycles)	θ	σ_{\max} (MPa)	Life (Cycles)
19	170	3900	71	38	150
19	150	20000	71	30	7000
19	90	60000	71	29	40000
19	80	190000	71	27	330000
19	80	500000	90	47	1
45	75	1	90	40	63
45	60	310	90	35	880
45	48	4000	90	30	4000
45	39	40000	90	28	180000
45	35	200000	90	26	61000
45	29	1000000	90	21	150000
71	50	1	90	19	10000000

Table A1-3: Fatigue data of GRP composites tested by Ellyin-El Kadi [6] at various off-axis angles θ (degrees) at the stress ratio of $R=0.5$.

θ	σ_{\max} (MPa)	Life (Cycles)	θ	σ_{\max} (MPa)	Life (Cycles)
0	800	1	45	57	9000
0	780	1200	45	50	100000
0	700	2800	45	42	2000000
0	680	47000	71	50	1
0	590	180000	71	42	200
19	150	21000	71	40	600
19	140	51000	71	38	7000
19	145	100000	71	36	17000
19	130	2000000	90	47	1
45	72	1	90	42	90
45	62	4000	90	38	3000
45	59	5000	90	35	92000

Table A1-4: Fatigue data of GRP composites tested by Ellyin-El Kadi [6] at various off-axis angles θ (degrees) at the stress ratio of $R=-1$.

θ	σ_{\max} (MPa)	Life (Cycles)	θ	σ_{\max} (MPa)	Life (Cycles)
0	530	1400	45	42	10000
0	500	29000	45	29	900000
0	400	150000	71	37	480
0	450	270000	71	33	720
0	360	300000	71	29	2400
0	350	650000	71	30	7000
19	120	400	71	26	75000
19	90	4000	71	22	300000
19	69	6000	90	36	110
19	60	50000	90	32	4000
19	57	100000	90	21	40000
45	45	2700	90	27	50000
45	47	4000	90	18	500000

Table A1-5: Fatigue data of GRP composites tested by Hashin-Rotem [3] at various off-axis angles θ (degrees) at the stress ratio of $R=0.1$.

θ	σ_{\max} (MPa)	Life (Cycles)	θ	σ_{\max} (MPa)	Life (Cycles)
5	245.25	2600	20	63.765	1000
5	196.2	8200	20	53.955	2200
5	171.675	10000	20	70.632	3600
5	156.96	15000	20	58.86	8600
5	186.39	23000	20	51.012	10000
5	181.485	60000	20	49.05	27000
5	171.675	180000	20	48.069	86000
5	147.15	400000	20	41.202	90000
5	149.112	4500000	20	49.05	860000
5	161.865	900000	30	54.936	4000
10	137.34	860	30	51.012	900
10	139.302	5400	30	56.4075	1140
10	137.34	7000	30	46.107	1360
10	142.245	8000	30	55.917	2000
10	137.34	9000	30	45.126	7000
10	134.397	12000	30	40.221	30000
10	132.435	15000	30	37.7685	32000
10	127.53	32000	30	41.202	48000
10	78.48	60000	30	37.278	50000
10	112.815	80000	30	39.24	54000
10	122.625	85000	30	41.202	60000
10	117.72	90000	30	41.6925	70000
10	112.815	190000	30	42.183	72000
10	88.29	200000	30	36.7875	77000
10	98.1	220000	30	36.297	84000
10	107.91	320000	30	35.316	100000

10	93.195	500000	20	68.67	130
10	103.005	540000	20	67.689	200
10	98.1	600000	20	68.67	410
10	78.48	1000000	20	74.556	930
15	103.986	720	30	31.8825	270000
15	104.967	2000	30	32.373	400000
15	103.005	4500	30	31.392	770000
15	94.6665	6000	60	26.9775	600
15	93.195	7700	60	26.487	2200
15	88.29	10000	60	23.544	10000
15	87.7995	15000	60	21.582	36000
15	87.309	77000	60	27.468	65000
15	77.499	100000	60	20.601	63000
15	66.708	500000	60	21.0915	86000
15	66.708	600000	60	23.544	180000
20	76.518	100	60	15.696	630000

Table A1-6: Fatigue data of GRP composites tested by Xiao-Bathias [43] at various off-axis angles θ (degrees) at the stress ratio of $R=-1$.

θ	σ_{\max} (MPa)	Life (Cycles)	θ	σ_{\max} (MPa)	Life (Cycles)
0	660.6934	79213.65	45	30.19952	2228435
0	741.3102	9727.472	71	45.70882	28.84032
0	822.2426	4677.351	71	36.30781	229.0868
0	870.9636	2172.701	71	30.19952	1717.908
0	954.9926	61.0942	71	30.19952	8511.38
19	147.2313	229.0868	71	26.30268	67608.3
19	131.8257	501.1872	90	38.01894	15.13561
19	158.4893	831.7638	90	36.30781	199.5262
19	114.8154	14354.89	90	28.84032	1071.519
19	100	14354.89	90	28.84032	3981.072
19	95.49926	39810.72	90	34.67369	4466.836
45	66.06934	63.09573	90	26.30268	14125.38
45	54.95409	1766.038	90	21.87762	31622.78
45	47.86301	8511.38	90	30.19952	165958.7
45	38.01894	40364.54	90	15.13561	2187762

Table A2-1: Material Properties of CFRP

Material Properties of CFRP	Values
Modulus of Elasticity in Direction 1	$E_1 = 137000 \text{ MPa}$
Modulus of Elasticity in Direction 2	$E_2 = 9600 \text{ MPa}$
Shear Modulus in Direction 1-2	$G_{12} = 5240 \text{ MPa}$
Ultimate Tensile Strength of Carbon Fiber	$\sigma_{\text{UTS}} = 2610 \text{ MPa}$
Modulus of Elasticity of Carbon Fiber	$E = 194300 \text{ MPa}$
Volume Fraction of Carbon Fiber	$V_f = 70\%$
Shear Strength of Epoxy Resin	$\sigma_{\text{UST}} = 55 \text{ MPa}$
Shear Modulus of Epoxy Resin	$G = 1822 \text{ MPa}$

Table A2-2: Fatigue data of CFRP composites tested by Kawai [14] at various off-axis angles θ (degrees) at the stress ratio of $R=0$.

θ	σ_{\max} (MPa)	Life (Cycles)	θ	σ_{\max} (MPa)	Life (Cycles)
0	2500	1	30	133	1
0	1900	275	30	90	2700
0	1710	4000	30	85	19000
0	1500	41000	30	80	69000
0	1420	230000	30	75	2000000
0	1280	1500000	45	80	1
10	330	1	45	55	6000
10	300	2000	45	50	10000
10	290	13000	45	45	180000
10	270	410000	45	42	2000000
10	220	2000000	90	50	1
15	260	1	90	32	3000
15	200	1100	90	29	15000
15	190	40000	90	23	18000
15	170	41500	90	20	390000
15	175	80000	90	18	2000000
15	140	160000			

Table A2-3: Fatigue data of CFRP composites tested by Kawai [14] at various off-axis angles θ (degrees) at the stress ratio of $R=0.5$.

θ	σ_{\max} (MPa)	Life (Cycles)	θ	σ_{\max} (MPa)	Life (Cycles)
0	2500	1	30	120	1000
0	2000	500	30	100	100000
0	1900	2000	30	110	400000
0	1800	60000	30	120	1300000
0	1800	70000	30	90	2000000
0	1700	2000000	45	80	1
10	340	1	45	70	10
10	330	50000	45	55	45000
10	320	500000	45	52	300000
10	310	850000	45	51	350000
10	300	2000000	90	50	1
15	250	1	90	35	6
15	240	2500	90	42	30
15	230	31000	90	40	150
15	230	60000	90	30	550
15	225	2000000	90	31	2500
15	140	1600000	90	30	350000
30	130	1.			

Table A2-4: Fatigue data of CFRP composites tested by Kawai [14] at various off-axis angles θ (degrees) at the stress ratio of $R=-1$.

θ	σ_{\max} (MPa)	Life (Cycles)	θ	σ_{\max} (MPa)	Life (Cycles)
0	2500	1	15	100	2000000
0	1600	1000	30	135.7	1
0	1280	15000	30	80	2200
0	1140	60000	30	70	3500
0	1000	12800	30	60	40000
0	900	200000	30	55	130000
10	350	1	30	45	2100000
10	215	1200	45	80	1
10	190	3800	45	47	320
10	157	41000	45	40	700
10	150	370000	45	28	800000
10	142	1500000	90	47	1
15	250	1	90	29	2000
15	190	700	90	23	6000
15	150	3100	90	18	90000
15	140	9000	90	15	2000000
15	120	380000			

Table A2-5: Fatigue data of CFRP composites tested by Zheng-Ming [41] at various off-axis angles θ (degrees) at the stress ratio of $R=0.1$.

θ	σ_{\max} (MPa)	Life (Cycles)	θ	σ_{\max} (MPa)	Life (Cycles)
0	1266	6490	45	67	1150
0	1233	10000	45	68	2050
0	1166	22100	45	54	5620
0	1200	126000	45	68	6490
10	287.5	2740	45	54	7500
10	287.5	3160	45	60	12600
10	258	3650	45	61	16500
10	287.5	4220	45	55	86600
10	241	12400	60	48	1260
10	241	15400	60	43	3550
10	241	19100	60	40	5620
10	266	32700	60	44	7500
10	266	31600	60	49	12600
10	200	56200	60	44	25100
10	200	100000	60	48	42200
10	200	175000	60	40	25100
10	210	1000000	60	41	1120000
20	155	1000	90	42	1260
20	142.5	5620	90	42	1580
20	157	3980	90	42	2510
20	157	6490	90	27	3980
20	142	10000	90	36	4220
20	130	20500	90	34	5620
20	132	31600	90	33	12600
20	142	1.00E+05	90	33	56200
20	130	115000	90	36	398000
20	110	126000			

APPENDIX B

B.1 Java-Programming of Fatigue Damage Analysis

Appendix B contains the program-listing for the fatigue damage analysis of unidirectional GRP and CFRP composites based on a fatigue damage approach developed in this thesis. In this program, the algorithm included the following analysis:

1. Calculation of material properties (E_x , E_y , G_{xy}) in x, y coordination,
2. Calculation of maximum normal and shear strain ranges in the critical plane,
3. Calculation of the normal and the shear stress ranges along the matrix-fiber interface,
4. Calculation of the normal and the shear strain ranges along the matrix-fiber interface,
5. Calculation of the fatigue damage in region II,
6. Calculation of the fatigue damages in regions I and III,
7. The total fatigue damage accumulation in regions I, II, and III

B.2 Symbols and Description in the Program

Symbols (in Code)	Symbols (in Text)	Variable description
TETA	θ	Off-axis angle
S_MAX	σ_{\max}	Maximum applied stress
S_MIN	σ_{\min}	Minimum applied stress
E_MAX_UL	$\epsilon_{\max}(\theta_1)$	Maximum normal strain in the unloading reversal
E_MAX_L	$\epsilon_{\max}(\theta_2)$	Maximum normal strain in the loading reversal
E_MIN_UL	$\epsilon_{\min}(\theta_1)$	Minimum normal strain in the unloading reversal
E_MIN_L	$\epsilon_{\min}(\theta_2)$	Minimum normal strain in the loading reversal
DSN	$\Delta\sigma_n$	Normal stress range
DS	$\Delta\sigma$	Range of stress
D_EN	$\Delta\epsilon_n$	Maximum normal strain range
D_G_MAX	$\Delta(\frac{\gamma_{\max}}{2})$	Maximum shear strain range
DTMAX	$\Delta\tau_{\max}$	Maximum shear stress range
EX	E_x	Modulus of elasticity in x direction
EY	E_y	Modulus of elasticity in y direction
GXY	G_{xy}	Shear modulus in x-y plane
E1	E_1	Modulus of elasticity in 1 direction
E2	E_2	Modulus of elasticity in 2 direction
G12	G_{12}	Shear modulus in 1-2 plane
N_STRESS	$\Delta\sigma_{12}$	Normal stress range in 22 direction
N_STRIAN	$\Delta\epsilon_{12}$	Normal strain range in 22 direction
S_STRESS	$\Delta\tau_{12}$	Shear stress range in 1-2 plane
S_STRAIN	$\Delta\gamma_{12}$	Shear strain range in 1-2 plane
W_SHO	W_{II}	Fatigue damage parameter in region II
NORMAL_E	$\Delta\sigma_n \times \Delta\epsilon_n$	Fatigue damage parameter in region I and III due to normal stress
SHEAR_E	$\Delta\tau_{\max} \times \Delta(\frac{\gamma_{\max}}{2})$	Fatigue damage parameter in region I and III due to shear stress
W_1_MODE L	$W_{III} + W_I$	Total fatigue damage parameter in regions I and III
W_2_MODE L	$W_I + W_{II} + W_{III}$	Total fatigue damage parameter in regions I, II, and III
MODIFIED MODEL	W	Modified fatigue damage parameter based on the proposed model

Fatigue Damage Assessment of Unidirectional GRP and CFRP

```
import type.lang.*;
import java.lang.*;

public class Main {
    public static void main(String[] args) {

        double S_MAX = 0, TETA = 0, S_MIN = 0, E1 = 0, E2 = 0, G12 = 0, R = 0,
        D = 0, F = 0, G = 0, H = 0, C = 0, EX = 0, GXY = 0, EY = 0, DSN = 0,
        DTMAX = 0, E_MAX_L = 0,
        E_MIN_L = 0, E_MAX_UL = 0, E_MIN_UL = 0, D_EN = 0,
        D_G_MAX = 0, D_S = 0, N_STRESS = 0, S_STRESS = 0, N_STRIAN = 0
        , S_STRAIN = 0, W_SHO = 0, NORMAL_E = 0, SHEAR_E = 0, W_1_MODEL = 0
        , W_2_MODEL = 0, TETA_FAKE = 0, MODIFIED_MODEL = 0, A=0;

        boolean GRP = false, CFRP = false;

        IO.print("Is it GRP (true / false) : ");
        GRP = IO.readBoolean();

        if (GRP)
        {
            CFRP = false;
            IO.println("CFRP = false");
        }
        else CFRP = true;

        IO.print("Please Input R : ");
        R = IO.readDouble();

        IO.print("Please Input S_MAX : ");
        S_MAX = IO.readDouble();

        IO.print("Please Input TETA : ");
        TETA = IO.readDouble();
```

```

if (GRP) {
E1 = 38500;
E2 = 17600;
G12 = 4400;
A=0.211688311;
}

```

```

if (CFRP) {
E1 = 137000;
E2 = 9600;
G12 = 5240;
A=0.186460132;
}

```

Calculation of material properties (E_x , E_y , G_{xy}) in x, y coordination:

$S_MIN = S_MAX * R;$

$D = \text{Math.pow}(\text{Math.cos}(\text{Math.toRadians}(TETA)), 4);$
 $D = D / (E1 / 1000);$

$F = \text{Math.pow}(\text{Math.sin}(\text{Math.toRadians}(TETA)), 2);$

$G = \text{Math.pow}(\text{Math.cos}(\text{Math.toRadians}(TETA)), 2);$

$H = \text{Math.pow}(\text{Math.sin}(\text{Math.toRadians}(TETA)), 4);$

$C = \text{Math.pow}(\text{Math.cos}(\text{Math.toRadians}(TETA)), 4);$

$EX = D + (A * F * G) + (H / (E2/1000));$

$EX = 1 / EX;$

$EX = EX * 1000;$

$GXY = (0.096485 * F * G) + ((H + C) / (G12/1000));$

$GXY = 1 / GXY;$

$GXY = GXY * 1000;$

$EY = (H / (E1/1000)) + (0.211688311 * F * G) + (C / (E2/1000));$

$EY = 1 / EY;$

$EY = EY * 1000;$

if (R != -1 && GRP) {

Calculation of maximum normal and shear strain ranges in the critical plane:

$DSN = (S_MAX / 2) - (S_MIN / 2);$

$$DTMAX = (S_MAX / 2) + (S_MIN / 2);$$

$$E_MAX_L = S_MAX / EX;$$

$$E_MIN_L = E_MAX_L * (-0.3);$$

$$E_MAX_UL = S_MIN / EX;$$

$$E_MIN_UL = E_MAX_UL * (-0.3);$$

$$D_EN = ((E_MAX_L - E_MIN_L) / 2) - ((E_MAX_UL - E_MIN_UL) / 2);$$

$$D_G_MAX = ((E_MAX_L - E_MIN_L) / 2) + ((E_MAX_UL - E_MIN_UL) / 2);$$

$$D_S = S_MAX - S_MIN;$$

Calculation of the normal and the shear stress ranges along the matrix-fiber interface:

$$N_STRESS = D_S * F;$$

$$N_STRESS = D_S * \text{Math.sin}(\text{Math.toRadians}(TETA)) * \text{Math.cos}(\text{Math.toRadians}(TETA));$$

Calculation of the normal and the shear strain ranges along the matrix-fiber interface:

$$N_STRAIN = N_STRESS / EY;$$

$$S_STRAIN = S_STRESS / GXY;$$

Calculation of the fatigue damage in region II:

```
if ( TETA ==90) {
    G = 1;
}
```

$$W_SHO = (G * N_STRESS * N_STRAIN) / ((\text{Math.pow}(1726, 2)) / 75000) + \text{Math.sin}(\text{Math.toRadians}(TETA)) * \text{Math.cos}(\text{Math.toRadians}(TETA)) * ((S_STRESS * S_STRAIN) / ((\text{Math.pow}(55, 2)) / 1822));$$

Calculation of the fatigue damages in regions I and III:

$$NORMAL_E = (DSN * D_EN) / ((\text{Math.pow}(1726, 2)) / 75000);$$

$$SHEAR_E = (D_G_MAX * DTMAX) / ((\text{Math.pow}(55, 2)) / 1822);$$

The total fatigue damage accumulation in regions I, II, and III:

```
W_1_MODEL = (G * NORMAL_E) +
    (Math.sin(Math.toRadians(TETA)) * Math.cos(Math.toRadians(TETA)) *
    SHEAR_E);
```

```
W_2_MODEL = W_SHO + W_1_MODEL;
```

```
if (84 <= TETA && TETA <= 90) {
    TETA_FAKE = 84;
}
else {
    TETA_FAKE = TETA;
}
}
```

```
MODIFIED_MODEL = ( W_2_MODEL ) /
    ( Math.pow(Math.cos(Math.toRadians(TETA_FAKE)), 2 ));

}
```

```
if (R != -1 && CFRP) {
```

```
    DSN = (S_MAX / 2) - (S_MIN / 2);
```

```
    DTMAX = (S_MAX / 2) + (S_MIN / 2);
```

```
    E_MAX_L = S_MAX / EX;
```

```
    E_MIN_L = E_MAX_L * (-0.3);
```

```
    E_MAX_UL = S_MIN / EX;
```

```
    E_MIN_UL = E_MAX_UL * (-0.3);
```

```
    D_EN = ((E_MAX_L - E_MIN_L) / 2) - ((E_MAX_UL - E_MIN_UL) / 2);
```

```
    D_G_MAX = ((E_MAX_L - E_MIN_L) / 2) + ((E_MAX_UL - E_MIN_UL) / 2);
```

```
    D_S = S_MAX - S_MIN;
```

```
    N_STRESS = D_S * F;
```

```
    S_STRESS = D_S * Math.sin(Math.toRadians(TETA)) *
```



```

    Math.cos(Math.toRadians(TETA));

N_STRIAN = N_STRESS / EY;

S_STRAIN = S_STRESS / GXY;

if ( TETA == 90) {
    G = 1;
}

W_SHO = (G * N_STRESS * N_STRIAN) / ( (Math.pow(2610, 2)) / 194300) +
    Math.sin(Math.toRadians(TETA)) * Math.cos(Math.toRadians(TETA)) *
    ((S_STRESS * S_STRAIN) / ( (Math.pow(55, 2)) / 1822));

NORMAL_E = (DSN * D_EN) / ( (Math.pow(2610, 2)) / 194300);

SHEAR_E = (D_G_MAX * DTMAX) / ( (Math.pow(55, 2)) / 1822);
W_1_MODEL = (G * NORMAL_E) +
    (Math.sin(Math.toRadians(TETA)) * Math.cos(Math.toRadians(TETA)) *
    SHEAR_E);

W_2_MODEL = W_SHO + W_1_MODEL;

    if (84 <= TETA && TETA <= 90) {
        TETA_FAKE = 84;
    }
    else {
        TETA_FAKE = TETA;
    }

MODIFIED_MODEL = ( W_2_MODEL ) /
    ( Math.pow(Math.cos(Math.toRadians(TETA_FAKE)), 2 ));

}

if (R == -1 && CFRP) {

DSN = (S_MAX / 2) - (S_MIN / 2);

DTMAX = (S_MAX / 2) - (S_MIN / 2);

E_MAX_L = S_MAX / EX;

E_MIN_L = E_MAX_L * (-0.3);

```

```

E_MAX_UL = S_MIN / EX;
E_MIN_UL = E_MAX_UL * (-0.3);
D_EN = ((E_MAX_L - E_MIN_L) / 2) + E_MIN_UL;
D_G_MAX = ((E_MAX_L - E_MIN_L) / 2) - ((E_MAX_UL - E_MIN_UL) / 2);
D_S = S_MAX - S_MIN;
N_STRESS = D_S * F;
S_STRESS = D_S * Math.sin(Math.toRadians(TETA)) *
    Math.cos(Math.toRadians(TETA));
N_STRIAN = N_STRESS / EY;
S_STRAIN = S_STRESS / GXY;

    if (TETA == 90) {
        G = 1;
    }

W_SHO = (G * N_STRESS * N_STRIAN) / ((Math.pow(2610, 2)) / 194300) +
    Math.sin(Math.toRadians(TETA)) * Math.cos(Math.toRadians(TETA)) *
    ((S_STRESS * S_STRAIN) / ((Math.pow(55, 2)) / 1822));
NORMAL_E = (DSN * D_EN) / ((Math.pow(2610, 2)) / 194300);
SHEAR_E = (D_G_MAX * DTMAX) / ((Math.pow(55, 2)) / 1822);

W_1_MODEL = (G * NORMAL_E) +
    (Math.sin(Math.toRadians(TETA)) * Math.cos(Math.toRadians(TETA)) *
    SHEAR_E);
W_2_MODEL = W_SHO + W_1_MODEL;

    if (84 <= TETA && TETA <= 90) {
        TETA_FAKE = 84;
    }
    else {
        TETA_FAKE = TETA;
    }

```

```

    }
MODIFIED_MODEL = ( W_2_MODEL ) /
    ( Math.pow(Math.cos(Math.toRadians(TETA_FAKE)), 2 ));

    }

    if (R == -1 && GRP) {

DSN = (S_MAX / 2) - (S_MIN / 2);

DTMAX = (S_MAX / 2) - (S_MIN / 2);

E_MAX_L = S_MAX / EX;

E_MIN_L = E_MAX_L * (-0.3);

E_MAX_UL = S_MIN / EX;

E_MIN_UL = E_MAX_UL * (-0.3);

D_EN = ((E_MAX_L - E_MIN_L) / 2) + E_MIN_UL;

D_G_MAX = ((E_MAX_L - E_MIN_L) / 2) - ((E_MAX_UL - E_MIN_UL) / 2);

D_S = S_MAX - S_MIN;

N_STRESS = D_S * F;

S_STRESS = D_S * Math.sin(Math.toRadians(TETA)) *
    Math.cos(Math.toRadians(TETA));

N_STRIAN = N_STRESS / EY;

S_STRAIN = S_STRESS / GXY;

    if ( TETA == 90) {
        G = 1;
    }

W_SHO = (G * N_STRESS * N_STRIAN) / ((Math.pow(1726, 2)) / 75000) +
    Math.sin(Math.toRadians(TETA)) * Math.cos(Math.toRadians(TETA)) *
    ((S_STRESS * S_STRAIN) / ((Math.pow(55, 2)) / 1822));

NORMAL_E = (DSN * D_EN) / ((Math.pow(1726, 2)) / 75000);

```

```

SHEAR_E = (D_G_MAX * DTMAX) / ( (Math.pow(55, 2)) / 1822);

W_1_MODEL = (G * NORMAL_E +
    (Math.sin(Math.toRadians(TETA)) * Math.cos(Math.toRadians(TETA)) *
    SHEAR_E);

W_2_MODEL = W_SHO + W_1_MODEL;

    if (84 <= TETA && TETA <= 90) {
        TETA_FAKE = 84;
    }
    else {
        TETA_FAKE = TETA;
    }

MODIEFIED_MODEL = ( W_2_MODEL ) /
    ( Math.pow(Math.cos(Math.toRadians(TETA_FAKE)), 2 ));

}
IO.print("Modeified Model = ");
IO.println(MODIEFIED_MODEL);

IO.print("W_SHO = ");
IO.println(W_SHO);

IO.print("W_1_Model = ");
IO.println(W_1_MODEL);
IO.print("W_2_Model = ");
IO.println(W_2_MODEL);

IO.print("EX = ");
IO.println(EX);

IO.print("EY = ");
IO.println(EY);

IO.print("GXY = ");
IO.println(GXY);

IO.print("NORMAL_E = ");
IO.println(C);

IO.print("SHEAR_E = ");
IO.println(C);
}
}

```

2BL-14-105